UNIVERSITY OF CALIFORNIA SAN DIEGO

SAN DIEGO STATE UNIVERSITY

Understanding the role of NEMO in IKK activation

in a Joint Doctoral Program

A dissertation submitted in partial satisfaction of the requirements for the degree Doctor of Philosophy

in

Chemistry

by

Myung Soo Ko

Committee in charge:

University of California San Diego:

Professor Geoffrey Chang
Professor Gourisankar Ghosh
Professor Wei Wang
Professor Jerry Yang

San Diego State University:

Professor Tom Huxford, Chair
Professor Manal Swairjo

2020

The dissertation of Myung Soo Ko is approved, and it is acceptable in quality and form for publication on microfilm and electronically:

_____

_____

_____

_____

_____

_____

Chair

University of California San Diego

San Diego State University

2020

TABLE OF CONTENTS

LIST OF FIGURES

LIST OF TABLES

ACKNOWLEDGEMENTS

Chapter two, in full, has been published for publication of the material as it may appear in BBA - Proteins and Proteomics, 2020, Myung Soo Ko; Tapan Biswas; Maria Carmen Mulero; Andrey A Bobkov; Gourisankar Ghosh; Tom Huxford. The dissertation/thesis author was the primary investigator and author of this paper.

VITA

2006	Bachelor of Science/Master of Science at Silla University
2006-2008	Student trainee at Korea FDA
2009-2012	Research Assistant at University of California Los Angeles
2013	Associate in Arts, Santa Monica College
2013 - 2014	Optional Practical Training Program at University of Southern California
2015 - 2016	M.S. program at San Diego State University
2020	Doctor of Philosophy in the Joint Doctoral Program at University of California San Diego and San Diego State University

ABSTRACT OF THE DISSERTATION

Understanding the role of NEMO in IKK activation

by

Myung Soo Ko

Doctor of Philosophy in Chemistry

University of California San Diego, 2020
San Diego State University, 2020

Professor Tom Huxford, Chair

Two key events are associated with IKK activation through the canonical NF-kB pathway. Phosphorylation of two serine residues within the activation loop (AL) of IKK2/β has long be known to be a requirement for IKK activation and serves as the signature for IKK in its active state. What is much less well understood is the necessary role of non-covalent interaction between linear polyubiquitin chains and the NEMO subunit in promoting AL phosphorylation of IKK2/β.

In order to better understand the solution behavior of the enigmatic NEMO protein and gain insight into its influence over multisubunit IKK complexes, I undertook biophysical characterization of purified a series of recombinant human NEMO proteins and disease-associated point mutant proteins as well as various NEMO:IKK2/β complexes. Through size exclusion chromatography-multiangle light scattering and

analytical ultracentrifugation, NEMO is predominantly a dimer in solution. However, by virtue of its modular coiled coil segments NEMO exhibits complicated solution dynamics that causes it to behave as a significantly elongated molecule. Analyses of NEMO in complex with IKK2 indicate that NEMO preserves this structurally dynamic character within the multisubuit complex and exacerbates the previously observed propensity of IKK2 towards homo-oligomerization. These observations provide critical information on the structural plasticity of NEMO which helps clarify its role in diseases and IKK regulation through oligomerization-dependent phosphorylation of catalytic IKK2 subunit dimers.

As further effort to understand how NEMO induces phosphorylation of the IKK2AL serines, I proposed that upon binding to the polyubiquitin chains synthesized during signaling, NEMO might mediate additional contacts with IKK2, which could induce the conformational changes in IKK2 necessary for AL phosphorylation. Using a series of *in vitro* and cell-based experiments, a short 6-residues segment located near the C-terminus of NEMO weakly contacts IKK2. A peptide derived from NEMO encompassing these contact residues blocks IKK2 activation *in vitro* and in cells. Finally, I could show that this novel inhibitory NEMO-based peptide protects mice from LPS-induced lethality. Furthermore, the native sequence NEMO peptide disrupts systemic cytokine induction by LPS while a mutated version of the peptide fails to do. Thus, this NEMO peptide could be developed for therapeutic purposes.

CHAPTER ONE

1. INTRODUCTION

1.1 Inducible gene expression

Cells must be able to rapidly respond to changes in their external environment to survive and benefit from new circumstances [101]. Even in multicellular organisms, cells need to respond to signaling molecules to determine when to divide, migrate, activate survival programs, or die. New proteins are produced in response to detection of changing external stimuli as a result of rapid activation of specific target gene transcription. This process, which is typically one of the terminal effector outputs of signal transduction, is known as inducible gene expression [101,108].

Inducible gene expression has several features that distinguish it from the regular or constitutive expression of “housekeeping” genes. Expression of inducible genes is tightly regulated and must be able to be rapidly and specifically activated in response to external stimuli [101-102]. However, the rate-limiting step of transcription can differ between various inducible genes. Once the stimulus is removed, an inducible gene must then be able to quickly return to its basal, inactive state. For example, signaling kinases such as MAPKs sometimes localize to the promoters of target genes where they can function as transcriptional activators, rapidly facilitating the switch between activated and repressed states of gene expression [103,108-111]. Furthermore, multiple genes must often be synchronously activated in response to the same stimulus, such that the proteins required to respond to the stimulus are produced simultaneously at the appropriate relative levels [101-103]. Similarly, multiple cells in an organism must respond to

developmental signs in a coordinated work so that the appropriate morphogenetic process occurs over a broad section of cells [102,109].

1.2 Inducible gene expression through the activation of human B cells

Human lymphocytes (cells) consist of T cells, B cells and, natural killer cells. T cells are mainly responsible for cell-mediated immunity [105]. B cells play the essential roles in the humoral immunity to activate immune system by secreting antibodies. B cells are also present antigens to T cells and can release a range of potential immune-regulating cytokines. It was first discovered by Chang and Glick [104]. B cells mature in the bone marrow in mammals. B cells express B cell receptors on their cell membrane and the receptors allow the cell to bind to a specific antigen and initiate an antibody response. Each B cell transmits a unique receptor for antigen that is consisted of the membrane-band form of its antibody. After antigen recognition by the membrane-bound receptor, the B cells can proliferate to increase their numbers and differentiate to secrete their antigen-specific antibodies [108].

Human B cells are generated in bone marrow from progenitor cells that are committed to the B cell linages (pro-B cells). Each pro-B cell undergoes independent rearrangement of diverse immunoglobulin L- and H- chain gene segments [106]. Rearrangement of the H-chain locus creates in each B cell and drives the expression of H-chain protein and then proliferate and differentiate to start L-chain gene recombination [108]. When a B cell expresses L-chain protein, it pairs with the previously arranged H chain and is expressed as membrane immunoglobulin on the cell surface [107].

Human immune system can generate a diversity of specific antibodies in response to antigen stimulation. This process is of fundamental importance to acquired immunity [107,111]. The process of human B cell development is very complicated and is controlled by many transcription factors [105].

1.3 NF-kB and the immune system

Systems analyses and bioinformatics metadata mining are commonly used today as state-of-the-art approaches for recognizing nodal components, whether proteins, genes or regulatory pathways, that intersect to affect biological processes or influence phenotypes [111-112]. This approach allows linkage to be made where none are readily apparent. Twenty-five years ago, David Baltimore and his researchers identified a DNA-binding factor using a simple gel-electrophoresis mobility-shift assay, which has since been found to be ancient and evolutionarily conserved and to be connected to many biological pathways [112]. This factor is associated with its specific DNA sequence 5'-GGGACTTTCC-3' located within the enhancer of the immunoglobulin kappa light chain gene in activated B cells [38,112]. This factor is NF-κB [112]. Today, more than three decades and literally tens of thousands of reported studies later, NF-κB is recognized as a crucial key of gene expression that immensely influences many aspects in immunology such as inflammation, immediate antimicrobial responses, the immune system, lymphoid organogenesis, pathogen recognition and innate immune responses, and initiation of the adaptive immune response [39-40].

1.4 NF-kB activation signaling pathways

NF-kB transcription factors play crucial roles in an intricate system that regulates cells to adapt and respond to environmental changes, which is a process that is critical for survival [21]. A large number of diverse external stimuli lead to NF-kB activation and the genes whose expression is regulated by NF-kB play important and conserved roles in immune and stress responses, and impact processes such as apoptosis, proliferation, differentiation, and development [1-4,11]. A lack of regulation and consequent aberrant NF-kB activity cause various pathological conditions, including chronic inflammatory and metabolic diseases, autoimmune disorders, and cancer [6,23]. Cellular responses to various pathogenic and pro-inflammatory signaling molecules, including viral and bacterial nucleic acids, lipopolysaccharide (LPS), interleukin-1β (IL-1β), and tumor necrosis factor alpha (TNF-α), depend on the NF-kB activation.

In their resting state, NF-kB dimers exist in a stable cytosolic complex, in inactive forms, through their association with a member of the inhibitor IkB family. Two major signaling pathways, “canonical” and “noncanonical”, are activated through upstream signal complexes then lead these factors to transmit to the nucleus and promote transcription (12-13). In canonical pathway, signaling is promoted through complexes such as TRAFs and RIPs and a central effector kinase complex, called the inhibitor of kB kinase (IKK) associated with NEMO (Figure 1). IKK1/α, IKK2/β, and NEMO/IKKγ are present within a IKK complex. NEMO regulates NF-kB activation through the canonical pathway that is essential for inflammation and innate immunity in response to pathogens [16,28]. IKK2/β is primarily responsible for the phosphorylation of specific residues of prototypical IkB proteins (IkBα, -β, and -ε) bound to NF-kB as well as an atypical IkB

protein, NF-kB1/p105, which is the precursor of the NF-kB subunit p50 [7,15,26-27]. IKK2-mediated phosphorylation-dependent ubiquitylation and proteasomal degradation of the IkB proteins (to process from p105 to p50) induce the release of active NF-kB dimers to the nucleus. NF-kB dimers (homo or hetero) bind to kB sites within the promoters/enhancers of target genes and regulate transcription through the recruitment of co-activators and co-repressors, primarily through its TAD [8-9].

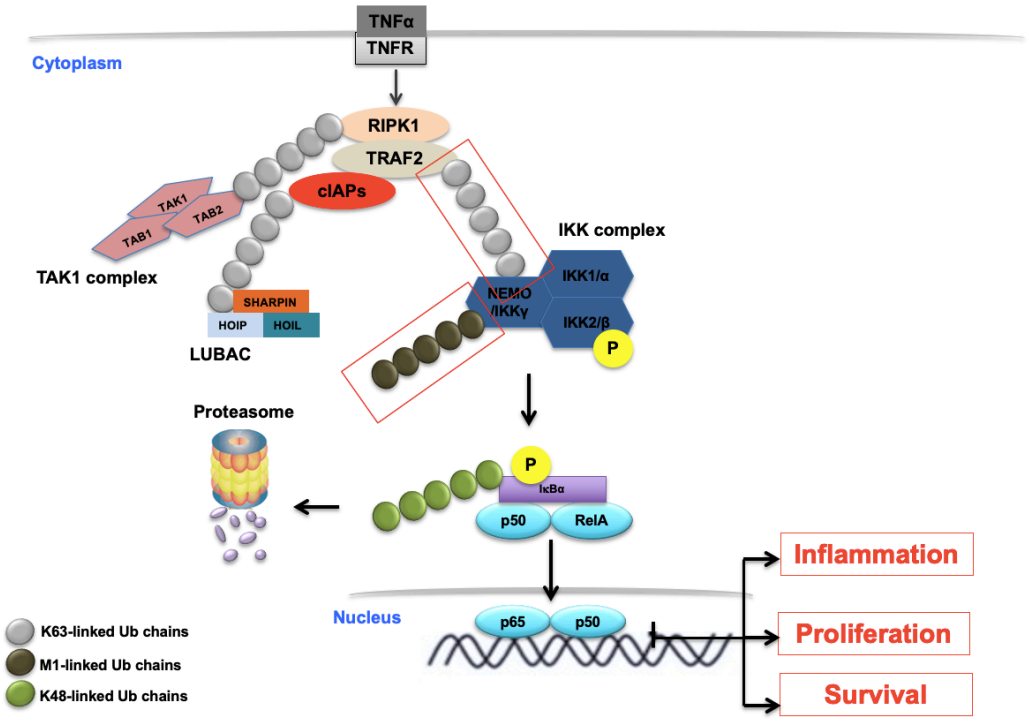

Figure 1. TNF-α-Induced IKK-NF-kB Activation Pathway: Current Model.
The interaction between ligand and its receptor through a cell membrane induces non-degradable poly-Ub chain synthesis which is covalently attached to different adapter proteins. Ub-chain binds NEMO subunit of the IKK complex that induce IKK2 undergoing activation. IKK2 phosphorylates IkBα and then IkBα undergoes degradable ubiquitination. Proteasome degrades IkBα. Free NF-kB can go to the nucleus to induce it target gene expression.

The non-canonical pathway is mediated through TRAFs and IKK1/α:NIK:p100 complexes but does not require NEMO (Figure 2). In contrast, the non-canonical pathway requires another kinase domain-containing cellular factor, NF-kB-inducing kinase (NIK) [29], to induce IKK activation. IKK1/α phosphorylation regulates NF-kB activation through the non-canonical pathway. IKK1/α phosphorylates specific residues of NF-kB2/p100 on its C-terminal IkBδ segment. This promotes to signal induced p100 processing and generation of the NF-kB subunit p52 [17]. Kinase activities of both NIK and IKK1/α are crucial for processing of p100 into p52 [14,18]. IKK1/α and NIK phosphorylate three serines (866, 870, and 872) of NF-kB2/p100 within its C-terminal IkBδ segment, conducting the processing of p100 to p52 [7,15,18,54].

As such, activation of NF-kB dimers is the result of IKK activation-mediated, which act as a central hub of these two pathways, promoting phosphorylation-induced degradation of the IkB inhibitors, which enables the NF-kB dimers to translocate into the nucleus and induce its specific target gene expression.

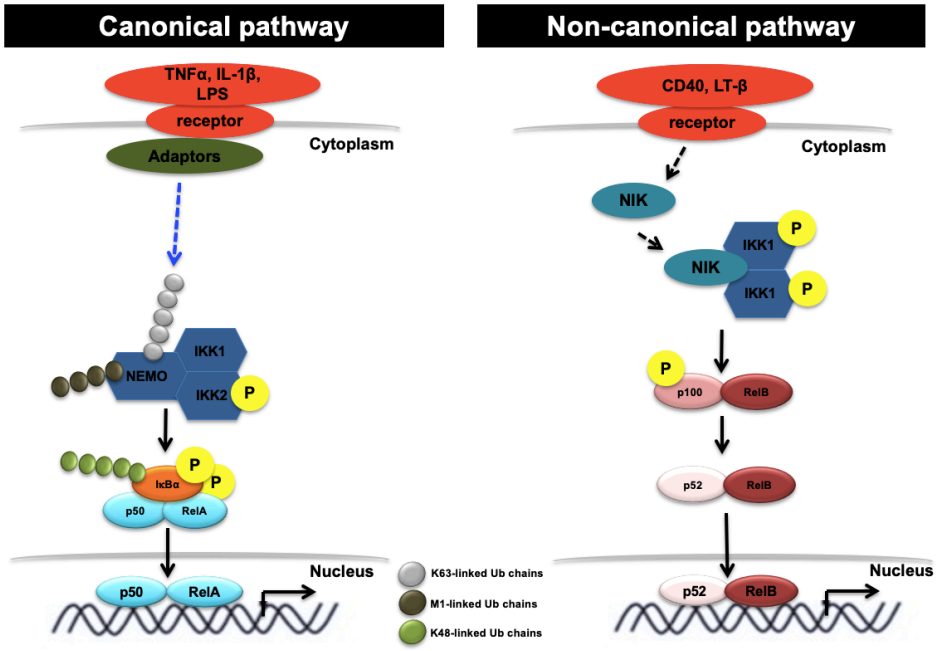

Figure 2. Two distinct NF-kB activation pathways.
Canonical and noncanonical pathways. Canonical pathway requires NEMO to activate IKK complex. However, non-canonical pathway requires NIK to induce IKK activation. Canonical signaling remains mostly intact even in the absence of IKK1. Thus, IKK2: NEMO Is a functional IKK complex.

1.5 NF-kB and IkB family members

The NF-κB family in mammals consists of five members, RelA (p65), RelB, c-Rel, p50 (generated from the p105 precursor protein), and p52 (generated from the p100 precursor), which associate noncovalently as homo- and heterodimers and activate select target gene transcription (Figure 3) [5-6]. 15 different NF-κB homo- or heterodimers are possible through the combinatorial association of the five subunits. Some of these homo- or heterodimer formations are plentiful in diverse cell types while others are uncommon. The NF-κB p50:p65 heterodimer, for instance, is appears at significant levels in many cells. However, c-Rel subunit-containing dimers are much less common and limited primarily to lymphoid cells. The p50:p52 heterodimer and RelB homodimer have not been identified in cells [10,12-13].

Each of the five NF-κB subunits contains the Rel homology region (RHR). The RHR is an N-terminal region that encompass roughly 300 residues with a high degree of amino acid conservation. X-ray crystallographic analyses have shown that the RHR consists of three independent structural elements: the N-terminal domain (NTD), the dimerization domain (DD), and the nuclear localization signal (NLS). Both NTD and DD are folded, globular domains, but the structure of the region including the NLS depends upon its partner proteins. Unique amino acid sequences C-terminal to their respective RHR exist in RelA, RelB, and c-Rel subunits, but not p50 or p52 [32-33]. These unique C-terminal regions are responsible for carrying out the particular transcriptional activation (TA) functions of the various NF-kB subunits. NF-kB p50 and p52 subunits do not possess this TA region. Rather, the C-termini of these two subunits contain a glycine-rich region (GRR) that seems to be a result of their incomplete proteolytic processing from

p105 and p100, respectively. Consequently, p50 or p52 homodimers function as transcriptional inhibitors. However, these two NF-κB proteins can become involved in selective target gene activation through their association with co-activating proteins in the nucleus [21, 29].

IκB proteins regulate induction of NF-κB in a stimulus-specific manner (Figure 3). The rapid and transient activation of NF-κB that is required to many immune and inflammatory responses is controlled by the degradation of classical IκB proteins, predominantly IκBα, and the subsequent transcriptional upregulation of response genes. IkBβ regulates NF-kB differently by controlling a more prolonged response and IkBε is thought to function as a modulatory factor to optimize the timing of waves of NF-kB activation through removal of IkBα. The non-classical IκB proteins, p105 and p100, induce more specialized gene activation programs, as these IκB proteins are co-opted for distinct degradation or partial proteolytic processing events. Additionally, the atypical "nuclear" IκB proteins, Bcl-3, IκBζ, and IκBNS, also regulate NF-κB activity by interacting with the transcription factors in the nucleus at the level of transcription [18, 20, 54].

In the case of IκBα, it was known that NF-kB became activated after phosphorylation of IkB and its subsequent polyubiquitylation and degradation via the 26 S Proteasome. The inducible phosphorylation sites were mapped to serines (S) 32 and 36, whose substitution with alanines (A) or threonines (T) prevents phosphorylation, ubiquitination and degradation [113]. As a result, nonphosphorylatable IκBα mutants, such as IκBα (A32/36), are potent and specific inhibitors of NF-κB activation. What was not clear is what was the protein kinase activity responsible for the IkB phosphorylation. After many years, multiple labs identified a kinase, which had previously been

characterized as a protein called CHUK, that was capable of phosphorylating both Serines 32 and 36 of IkBα *in vitro* [113-116]. Once it was recognized that the key initiating step in NF-κB activation was IκB phosphorylation by the IkB Kinase, much of the effort to understand the regulation of this signaling pathway has focused on identification of the protein kinase(s) responsible for this event. Purification of the CHUK enzyme (which turned out to be IKK1/a) from TNF-a-induced HeLa cells revealed it to be part of a complex with a closely homologous kinase (IKK2/β) and the novel NEMO protein subunit [117]. Mutational studies quickly proved that the IKK2/β subunit was chiefly responsible for activating NF-kB in response to typical pro-inflammatory stimuli. However, IKK1/α was soon identified as the critical activity in inducible control over production of p52 subunits through the “noncanonical” NF-kB pathway.

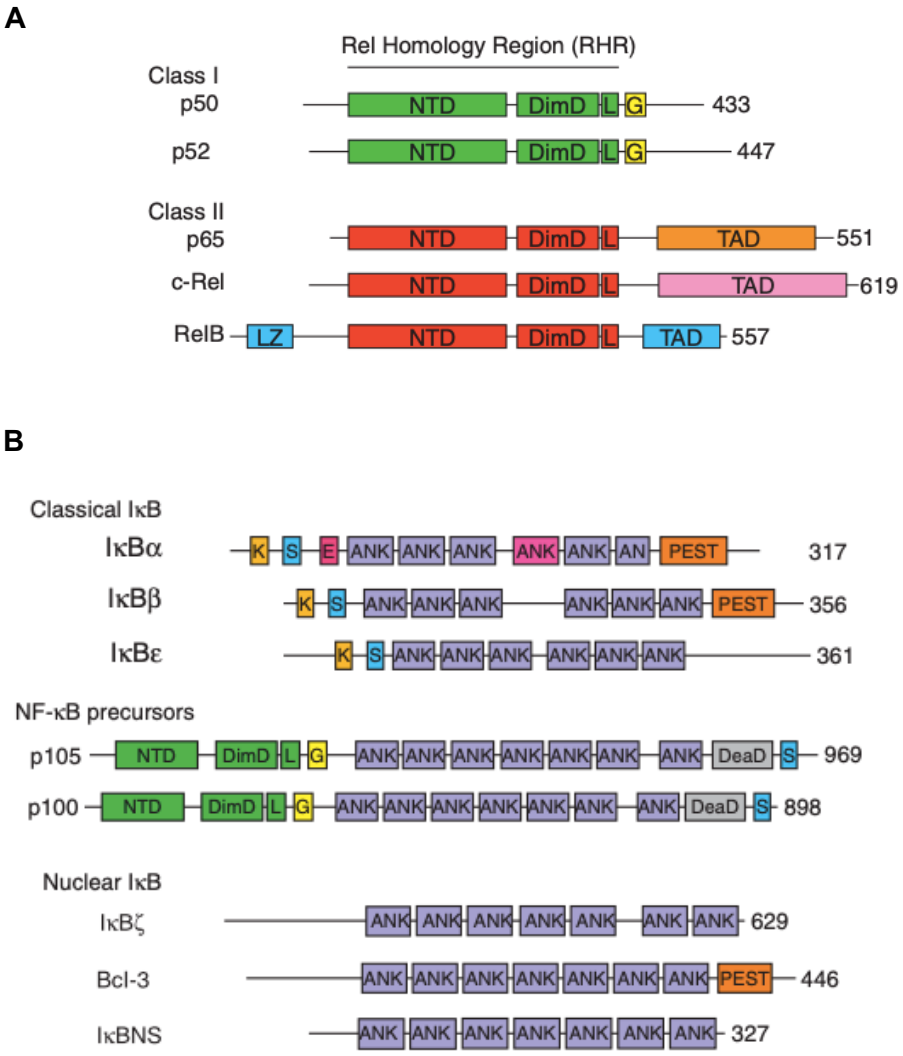

Figure 3. Schmatic representation of members of the nuclear factor-kB (NF-kB) and IkB protein families [54].
(A) All five members have a conserved DNA-binding/dimerization domain(RHD). RHD also has sequences important for nuclear localization and IkB inhibitor binding. The halves of C-terminal in the Rel proteins have tanscriptional activation domains (TAD). The C-terminal halves of the NF-kB subfamily proteins have ankyrin repeat-containing inhibitory domains that can be removed by proteasome-mediated proteolysis. (B) As with the C-terminal domains of the NF-kB proteins, the independent IkB proteins mainly contain ankyrin repeats, and several (IkBα, IkBβ, IkBε, Bcl3, IκBζ, and IκBNS) have two N-terminal serine residues (S) that serve IKK phosphorylation sites, which signal the protein for ubiquitination and degradation.

1.6 The IKK complex

1.6.1 Activation of IKK complex

The IKK holocomplex is activated in response to diverse extra-cellular stimuli ranging from pathogen-derived substances (PAMPs) to inflammatory cytokines, to MHC-presented antigens, to metabolic and genotoxic stresses [18]. These stimuli act on their specific receptors to initiate the signaling. The PAMSs and cytokines bind toll-like receptors (TLRs) and tumor necrosis factor receptors (TNFR) to activate NF-κB through signaling pathways referred to as the “canonical” signaling. Among many other cellular functions, NF-κB activity is essential for immunity and inflammation. Despite the presence of two catalytic IKK subunits (IKK1 and IKK2) within the IKK holocomplex, only IKK2 is activated by canonical signaling marked by the phosphorylation of two serines (Ser177 and Ser181) within the activation loop (AL) [15,26].

Activated IKK2 of the IKK holocomplex is responsible for the phosphorylation of two specific serine residues of NF-κB-bound prototypical IκB (α, -β, and ε) proteins, and also an atypical IκB protein, NF-κB1/p105 [18,26]. Phosphorylation of both serines of IκB leads to its ubiquitination and proteasomal degradation. Degradation of each of these IκBs releases a specific subset of NF-κB dimers, e.g. degradation of IκBα releases NF-κB p50:RelA heterodimer and degradation of IκBβ releases RelA:RelA homodimer because of the interaction specificity [25].

In contrast, IKK1 regulates the activation of NF-κB signaling by the non-canonical pathway, which is essential for lymphoid organogenesis and adaptive immunity among other functions. IKK1 phosphorylates specific residues on the C- terminal segment of NF-κB2/p100, leading to processing of p100 and generation of a different class of NF-κB

dimers [67]. The non-canonical pathway is dependent upon the catalytic activity of another kinase, NIK (NF-κB Inducing Kinase), but not on IKK2 or NEMO [28,67].

It is still debated if a single IKK complex control both pathways or there are distinct IKK complexes *in vivo*. Earlier reports suggested that in at least some cells IKK2 exists as the IKK2:NEMO complex in addition to the trimeric IKK1:IKK2:NEMO complex [57]. Similarly, a small pool of IKK1 is thought to exists as a homodimer which is targeted by the non-canonical pathway. The IKK1:IKK2:NEMO complex is undoubtedly the most abundant, if not the sole IKK complex. The heterotrimeric IKK complex is large containing multiple but an unknown number of copies of each subunit. NEMO binding domain of both IKK1 and IKK2 regulate the formation of IKK1:IKK2:NEMO ternary complex [58,71].

However, the mechanism of larger assembly is still unknown. How specific signals selectively activate IKK1 and IKK2 within an IKK holocomplex, with the help of pathway-specific modulators, NEMO and NIK, has remained elusive. Another related fundamental unanswered question is the role of IKK1, if any, in activation of IKK2 in canonical signaling.

1.6.2 Structures of IKK1, IKK2, and NEMO

1.6.2.1 Catalytic subunits, IKK1 and IKK2

IKK1 and IKK2 share ~50% sequence identity over the entire length and ~65% within the kinase domain (KD) [12,58]. A small but homologous C- terminal segment spanning residues ~700-740 of both IKK1 and IKK2, referred to as the NEMO binding domain (NBD), binds the N-terminal region of NEMO (Figure 4) [72-73]. IKK1/2 binding region of NEMO encompassing residues 50 to 110 is the kinase binding domain (KBD)

[75]. Whereas both IKK1 and IKK2 can bind NEMO independently, IKK2 displays a higher affinity for NEMO [75].

The first structures of an IKK sub-complex were reported in 2008 which revealed how helical NBD of IKK binds coiled-coil KBD [75]. The structure of the core segment of IKK2 of Xenopus was published in 2011, which showed that the core of IKK2 is composed of three domains, KD, ubiquitin-like domain (ULD) and an extended helical domain known as the scaffold dimerization domain (SDD) [59]. These domains interact closely to maintain the structural integrity and regulatory capacity of IKK2.

In 2013, structures of human IKK2 were reported from two groups (Figure 4) [60-61]. These structures of IKK2 determined in inhibitor-free (poised and active) and inhibitor-bound states the IKK2 homodimer provide snapshots of four different conformational states of IKK2. The three-dimensional structures of IKK1 determined by both cryo-EM and X-ray crystallography (Figure 4) [65]. These structures revealed that IKK1 forms stable dimers, similar to IKK2. In the crystal lattice, IKK1 forms a hexameric scaffold arising from trimeric arrangements of the dimers. Surprisingly, in solution, approximately 1-2 % of IKK1 exist in similar hexameric form [65]. Structure-guided cellular and biochemical studies indicate that this supra-molecular assembly of IKK1 triggers non-canonical NF-κB signaling by directly interacting with NIK. Mutations at the IKK1 trimer interface reduced binding of the mutants to NIK and affected non-canonical signaling. However, the IKK1 mutants do not impact canonical signaling mediated by IKK2 [65]. These results suggest that IKK1 in its free state tends to oligomerize differently than its assembly as part of the IKK1:IKK2:NEMO holocomplex.

1.6.2.2 The NEMO adaptor subunit

The third subunit of the IKK complex is a non- catalytic 48 kDa protein, called NEMO (Figure 4). NEMO is a 419 amino acid protein and its three-dimensional structures of several other segments of varying lengths are known to interact their partner proteins [35]. For examples, these include the kinase binding domain (44-111) [27,35] the vFLIP binding domain spanning residues 192 to 252 [76] the CC2-LZ domain (263-333) [77-79] a peptide that binds deubiquitinase (DUB) and M1-linked or K63- ubiquitin chains [81] and the C-terminal Zn finger domain interacting with K63 linked ubiquitin chains and IkBα (394-419) [118].

Although devoid of catalytic activity, NEMO is absolutely required for the canonical NF-kB activation pathway. Structure prediction, confirmed by recent X-ray crystallography data [27,35,77-79,81,118], indicates that it is essentially a long parallel dimeric intermolecular coiled coil, except for the carboxyl terminus. The amino-terminal part of NEMO (aa 47 – 120 in human NEMO) is responsible for interaction with the kinase subunits [27]. The X-ray structure of amino acids 44 – 111 of NEMO bound to amino acids 701 – 746 of IKK2/β has been reported recently (Figure 4) [27,35]. It forms an asymmetrical four-helix bundle made of a parallel NEMO dimer, each monomer being a crescent shape a-helix associated with two mainly helical IKK2/β peptides, which do not interact with each other. Interestingly, replacement of a phosphoacceptor Ser at position 68 by a phosphomimetic Glu decreases NEMO dimerization and reduces IKK2/β binding [75]. However, the kinase responsible for targeting Ser68 has not been unambiguously identified.

The structure provides detailed insight into the earlier discovery of a small peptide

inhibitor of the NEMO/IKKβ interaction, named the “NEMO binding domain” or NBD peptide and corresponding to the IKKβ sequence 737–742 [72]. Despite the weak affinity for NEMO, the peptide has proven to be an important physiological tool and its efficacy has been demonstrated in over 70 cellular and *in vivo* studies [72-73]. The task of determining the structure of the unliganded IKKβ-binding domain of NEMO has been challenging, as the domain, when truncated from the full-length protein, is conformationally heterogenous and appears only partially folded [85]. Moreover, recent studies showed that in the resting state, binding affinity of the central CC region interacting with short poly ubiquitin such as M1-di-ubiquitin by full length NEMO is very week due to NEMO existing in an auto-inhibited conformation through intramolecular interactions [30,34-35]. Long Met1-linked linear poly-ubiquitin such as tetra-ubiquitin seemed to be able to overcome NEMO auto-inhibition [31,36-37].

1.6.3 IKK complex assembly

A catalytically active complex of apparent molecular weight 700-900 kDa that contains all three subunits (IKK1/α:IKK2/β:NEMO) is present in both unstimulated and stimulated cells, but both IKK1/α and IKK2/β homodimers also seem to exist in cells. Some researchers showed that recombinant NEMO with either IKK1/α or IKK2/β assembles into a complex with an apparent molecular weight that is similar to the purified IKK complex [10].

The 3-dimensional structures of over 90% of the molecular mass of IKK1 and IKK2, and over 55% of NEMO are now known [60,65]. These structures provide clues to how an IKK1:IKK2 heterodimer or IKK2 homodimer could associate with a NEMO dimer

forming the basic IKK1:IKK2:NEMO or IKK2:NEMO complexes. The partial structures of the subunits and information derived from biochemical and biological studies, do not allow us to understand how the oligomeric IKK holocomplexes could form from the basic trimeric units [12]. These point towards complex biochemical properties of the IKK complex. Perhaps when all three components (or just NEMO and IKK2) associate, a large structural change ensues leading to oligomerization. Detailed structural information about the NEMO/IKK interaction is still unclear and whether this is the exclusive composition characteristic for a ubiquitously expressed IKK complex or whether other variants of the assembly exist. Therefore, knowledge of the structure of the IKK holocomplex, or any subcomplex that mimics the larger assembly, is required.

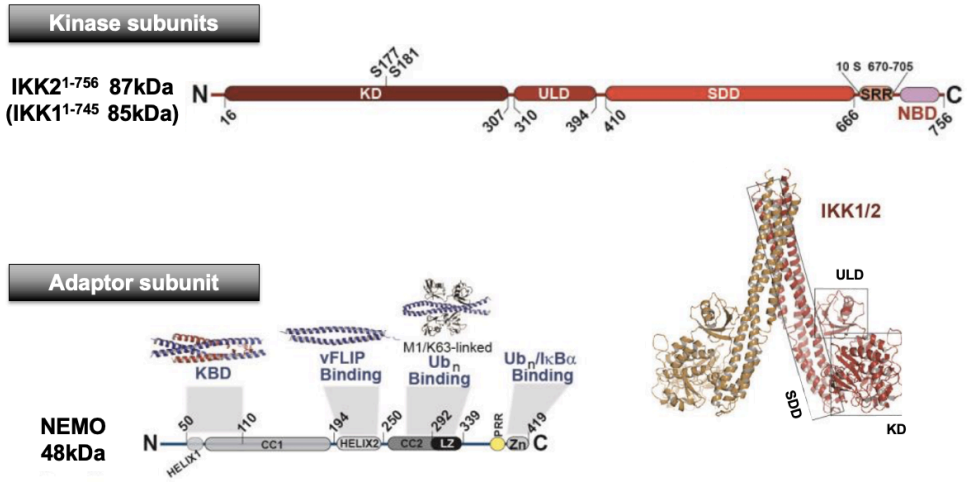

Figure 4. Domain Architectures of the Subunits of the IKK Complex: IKK1/α, IKK2/β, and NEMO.

Domain organization of IKK catalytic subunits and NEMO, and primary interaction sites with each other and ubiquitin. Also shown are available X-ray structural models of the core domain of IKK1/2 lacking the NBD. The high affinity interaction that hold the subunits together is between the NBD of IKK (~residues 705 to 740 shown in red ribbon) and KBD (~residues 50 to 110- shown in blue ribbon) of NEMO. The Ub-binding domain of NEMO spans residues ~260 to 333.

1.7 Ubiquitylation in immune response

Ubiquitylation is a posttranslational mechanism of protein modification involving covalent conjugation of ubiquitin to lysine (K) residues of target proteins, a process that is catalyzed by the sequential action of ubiquitin-activating (E1), ubiquitin-conjugating (E2), and ubiquitin-ligating (E3) enzymes [119,126].

Formation of polyubiquitin chains involves isopeptide bond connection between the carboxyl-terminal glycine residue of ubiquitin and an internal K residue or the amino-terminal methionine (M1) of another ubiquitin. The presence of seven Ks, along with the M1, creates a large variety of ubiquitin chains, including K6-, K11-, K27-, K29-, K33-, K48-, K63-, and M1-linked ubiquitin chains, as well as mixed ubiquitin chains [126]. The substrate specificity of ubiquitination is mainly determined by E3s, a family of > 600 mammalian members that recognize protein substrates and assist or directly catalyze the transfer of ubiquitin from E2s to the substrates [120-121]

Ubiquitination is a reversible and dynamic event, since the conjugated ubiquitin chains can be cleaved by a family of ubiquitin-specific proteases, termed deubiquitinases (DUBs) [126]. Although the best-known function of ubiquitination is to target substrate proteins for degradation in the 26S proteasome, it is now clear that some ubiquitin chains, such as the K63-linked and M1-linked (also called linear) ubiquitin chains, mediate signal transduction via nondegradative mechanisms [122-123].

Such ubiquitin chains can function as a platform that facilitates protein-protein interactions in signal transduction. A growing family of proteins with ubiquitin-binding domains (UBDs) recognize target proteins when they are attached with specific types of ubiquitin chains and, thereby, mediate assembly of signaling complexes [124-125].

1.7.1 Ubiquitylation in IKK-NF-kB Activation

Early studies established Lys48-linked ubiquitylation as a mechanism for inducing the degradation of negative regulators of NF-κB, such as the NF-κB inhibitor IκBα, but later work suggested that ubiquitin chains linked through other Lys residues can regulate the canonical IKK complex by a non-degradative mechanism [127]. The molecular mechanisms underlying these non-degradative actions of ubiquitin are now being rapidly uncovered and are leading to new insights into how signal transduction networks, in general, can be controlled [127].

At the heart of this new knowledge is the discovery that NEMO interacts with linear Met1-linked ubiquitin dimers [128-129] and that mutations in NEMO that interfere with ubiquitin binding reduce the activation of the canonical IKK complex [128-130]. Moreover, four other proteins that possess a ubiquitin-binding domain similar to that found in NEMO have been identified, namely ABIN1 (A20-binding inhibitor of NF-κB 1), ABIN2, ABIN3 and optineurin (OPTN; also known as NEMO-related protein) [132-134].

Several of these proteins also have distinct key roles in regulating the innate immune system. The interaction of NEMO with ubiquitin oligomers is crucial for the activation of the canonical IKK complex, because interleukin-1 (IL-1) or tumour necrosis factor (TNF) fail to induce robust activation of IKKα and IKKβ in cells expressing NEMO mutations that prevent interaction with ubiquitin chains [129-131].

Although the role of ubiquitination in targeting proteins for proteasome-dependent degradation have been extensively studied and well-characterized, the critical non-proteolytic functions of ubiquitination, such as how ubiquitin chains non-covalently binding to NEMO activate IKK and further involved in cell survival and cancer development are still unclear[128-130]. Therefore, there are starting to emerge in elucidating the non-

proteolytic function of ubiquitination signaling in protein kinase activation and its implications in human diseases.

1.8 IKK, disease and drug development

Gene knock out studies in mice have demonstrated the essential function of all three IKK subunit *in vivo* [41,43]. Constitutive IKK activity leads to cancer and results from acquired mutations of several IKK regulatory proteins, although mutations are mostly observed in signaling proteins upstream of the IKK complex that affect both pathways [45]. However, acquired mutations are also observed in the catalytic IKK subunits albeit rarely. Rare mutations of the IKK subunits identified so far result in reduced IKK catalytic activity which accounts for immunological disorders. Non-sense IKK2/β mutations causing severe combined immunodeficiency (SCID) have also been reported [42]. SCID are heritable deficiencies of humoral and cell-mediated immunity where lymphocytes cannot be properly activated. In IKK2-mutated SCID, non-sense mutations result in truncation of the protein at residues 272, 286 and 432. The kinase domain of IKK2/β of the last truncation remains intact whereas it is shortened in the first two. All three truncations severely block canonical NF-κB activation through TLR and TNFR pathways. These truncations are expected to completely block IKK2/β activity since the complete loss of IKK2/β causes premature death in mice [45]. It is possible that the requirement of IKK2/β might be different in human vs mice.

The gene encoding *NEMO* is in the X chromosome. NEMO subunit is frequently mutated in two types of disorders, Anhidrotic Ectodermal Dysplasia, with ImmunoDeficiency (EDA- ID) and Incontinentia Pigmenti (IP). In EDA-ID patients, always

males, hemizygous *NEMO* mutations retains a residual NF-κB activation (hypomorphic mutations); in female patients, the NEMO mutation is always in a heterozygous state and can either maintain a residual NF-κB activation (EDA-ID) or its near abolition (IP) [48-49].

Mutations in IKK1/α result in lethal cocoon syndrome, characterized by fetal encasement and malformations [44]. These relatively unrelated phenotypes in IKK1/α, IKK2β and NEMO mutants suggest unique subtlety in signal processing by IKK which may or may not be through targeting NF-κB. Heterozygous mutations in NFKB1A (IκBα gene) cause autosomal dominant (AD) EDA-ID due to a severe defect in NF-κB p50:RelA activation by stimuli of canonical pathways including pathogens. Mutations mostly occur within the N-terminal region encompassing residues 1 to 36. Several are point mutations, and some are deletion mutant where N-terminal 36 residues are deleted. Surprisingly, point mutants are more severely defective in NF-κB activation than the deletion mutants [46-47]. It has also been shown that the mutant proteins are stable; thus, the defect in NF-κB activation is not due to protein expression or stability.

Targeting constitutively active IKK1/2 with inhibitors for therapeutic purposes has attracted much attention from both academics and pharmaceutical companies [45]. As of 2013, more than 130 patents have been filed for small molecule inhibitors of IKK activity [50]. None of these efforts resulted in a clinical success, due to intolerable side effects upon prolonged treatment with inhibitors. There has been no effort to induce IKK activity in cases where low IKK activity causes disease. Some of the patients with EDA-ID have undergone hematopoietic stem cell transplantation (HSCT) [47]. The positive outcome of HSCT is greater in XL-EDA-ID (NEMO mutations) than in AD-EDA-ID (IκBα mutations).

1.9 Focus of the dissertation research

The IkB Kinase (IKK) complex is a signaling hub that integrates many diverse cell signaling inputs and transmits them to downstream effectors including the NF-kB family transcription factors. The end result of this process is the inducible control over select response gene expression via transcription factor NF-κB. Signals are processed during the input-output event in the form of IKK activation from its inactive or resting state to a state of catalytic activity. However, the precise mechanism through which specific cellular signaling events serve to activate the protein kinase catalytic activity within the IKK2/β subunit of the heterotrimeric IKK complex has remained elusive. What is clear is that the modulator protein NEMO is required for IKK activation in response to canonical NF-kB signaling in response to proinflammatory signals. Regardless of extensive efforts in past years, the mechanism of activation of the IKK complex from its catalytically inactive to the active form by proinflammatory cytokines or environmental hazards remains unclear.

A key event of canonical signaling is the synthesis of multiple types of poly-ubiquitin chains- linear (M1-linked), lysine 63-linked (K63) and mixed. These chains could be linked to adapter proteins including NEMO. NEMO also non-covalently interacts with high affinity to linear Ub-chain and weakly to K63-lined Ub-chain. Irrespective of the covalently linked linear Ub-chain, the non-covalent interaction between the linear Ub-chain and NEMO is essential for the AL phosphorylation of IKK2/β. Different stimuli of canonical IKK2/β activation pathways may form different kinds of poly-ub chain that are covalently linked to different adapter molecules giving rise variations in kinetics and amplitudes of IKK2 activity. The biochemical mechanism of IKK2 activation is largely unknown.

In this study, I highlight the progress in my understanding of the molecular mechanisms by which the binding of ubiquitin to NEMO controls IKK activation through cell signaling networks and how defects in this process underlie the pathogenesis of human disease. To this end, I examined biophysical characterization of purified a series of recombinant human NEMO proteins including full length NEMO, NEMO deletion variants, and disease-associated point mutant proteins as well as various NEMO:IKK2/β complexes. Furthermore, I developed a novel inhibitory NEMO-based peptide which selectively inhibited canonical NF-kB signaling in vitro and in cells and protected mice from bacterial lipopolysaccharide (LPS)-induced lethality. The inhibitor provides a useful tool for investigating the biological functions of IKK/NF-kB and a potential candidate for further development of anti-inflammatory and anticancer drugs.

CHAPTER TWO

2. Structurally plastic NEMO and oligomerization prone IKK2 subunits define the behavior of human IKK2:NEMO complexes in solution

2.1 ABSTRACT

The human IκB Kinase (IKK) is a multisubunit protein complex of two kinases and one scaffolding subunit that controls induction of transcription factor NF-κB activity. IKK behaves as an entity of aberrantly high apparent molecular weight in solution. Recent X-ray crystallographic and cryo-electron microscopy structures of individual catalytic subunits (IKK1/α and IKK2/β) reveal that they are both stably folded dimeric proteins that engage in extensive homo- oligomerization through unique surfaces that are required for activation of their respective catalytic activities. The NEMO/IKKγ subunit is a predominantly coiled coil protein that is required for activation of IKK through the canonical NF-κB signaling pathway. Here I report size-exclusion chromatography, multi-angle light scattering, analytical centrifugation, and thermal denaturation analyses of full-length and mutated recombinant human NEMO. I observe that NEMO is predominantly a dimer in solution, although by virtue of its modular coiled coil regions NEMO exhibits complicated solution dynamics that causes it to behave as a significantly larger sized particle. Analyses of NEMO in complex with IKK2/β indicate that NEMO preserves this structurally dynamic character within the multisubuit complex and provides the complex-bound IKK2/β further propensity towards homo-oligomerization. These observations provide critical information on the structural plasticity of NEMO subunit dimers which

helps clarify its role in diseases and in IKK regulation through oligomerization-dependent phosphorylation of catalytic IKK2/β subunit dimers.

2.2 INTRODUCTION

Induction of transcription factor NF-κB in response to diverse environmental challenges and intracellular stresses requires activation of the IκB Kinase (IKK) [51-52]. Human IKK is a multisubunit complex that consists of two highly similar kinase domain-containing proteins known as IKK1/IKKα and IKK2/IKKβ as well as a necessary scaffolding subunit referred to as NF-κB Essential Modulator or NEMO/IKKγ (hereafter referred to as IKK1/α, IKK2/β, and NEMO, respectively) [53-54]. IKK was discovered biochemically as the only cellular activity in TNF-α-induced HeLa cell cytoplasmic extracts that could selectively phosphorylate the NF-κB inhibitor protein IκBα at serines 32 and 36 [55-57]. Early characterization of active IKK via size-exclusion chromatography (SEC) revealed that it behaves in solution as a 700-900 kDa complex [56-58]. While this suggests the presence of multiple copies of IKK1/α (85 kDa), IKK2/β (87 kDa), and/or NEMO (48 kDa), the precise number and arrangement of individual subunits in the functional IKK complex has been a matter of debate. Furthermore, the molecular mechanism by which IKK becomes active in response to a plethora of distinct cellular stimuli has also remained unclear. Detailed knowledge of the IKK activation mechanism to a level that can guide discovery of novel targeted therapeutic strategies requires a clearer understanding of the assembly and solution dynamics of IKK subunits.

Independent structural models for IKK1/α and IKK2/β subunits as well as analyses of their respective behavior in solution have emerged from experimental biophysical studies on purified, individual IKK subunit proteins. The X-ray crystal structure of nearly

full-length IKK2/β revealed it to be a stably folded homodimer [59-61]. IKK2 dimerization is mediated by interaction through its C-terminal scaffold dimerization domain (SDD) that exhibits hinge-like properties and, consequently, supports considerable variation in the distance between N-terminal kinase domains (KD) of IKK2/β homodimers. Engineered deletion of the distal portion of the SDD that mediates dimerization resulted in a stable monomeric version of IKK2/β that preserves its structure and catalytic specificity towards the IκBα substrate protein [62]. Interestingly, IKK2/β dimers demonstrate a propensity toward higher order oligomerization in solution. Structure-based scanning mutagenesis of residues from different areas on the surface of the KD that stabilize the "open" conformation of IKK2/β homodimers observed in some crystal structures implicated these surfaces as necessary for converting inactive IKK to its active state [60]. The hallmark of active IKK in response to canonical NF-κB signaling is the phosphorylation of serines 177 and 181, within the activation segment of the IKK2/β subunit kinase domain [63]. As with many protein kinases, phosphorylation within this region serves to arrange active site residues so that they are capable of supporting transfer of the gamma-phosphate from ATP to substrate proteins [64]. Structural studies of IKK1/α revealed that it adopts a similar homodimeric structure to IKK2/β and also tends toward self- association in solution [65]. However, IKK1/α oligomerization involves unique amino acid residues that map to different surfaces than those required for IKK2/β self-association. Mutation of these residues was sufficient to disrupt key steps in alternative NF-κB signaling, which is mediated through the catalytic activity of IKK1/α [65-67].

NEMO is an integral component of multisubunit IKK complexes that is required for canonical NF-κB signaling through IKK2/β [68-69]. The precise mechanism by which

NEMO serves to integrate diverse signaling inputs to yield phosphorylation-dependent activation of IKK2/β remains unknown. However, it is clear that inducible formation of polyubiquitin chains plays a vital upstream role in this process [70].

NEMO was predicted from its amino acid sequence to be a primarily coiled coil (CC) protein with a zinc finger domain at its extreme C-terminus [53, 71]. Although no structure for the full-length protein is known, X-ray crystal structures of several segments conform with this prediction. An N-terminal region spanning residues 49-109 in human NEMO has been shown to mediate the principal interaction with the C-terminal NEMO binding domain (NBD) in catalytic IKK2/β and IKK1/α subunits [72-73]. X-ray crystal structures of this kinase binding domain (KBD) portion in NEMO in complex with residues 705-743 from the C-terminus of IKK2/β and in its free form revealed the KBD to be a dynamic CC homodimer that can open slightly to accommodate binding of the catalytic subunit [74- 75]. Three-dimensional structures of several other segments of NEMO include the vFLIP binding CC1 spanning residues 192 to 252 [76], the CC2 at residues 263-333 (also commonly referred to as CoZi or UBAN) that binds to linear diubiquitin and the HOIP linear ubiquitin assembly complex (LUBAC) subunit NZF1 domain [77-80], a Pro-rich segment (residues 388-393) that binds the CYLD deubiquitinase (DUB) [81], and ubiquitin-binding C-terminal Zn finger domain (residues 394-419) [82].

NEMO is encoded by an X-linked gene and NEMO dysfunction due to point mutations or deletions is often associated with the inherited diseases incontinentia pigmenti (IP) and ectodermal dysplasia anhidrotic with immunodeficiency (EDA-ID) [83]. The severity of EDA-ID and IP is highly variable among patients and depends upon the specific NEMO mutation. Whereas functional defects arising from some mutations can be

readily explained, such as disruption of ubiquitin chain binding or NEMO ubiquitylation, the mechanisms through which many NEMO mutations confer disease phenotypes are not known.

Despite the direct observation of multiple homodimeric CC regions, the structure and oligomerization state of full-length human NEMO in solution remains a point for discussion. Early attempts at studying NEMO oligomerization via diverse methods including chemical crosslinking, sedimentation, and chromatography suggested various oligomeric states for NEMO in solution including monomer, dimer, trimer, and tetramer [71, 84-86]. The lack of clarity surrounding the solution behavior of NEMO is exacerbated by the aforementioned observation that multisubunit IKK complexes are routinely purified from cells with an apparent mass of 700-900 kDa.

In this study I used current structural understanding of individual IKK subunit proteins to engineer recombinant full-length, deletion mutant, and disease-linked point mutant human NEMO proteins. Purified NEMO protein constructs both independently and in complex with recombinant IKK2/β subunit homodimers were subjected to experimental biophysical approaches to characterize their oligomerization state and solution behavior. Size-exclusion chromatography coupled with multi-angle light scattering (SEC-MALS) and analytical ultracentrifugation (AUC) measurements clearly indicate that full-length human NEMO assembles predominantly as a homodimer. Some, but not all, of the truncated fragments and many disease-linked single residue mutant NEMO proteins exhibit defects in dimerization. In association with IKK2/β, the resulting IKK2:NEMO complexes form homodimer:homodimer tetramers that exhibit an even greater tendency toward higher order oligomerization than has been observed previously with human

IKK2/β homodimers alone. The NEMO truncation mutants and disease-linked mutants studied here assemble with IKK2/β in a manner similar to the full-length NEMO.

2.3 MATERIALS AND METHODS

2.3.1 Recombinant plasmid and baculovirus preparation

Full-length human NEMO and deletion mutants ($NEMO^{1-110}$, $NEMO^{1-130}$, $NEMO^{1-210}$, $NEMO^{1-250}$, $NEMO^{1-280}$, $NEMO^{1-365}$, $NEMO^{111-250}$, and $NEMO^{250-365}$) were subcloned individually into the NdeI and BamHI restriction sites of the pET15b vector in frame with an N-terminal hexahistidine tag. For site-directed mutagenesis, all substitutions of seven mutations causing EDA-ID in males and three that cause IP in females mapped within the IVD and CC1 regions (110-250) were generated within the pET15b plasmid harboring wild-type NEMO (Table 1). Ten single amino acid substitutions, $NEMO^{D113N}$, $NEMO^{R123W}$, $NEMO^{V146G}$, $NEMO^{L153R}$, $NEMO^{Q157P}$, $NEMO^{A162P}$, $NEMO^{R173G}$, $NEMO^{R173Q}$, $NEMO^{R175P}$, and $NEMO^{L227P}$, were prepared by PCR with base changes incorporated in the oligonucleotide primers (Table 2). Human IKK2/β cDNA was graciously provided by the laboratory of M. Karin (School of Medicine, UC, San Diego). Full-length IKK2/β (amino acids 1-756) was amplified by PCR and cloned in pFastBacHTb (Invitrogen) vector within BamHI and NotI sites in frame with an N-terminal hexahistidine-TEV cleavage site tag. Recombinant baculovirus production, amplification, and titer optimization were carried out in Sf9 insect cell suspensions (Figure 5).

Table 1. Oligonucleotides used to make full-length and truncated NEMO Constructs

NEMO construct		primer sequence
$NEMO^{FL}$	NdeI_F	5′ GTCATCCATATGAATAGGCACCTCTGGAAGAGC 3′
$NEMO^{250-365}$	NdeI_F	5′ GTCATCCATATGGTGGGCAGTGAGCGGAAG 3′
$NEMO^{111-253}$	NdeI_F	5′ GTCATCCATATGAAGCTCGATCTGAAGAGGCAG 3′
$NEMO^{1-110}$	BamHI_R	5′ GTAATCGGATCCTTATCACTCCAGGCCGAGTCTCTCCACCAG 3′
$NEMO^{1-130}$	BamHI_R	5′ GCGCATGGGATCCTCATCTCTTCAGGTGCTCCAC 3′
$NEMO^{1-210}$	BamHI_R	5′ CGGGATCCCTACTCCACGCTCTGGCCCTG 3′
$NEMO^{1-250}$	BamHI_R	5′ GTAATCGGATCCTTATCACTCACTGCCCACCACG 3′
$NEMO^{1-280}$	BamHI_R	5′ CAATACGGATCCTTATCAATCGATCACCTCCTGTTTGG 3′
$NEMO^{1-365}$	BamHI_R	5′ CAATACGGATCCTTATCACTGGGAGACCTCGAC 3′
$NEMO^{FL}$	BamHI_R	5′ GTAATCGGATCCTTATCACTCAATGCACTCCATG 3′

Table 2. Oligonucleotides used to disease causing single point mutants of NEMO

NEMO mutant		primer sequence
NEMO ^{D113N}	F	5′ GGAGAAGCTCAATCTGAAGAGGCAG 3′
NEMO ^{D113N}	R	5′ AGGCCGAGTCTCTCCACC 3′
NEMO^{R123W}	F	5′ GCAGGCTCTGTGGGAGGTGGAGC 3′
NEMO^{R123W}	R	5′ TCCTTCTGCCTCTTCAGATCGAGCTTC 3′
NEMO ^{V146G}	F	5′ GAAAGCCCAGGGGACGTCCTTGC 3′
NEMO^{V146G}	R	5′ ACAGAGGCCTTGTCCTCAGC 3′
NEMO ^{L153R}	F	5′ GCTCGGGGAGCGGCAGGAGAGCC 3′
NEMO ^{L153R}	R	5′ AAGGACGTCACCTGGGCTTTCACAG 3′
NEMO^{Q157P}	F	5′ GCAGGAGAGCCCGAGTCGCTTGG 3′
NEMO ^{Q157P}	R	5′ AGCTCCCCGAGCAAGGAC 3′
NEMO ^{A162P}	F	5′ TCGCTTGGAGCCTGCCACTAAGG 3′
NEMO ^{A162P}	R	5′ CTCTGGCTCTCCTGCAGC 3′
NEMO ^{R173G}	F	5′ TCTGGAGGGTCAAGCCCGGGCGG 3′
NEMO ^{R173G}	R	5′ GCCTGGCATTCCTTAGTGG 3′
NEMO ^{R173Q}	F	5′ TCTGGAGGGTCAGGCCCGGGCGG 3′
NEMO ^{R173Q}	R	5′ GCCTGGCATTCCTTAGTGGCAGCC 3′
NEMO ^{R175P}	F	5′ GGGTCGGGCCCCGGCGGCCAGCG 3′
NEMO ^{R175P}	R	5′ TCCAGAGCCTGGCATTCCTTAGTGGCAGC 3′
NEMO ^{L227P}	F	5′ GAAGAGGAAGCCAGCCCAGTTGCAGGTGGC 3′
NEMO ^{L227P}	R	5′ TCCTCCGAGGCGGCCTGG 3′

2.3.2 Protein expression and purification

All His-tagged NEMO proteins were expressed in BL21 (DE3) cells. 1 L cultures in LB media with 100 ug/mL ampicillin were grown at 37°C to OD600 of 0.2 before induction with 0.2 mM isopropyl β-D-1-thiogalactopyranoside (IPTG) (Biobharati) and stirring at 150 rpm for 22°C for 16 hours. Cells were harvested by centrifugation at 3,000 x *g* for 10 minutes (Beckman Coulter) and cell pellets were lysed by sonication (VWR Scientific) on ice in 200 mL of lysis buffer (20 mM Tris-HCl pH 8.0, 300 mM NaCl, 10% w/v glycerol, 10 mM imidazole, 0.2% TritonX, 1 mM PMSF, and 5 mM β-mercaptoethanol). Lysates were clarified by centrifugation at 15,000 rpm for 45 minutes. Supernatants containing soluble proteins were then applied to a 1 mL Ni NTA-Agarose (Biobharati) column that was preequilibrated with lysis buffer. Bound proteins were washed with 25 mL wash buffer (lysis buffer with 30 mM imidazole) and eluted in 10 mL elution buffer (lysis buffer containing 250 mM imidazole).

Sf9 insect cells from 1 L suspension cultures were harvested by centrifugation at 3,000 x *g* for 10 minutes at 4°C and lysed by sonication in 100 mL of lysis buffer (25 mM Tris-HCl, pH 8.0, 200 mM NaCl, 10 mM imidazole, 10% w/v glycerol, 5 mM β-mercaptoethanol). The lysate was clarified by centrifugation at 18,000 rpm for 45 minutes at 4°C. Pre-equilibrated Ni NTA-Agarose resin was added at a ratio of 1 mL of resin slurry/liter of lysed cell culture and the mixture was incubated on a rotator at 4°C for 3 hours. The Ni beads were pelleted at 1,000 rpm for 2 minutes in a swinging bucket centrifuge rotor. Supernatant was carefully decanted and the protein-bound resin was resuspended with wash buffer (lysis buffer containing 30 mM imidazole) and incubated at 4°C on a rotator for 2 minutes. The Ni beads were pelleted again and decanted (wash

1). This was repeated until the last wash fraction contained 0.01-0.1mg/mL of protein (Bio-Rad Protein Assay). Elution buffer (lysis buffer containing 250 mM imidazole) was added, and eluted fractions were collected and stored in -80°C.

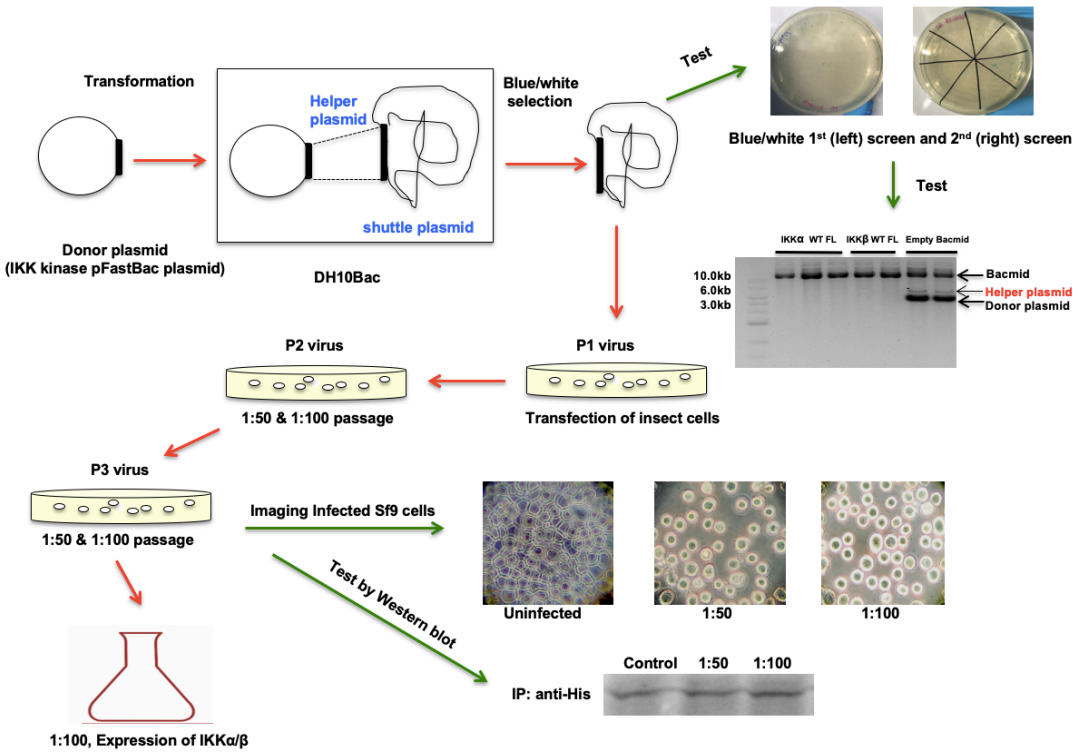

Figure 5. Recombinant baculovirus expression system in infected sf9 cells.
This is workflow for IKK1/α or IKK2/β baculovirus expression process. An expression vector pFast Bac with gene of interest is translocated into a baculovirus shuttle vector (bacmid) by helper plasmid. Translocation of IKK gene is checked by blue/white screen depending on whether containing beta galactosidase and agarose gel electrophoresis. Bacmid with gene is transfected in insect cells then undergoes amplification for producing P1, P2, and P3 viruses. Virus infection is verified by western blot and then proceeded to large scale cell culture and purified by Ni affinity chromatography.

2.3.3 Size-exclusion chromatography

To investigate the degree of self-association, all purified individual NEMO and IKK2/β proteins as well as NEMO:IKK2 complexes were subjected to gel filtration with a Superose6 Increase10/300 GL size-exclusion column (GE Healthcare) on an NGC™ Liquid Chromatography System (Bio-Rad). The column was equilibrated in a buffer with 25 mM Tris-HCl, pH 8.0, 250 mM NaCl, 2 mM DTT, and 5% glycerol at a flow rate of 0.2 mL/min at 22°C. Molecular weight standards used are as follows: thyroglobulin, 670 kDa; gamma-globulin, 158 kDa; ovalbumin, 44 kDa; myoglobin, 17 kDa; vitamin B12, 1.4 kDa (Bio-Rad). The calibration standard data fit to the function:

$$\text{Apparent Molecular Weight}(V_E) = 0.0101V_E^2 + 00307V_E + 3.6298$$

where V_E is the measured elution volume of the protein. Peak fractions were analyzed by SDS-PAGE.

2.3.4 Size-exclusion chromatography-multi-angle light scattering analysis

Size-exclusion chromatography coupled multi-angle light scattering (SEC-MALS) was performed on an Agilent Technologies 1200 Series HPLC chromatography system equipped with a miniDAWN TREOS MALS detector and an Optilab TrEX differential refractive index detectors (Wyatt Technology). The SEC-MALS system was calibrated with bovine serum album. An aliquot of 100 µl each sample was centrifuge-filtered prior to being loaded onto a Superose6 increase10/300 GL size-exclusion column (GE Life Science) and eluted in a buffer containing 25 mM Tris-HCl, pH 8.0, 250 mM NaCl, 2 mM DTT, and 5% glycerol at a flow rate of 0.4 mL/min at 22°C. Absorbance was measured at 280 nm, and the MW was determined from the Raleigh ratio calculated by measuring

the static light scattering and corresponding protein concentration of a selected peak using ASTRA VI software (Wyatt Technology).

2.3.5 Analytical ultracentrifugation analysis

Sedimentation velocity experiments were performed in a ProteomeLab XL-I (Beckman Coulter) analytical ultracentrifuge. NEMO and NEMO:IKK2 complex were purified and prepared as previously described. Protein samples at a concentration of 0.4 mg/mL in SEC buffer containing 1 mM TCEP were loaded in two-channel cells and spun in an An-50 Ti 8-place rotor at 30,000 rpm at 21°C for 16 hr. Absorbance at 280 nm was used for detection. Sedimentation velocity data were analyzed using Sedfit software [88].

2.3.6 Thermal stability analysis

Thermal melting experiments of NEMO and truncated mutants ($NEMO^{1-110}$, $NEMO^{1-130}$, $NEMO^{1-210}$, $NEMO^{1-250}$, $NEMO^{1-365}$, $NEMO^{250-365}$, $NEMO^{250-419}$ and single point mutants $NEMO^{D113N}$, $NEMO^{V146G}$, $NEMO^{L153R}$, $NEMO^{Q157P}$, $NEMO^{A162P}$, $NEMO^{R173G}$, $NEMO^{R173Q}$, $NEMO^{R175P}$, and $NEMO^{L227P}$ were performed using a Tycho NT.6 instrument (NanoTemper Technologies). In brief, the samples were loaded as duplicates and heated in a glass capillary. While heating, the thermal unfolding profiles by internal fluorescence at 330 nm and 350 nm were recorded. Data analysis, data smoothing, and calculation of derivatives were done using the internal evaluation features of the NT.6 instrument.

2.3.7 CD spectroscopy

Coiled-coil character and construct stability were assessed by circular dichroism (CD) spectroscopy. CD data were collected on an Aviv 420 instrument using a 2 mm path-length cuvette. NEMO samples were analyzed at 4.6 μM in buffer containing 20 mM potassium phosphate pH 7.8 and 150 mM NaF. CD spectra measurements were

performed from 190 to 280 nm at 20°C and the mean residue ellipticity was calculated from the raw signal. The degree of alpha-helical content was detected from the ratio of ellipticity at 222 nm to 208 nm. Thermal melting curves were obtained through variable temperature scans at fixed wavelength (222 nm) from 10°C to 85°C at a 2°C/minute ramp rate. The melting temperature (T_m) for each protein was estimated from the maximum of a plot of the first derivative of ellipticity against temperature. Helical content was estimated from the CD spectra using a method "beta-structure" through the BeStSel server [96].

2.4 RESULTS

2.4.1 NEMO exhibits complicated solution behavior

Previous attempts at determining the three-dimensional structure of full-length or nearly full-length human NEMO proteins have thus far not met with success. Therefore, in support of my efforts to characterize the size and oligomerization state of NEMO in solution, I generated a simplistic model of NEMO combining existing structural knowledge of its parts and secondary structure prediction algorithms [87]. My model contains an undefined N-terminal region composed of amino acids 1-48 and an enigmatic intervening domain (IVD) between residues 110-194, that is predicted to be entirely alpha-helical, in addition to regions defined structurally in previous studies (Figure 6).

I engineered DNA expression plasmids encoding full-length and fragments of NEMO and expressed each of them separately in *E. coli* as N-terminal poly-histidine fusion proteins. Some of the NEMO fragments were designed to begin and/or end within suspected CC domains. These include the $NEMO^{1-130}$, $NEMO^{1-210}$, and $NEMO^{1-280}$

protein fragments, where superscript numbering reflects amino acids of human NEMO. $NEMO^{1-365}$ is a curious case since the structure of the segment bracketed by the CC2 domain (ends at residue 337 in crystal structures) and Pro-rich region (begins at residue 375) is not known, but the Jpred 3 secondary structure prediction algorithm describes the whole of 259-360 as alpha-helical. The resulting recombinant proteins were purified to near homogeneity by nickel affinity and size-exclusion chromatography (SEC) (Figure 6C). When the apparent molecular weight of each recombinant NEMO protein was determined by analytical scale SEC using as calibration a standard set of globular enzymes, all were observed to elute as particles many times larger than that of any individual NEMO protein (Figure 6D; Figure 7; Table 3). This behavior is reflected in the endogenous multisubunit IKK complex that also exhibits high molecular weight by SEC [58, 60]. As SEC provides a measure of hydrodynamicity of a particle, and not a true measure of protein molecular weight, it is not clear from these analyses whether NEMO runs as a large oligomer, as an extremely elongated molecule, or some combination.

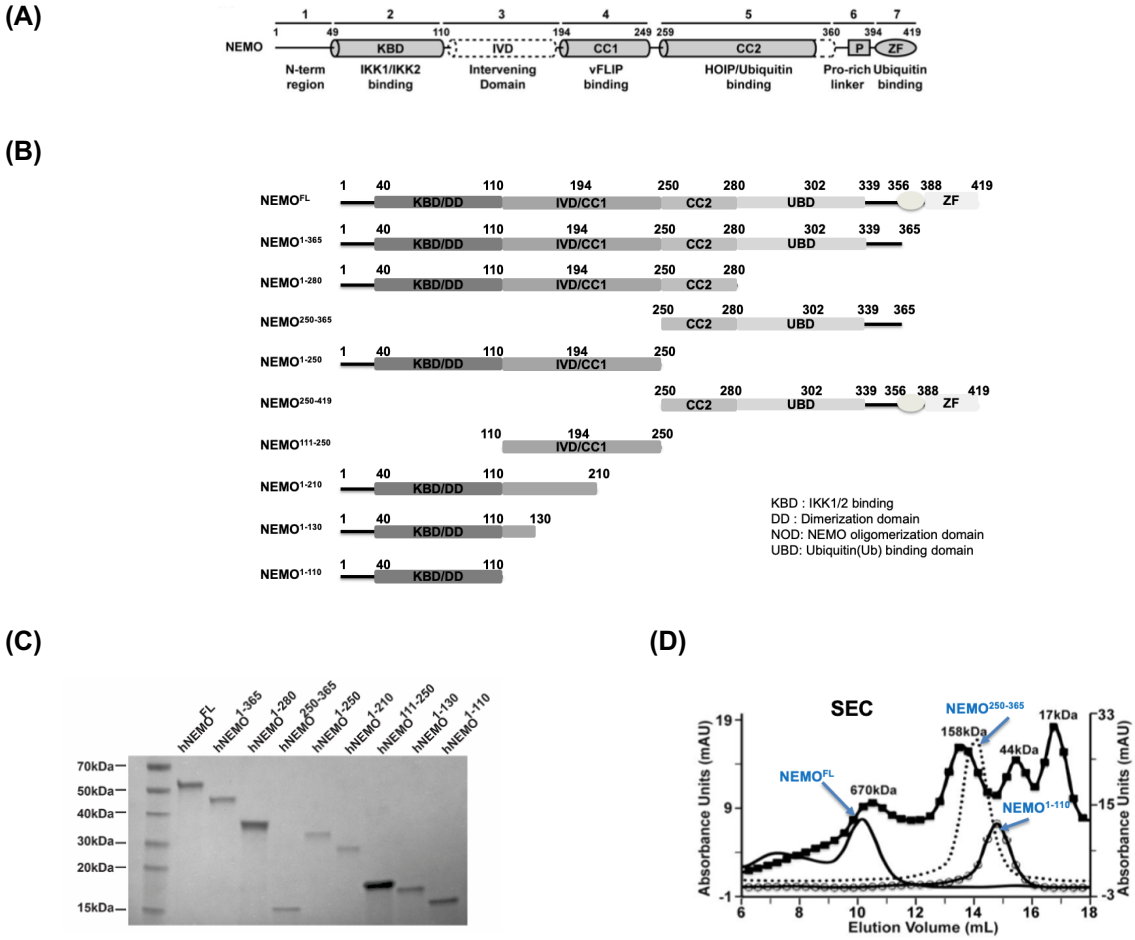

Figure 6. Recombinant full-length human NEMO protein and deletion constructs.
A) and B)Two-dimensional structural diagram of human NEMO protein. Portions of known structure are shaded grey and known or suspected helical regions are depicted as cylinders. The linear structure is divided into seven segments (numbered above): 1-An amino-terminal segment; 2-the kinase binding domain (KBD) that interacts through noncovalent association with the C-terminal NEMO-binding domain (NBD) of either IKK1 or IKK2; 3) an enigmatic intervening domain (IVD) that is predicted to be helical (dashed cylinder); 4) the first of two colied coil regions (CC1) that has been shown to interact with viral protein vFLIP; 5) a second coiled-coil (CC2) that associates with the HOIP protein of the LUBAC complex and linear ubiquitin; 6) a linker that ends in a Pro- rich sequence; 7) a zinc finger motif that has been shown to interact with ubiquitin. Approximate amino acid numbering (1-419) is given at each segment border. B) Coomassie-stained SDS-PAGE analysis of recombinant full-length (lane 2) and deletion mutant human NEMO proteins (lanes 3-10). C) Analytical SEC chromatograms of full-length NEMO (solid line) and NEMO deletion constructs $NEMO^{250-365}$ (dotted line) and $NEMO^{1-110}$ (solid line with hollow circles) overlaid on calibration standard (solid line with filled squares) with known MW of standard proteins labeled in kilodaltons (kDa).

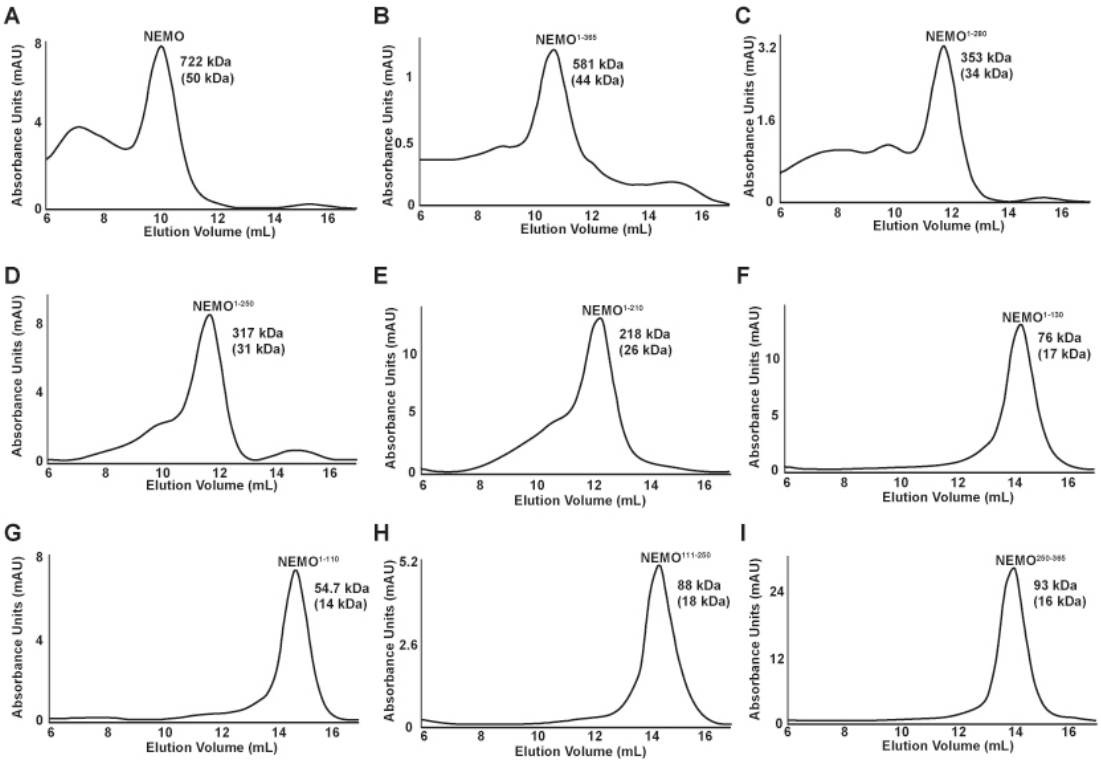

Figure 7. Analytical-scale size exclusion chromatography (SEC) chromatograms of NEMO full length and deletion proteins.

A) Full length NEMO. The peak elution volume corresponds to 722 kDa, when determined from a calibration curve generated by a set of standard, globular proteins (see Materials & Methods for details). Each His-tagged full length NEMO protein is 50 kDa (the molecular weight of individual proteins is given in parentheses). Similar data are presented for: B) $NEMO^{1-365}$, C) $NEMO^{1-280}$, D) $NEMO^{1-250}$, E) $NEMO^{1-210}$, F) $NEMO^{1-130}$, G) $NEMO^{1-110}$, H) $NEMO^{111-250}$, and I) $NEMO^{250-365}$.

Table 3. Apparent molecular weight of human NEMO and NEMO deletion proteins by size exclusion chromatography

Protein	MW of monomer (kDa)	Elution vol. (mL)	Apparent MW (kDa)
NEMO	50.2	10.39	721.9
$NEMO^{1-365}$	44.4	10.90	481.4
$NEMO^{1-280}$	34.6	11.98	353.2
$NEMO^{1-250}$	31.2	12.15	325.0
$NEMO^{1-210}$	26.3	12.93	217.9
$NEMO^{1-130}$	17.4	15.01	65.3
$NEMO^{1-110}$	14.9	15.54	46.5
$NEMO^{111-250}$	18.5	14.78	75.4
$NEMO^{250-365}$	13.8	14.68	80.2

2.4.2 Full-length human NEMO is a dimer in solution

In order to determine the shape-independent molecular weight of NEMO in solution, I employed size-exclusion chromatography coupled with multi-angle light scattering (SEC-MALS). Experiments performed at 60 μM protein concentration revealed an average molecular weight of 95.0 kDa, a value that was in close agreement with the calculated mass of 96.4 kDa for a NEMO homodimer (Figure 8A). This value varies significantly from the observed molecular weight of >700 kDa estimated from the elution volume of NEMO by SEC alone. This discordance suggests that the shape of the NEMO dimer in solution is extremely elongated rendering it to appear as a globular hydrodynamic particle of significantly larger mass.

In order to obtain an independent measure of its oligomerization state in solution, I next performed sedimentation velocity analytical ultracentrifugation (AUC) experiments on NEMO under conditions of protein concentration and buffer solution that were identical to that used in the SEC-MALS experiments. Data were analyzed by Sedfit [88]. The C(S) distribution of different NEMO species in solution was dominated by one peak (nearly 80% of total protein) with apparent molecular weight (MW) of 96 kDa, which is once again suggestive of a NEMO homodimer (Figure 8B). A major axis ratio of 31.4 for this particle indicates that the NEMO dimer is a highly elongated particle in solution. I also observed two minor species (roughly 10% each) with apparent MW of 217 kDa and 477 kDa, that are consistent with NEMO tetramers and octamers, respectively, though it is also possible that these larger species represent the beginning of nonspecific aggregation. Taken together, these SEC-MALS and AUC data strongly indicate that NEMO exists predominantly as an abnormally elongated homodimer in solution.

A

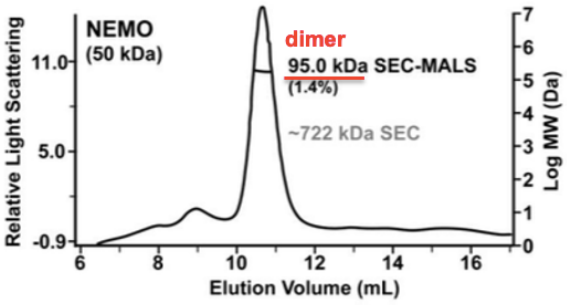

B

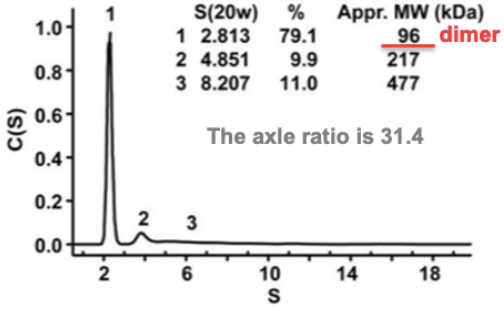

Figure 8. Shape-independent size determination of full length human NEMO in solution. A) Size exclusion chromatography with multi-angle light scattering (SEC-MALS) analysis. Determined molecular weight is given in kilodaltons (kDa) with percent error in measurement. Calculated molecular weight of the His-tagged monomer is given in parentheses in this and all other figures reporting SEC-MALS data. B) Analytical ultracentrifugation (AUC) sedimentation velocity measurement data for full length NEMO. Peaks are assigned to a percentage value (fraction of total protein detected) and approximate molecular weight.

2.4.3 NEMO dimerization stability is affected by deletion of structured elements

I next analyzed several NEMO deletion mutant proteins by SEC-MALS to determine their respective sizes in solution. These experiments were repeated multiple times and with different protein preparations. $NEMO^{1-110}$, $NEMO^{1-250}$, $NEMO^{250-365}$, and $NEMO^{111-250}$ yielded particles of 30, 69, 30, and 35 kDa, respectively (Figure 9A-D). Each of these measurements agrees well with mass of dimeric forms (28, 62, 32, and 36 kDa, respectively). Interestingly, $NEMO^{1-365}$ appeared as a trimer and $NEMO^{1-130}$ exhibited significant amounts of high MW species in addition to a clear dimeric species (Figure 9E,F). These results suggest that disruption of NEMO by deletion of parts from either end can drastically influence its propensity to associate into higher order oligomers. This idea was corroborated by two additional protein fragments, $NEMO^{1-210}$ and $NEMO^{1-280}$, which behave in solution as 377 and 140 kDa particles, respectively (Figure 10). Thus, it appears that disruption of NEMO within a particular structured element, rather than at borders of an element, hinders self-dimerization and leads to its stabilization through alternative modes of oligomerization. These observations point to a complex mode for NEMO dimerization in which multiple elements can interact but do so in a manner that is influenced strongly by their flanking regions.

To test the folding stability of NEMO and NEMO deletion mutant proteins, I performed nano differential scanning fluorimetry (nanoDSF) measurements. Under this approach kinetics of temperature-dependent protein unfolding can be rapidly monitored in solution by measuring fluorescence intensity simultaneously at two different wavelengths, 330 and 350 nm. Changes in fluorescence intensity and shift of the fluorescence maximum indicate protein unfolding at the apparent melting temperature

(T_m). By this method I found $NEMO^{250-365}$ to be the most stable of all NEMO proteins tested (Figure 9G). This construct corresponds generally to CC2 (Figure 6A). Increased thermal stability of this fragment relative to full-length NEMO suggests that either one or both flanking regions destabilize self-dimerization of CC2. $NEMO^{1-365}$, in particular, appears less stable than $NEMO^{250-365}$ suggesting that the IVD negatively affects the dimerization stability of CC2. I failed to detect a major folding transition for $NEMO^{1-210}$, $NEMO^{1-130}$, and $NEMO^{1-110}$ by nanoDSF suggesting these are kinetically unstable segments.

In order to experimentally investigate the nature of the NEMO IVD, secondary structure of the $NEMO^{1-210}$ protein was analyzed in solution under equilibrium conditions by circular dichroism (CD) spectroscopy. This fragment was found to be even more alpha-helical and slightly more thermally stable than the full-length NEMO (Figure 9H,I). The combined thermal stability data reveal several key properties regarding NEMO in solution. First, the NEMO IVD indeed appears to exhibit alpha-helical secondary structure as predicted, though it is kinetically unstable. Second, this portion promotes self-dimerization of NEMO while also serving to weaken the stability of dimerization through CC2. Finally, full-length NEMO exhibits relatively low native thermal stability in solution with T_m ~47°C. Therefore, it is possible that rapid association and dissociation of NEMO coiled coils could serve in part to explain the observed complex behavior of NEMO in solution.

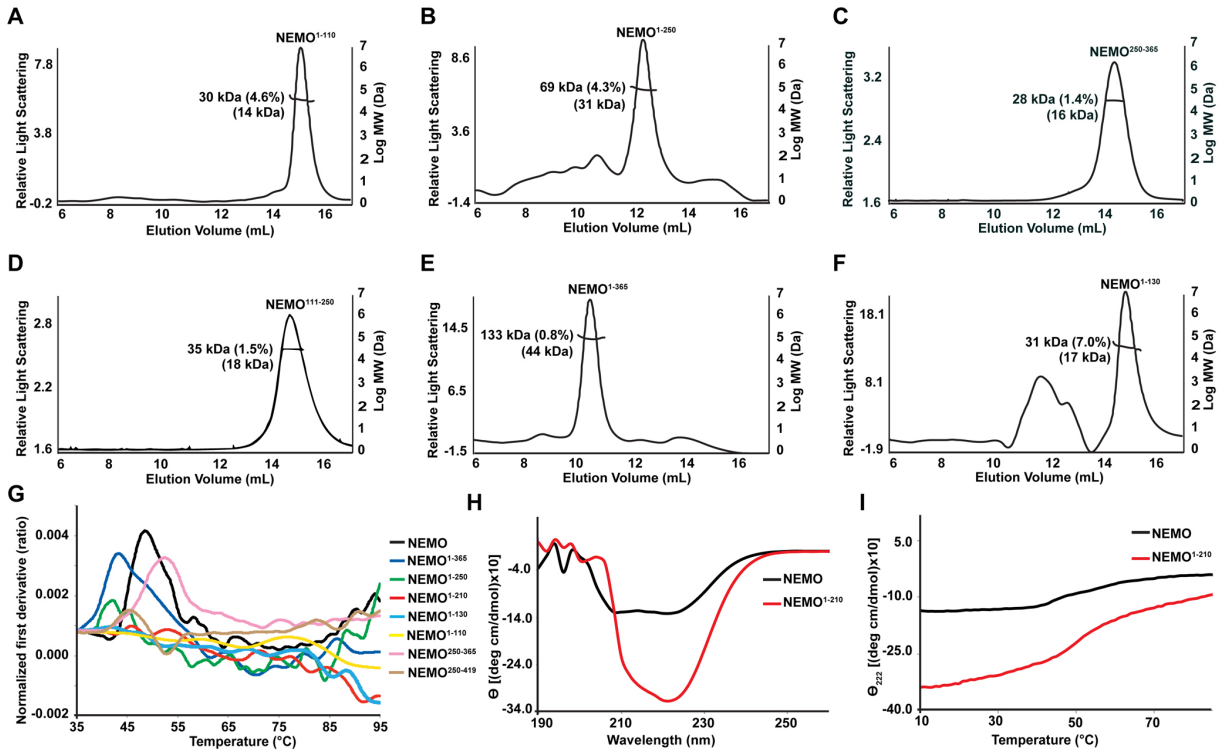

Figure 9. Analysis of NEMO deletion mutants in solution.
A) SEC-MALS analysis of NEMO$^{1-110}$, B) NEMO$^{1-250}$, C) NEMO$^{1-130}$, D) NEMO$^{1-110}$, E) NEMO$^{111-250}$, and F) NEMO$^{250-365}$. G) NanoDSF analysis of deletion mutant NEMO proteins. Each colored line represents measurement of the NEMO protein construct indicated. H) Circular dichroism (CD) spectroscopy of full-length NEMO (black line) and NEMO$^{1-210}$ (red line). I) Temperature-dependent CD signal at 222 nm of full-length NEMO (black) and NEMO$^{1-210}$ (red).

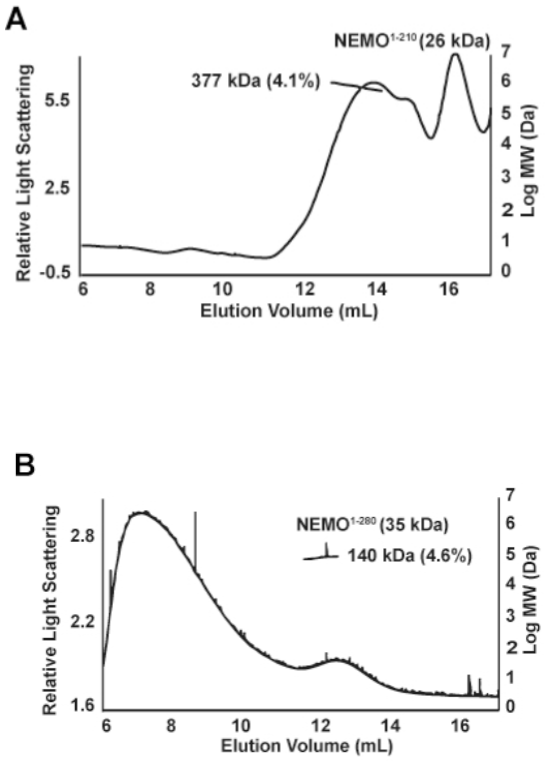

Figure 10. SEC-MALS analysis of A) NEMO1-210 and B) NEMO 1-280.

2.4.4 Disease-linked NEMO point mutations affect its solution behavior

Consistent with a complicated functional mechanism for NEMO, the severity of symptoms in patients with EDA-ID and IP is highly variable and dependent upon which specific mutations are present in NEMO. Using the same approach as I employed for generating recombinant full-length and deletion NEMO proteins, I prepared ten NEMO single amino acid mutant proteins: D113N (IP), R123W (IP), V146G (IP), L153R (EDA-ID), Q157P (EDA-ID), A162P (EDA-ID), R173G (EDA-ID), R173Q (EDA-ID), R175P (EDA-ID), and L227P (EDA-ID). Nine of these map to the IVD and the abbreviation for the disease associated with each of these mutations is given in parentheses after the mutation. Analysis via SEC-MALS (Table 2) revealed that the D113N and L153R mutants are dimers at 60 μM concentration similar to NEMO of native sequence (Figure 11A,B). Oddly, the R123W mutant was observed at 130 kDa, which is smaller than a trimer but larger than a dimer (Figure 11C). Each of the proline mutants, Q157P, A162P, R175P, and L227P, exhibited varying degrees of higher order oligomerization relative to the wild-type NEMO (Figure 11D-G).

I then tested the folding stability of the disease-linked mutant NEMO proteins by nanoDFS and found that the mutants can be classified into two groups based on their thermal stability. The D113N, V146G, L153R, and R173Q mutants each exhibit major unfolding transitions at temperatures similar to the wild-type NEMO, whereas Q157P, A162P, R173G, and R175P exhibit numerous small transitions across a broad range of temperatures (Figure 11H). Interestingly, L227P demonstrated no unfolding transition whatsoever across the entire temperature range tested suggesting it is highly kinetically unstable. I measured the secondary structure of the L227P mutant in solution by CD

spectroscopy and found that it displays alpha-helical structure to a similar degree as wild-type NEMO (Figure 11I). I note that the disease-linked mutant NEMO proteins display elevated MW in solution by SEC-MALS also fail to undergo the thermally induced ~47°C structural transition characteristic of wild-type NEMO. It is possible that the inability of these mutants to readily dissociate from one another in solution is linked to their association with diseases such as IP and EDA-ID.

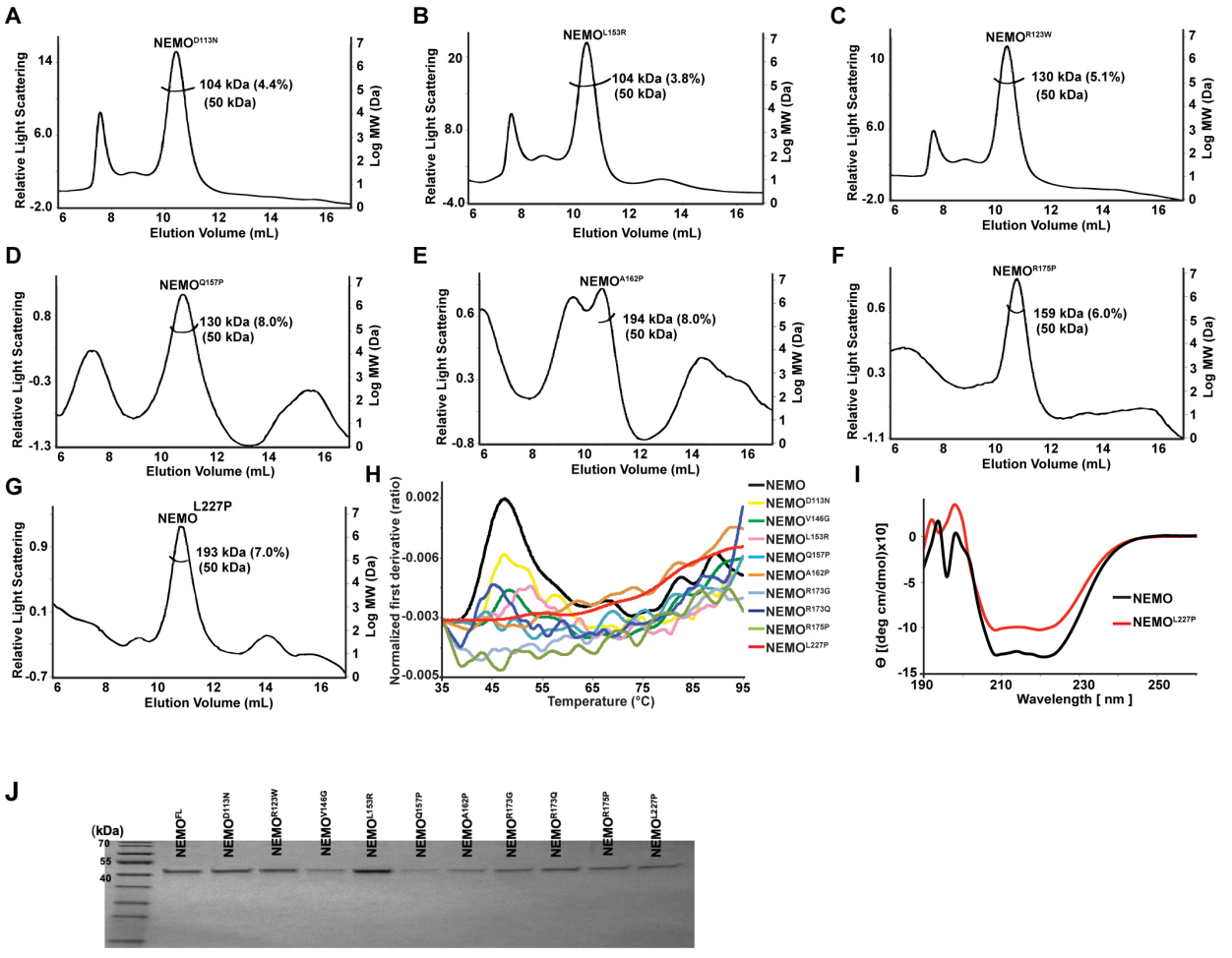

Figure 11. Analysis of disease-linked NEMO point mutants in solution.
A) SEC-MALS analyis of NEMO^{D113N}, B) NEMO^{L153R}, C) NEMO^{R123W}, D) NEMO^{Q157P}, E) NEMO^{A162P}, F) NEMO^{R175P}, and G) NEMO$^{250\text{-}365}$. H) NanoDFS analysis of disease-linked mutant NEMO proteins. Each colored line represents measurement of the NEMO mutant protein indicated. I) Circular dichroism (CD) spectroscopy of full length wild type NEMO (black line) and NEMO^{L227P} (red line). J) Coomassie-stained SDS-page gel analysis from SEC fractions for individual NEMO single point mutant.

Table 4. Molecular weight of full length human NEMO proteins measured in solution by SEC-MALS

single point mutant	concentration	MW by SEC-MALS (kDa)
hNEMO^{D113N}	60 μM	104.4 (4.4%)
hNEMO^{R123W}	60 μM	129.7 (5.1%)
hNEMO^{L153R}	60 μM	104.0 (3.8%)
hNEMO^{Q157P}	60 μM	no specific peaks
	6 μM	130.4 (8.0%)
hNEMO^{A162P}	60 μM	336.1 (4.0%)
	6 μM	194.0 (8.0%)
hNEMO^{R175P}	60 μM	159.2 (2.8%)
	6 μM	158.9 (6.0%)
hNEMO^{L227P}	60 μM	1792.1 (0.7%)
	6 μM	193.0 (7.0%)
	3 μM	103.6 (9.2%)

2.4.5 Binding to NEMO and its effect on the propensity of IKK2 to oligomerize

In order to observe the solution behavior of NEMO within the context of a multisubunit IKK complex, I combined our NEMO proteins with purified full-length IKK2 subunit proteins generated by recombinant baculovirus infection of Sf9 insect cell suspension cultures [89]. As described previously, NEMO and IKK2 are known to associate through noncovalent interaction between the KBD in NEMO (residues 49-109 in human NEMO) and the NEMO binding domain (NBD) of IKK2 (human IKK2 residues 705-743) (Figures 6A and 12A,B). Prior to formation of NEMO:IKK2 complexes, I analyzed IKK2 subunit oligomerization in solution via SEC-MALS and sedimentation equilibrium AUC (Figure 12C,D). Both approaches identified major peaks that correspond to homodimers, which agrees with previously reported X-ray crystal structures of nearly full-length IKK2 proteins [59-61]. I note that AUC also detects measurable amounts of higher order oligomers at multiples of the homodimer molecular weight. Transient higher order oligomerization is a signature of IKK2 homodimers in solution [60].

As mentioned previously, multisubunit IKK complexes purified directly from activated HeLa cells behave as 700-900 kDa particles in solution when analyzed by SEC. In light of the observation that NEMO behaves as an aberrantly large particle by SEC, I employed SEC-MALS to determine the shape-independent molecular weight of our NEMO:IKK2 complex preparations (Figure 12E). This revealed an apparent molecular weight of 303 kDa, which is only slightly larger than what one would expect for a $NEMO_2$:$IKK2_2$ heterotetrameric complex (calculated MW = 280 kDa). I next analyzed the complex by AUC sedimentation velocity and observed the major peak at 262 kDa, which I interpret as corresponding to the $NEMO_2$:$IKK2_2$ heterotetramer (Figure 12F).

Interestingly, I also observe clear signals that correspond to molecular weights for $NEMO_4$:$IKK2_4$ (heterooctamer), $NEMO_6$:$IKK2_6$ (heterododecamer), and so forth. IKK2 homodimers display a similar propensity to assemble into higher order oligomers in solution [60]. However, the addition of NEMO to IKK2 appears to strengthen its self-association into higher order oligomeric assemblies.

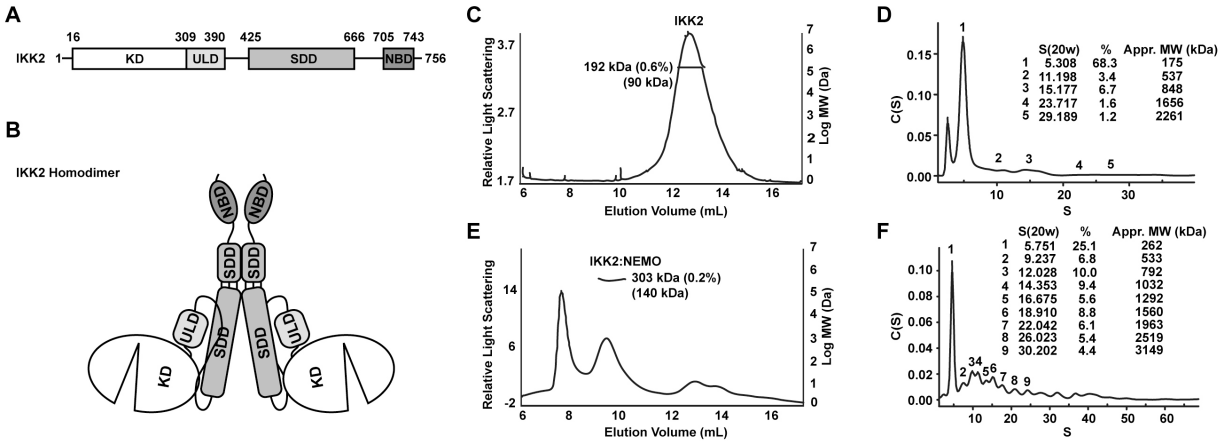

Figure 12. Solution analysis of recombinant full length IKK2 protein and NEMO:IKK2 complex.

A) Domain organization of the IKK2/β subunit with kinase domain (KD), ubiquitin-like domain (ULD), and scaffold-dimerization domain (SDD) labeled and human amino acid numbering indicated. B) Schematic representation of the IKK2/β homodimer depicting the relative arrangement of domains and homodimerization through the portion of the SDD distal to the KD and ULD. C) SEC-MALS chromatogram of full length human IKK2/β protein. D) AUC sedimentation velocity measurement of full length human IKK2/β in solution. E) SEC-MALS chromatogram of recombinant IKK2:NEMO complex. F) AUC sedimentation velocity measurement of the IKK2:NEMO complex.

2.4.6 Effects of NEMO truncation or mutation on multisubunit IKK complex formation

I next tested whether NEMO deletion mutants assemble with IKK2/β. For this study, I were limited to only those mutants that retained the N-terminal KBD, which is known to mediate a strong association with the C-terminal NBD of IKK2/β. I mixed purified recombinant IKK2/β in excess with various NEMO deletion mutant proteins and then analyzed the resultant complexes by SEC-MALS. Most of the mixtures yielded peaks that correspond to $IKK2_2$:$NEMO_2$ heterotetrameric complexes (Figure 13A-E). Other than nonspecific extremely large aggregates that accompanied all NEMO protein preparations, only $NEMO^{1-365}$ of the deletion mutant proteins tested assembled into complexes with IKK2 that were significantly larger than the heterotetramer. This reinforces what I observed when studying the $NEMO^{1-365}$ protein alone that deletion within the Pro-rich linker leaves NEMO prone to self-association, perhaps by leaving CC2 uncapped and capable of interaction with additional NEMO protein monomers. Finally, these observations suggest that NEMO could serve to modulate the natural propensity of IKK2 dimers to form higher order oligomers in solution and therefore control activation of multisubunit IKK complexes.

Finally, I tested whether the EDA-ID disease-associated L227P NEMO mutant protein would also associate with IKK2/β similar to the truncated NEMO mutants. I combined $NEMO^{L227P}$ with IKK2/β and analyzed the resultant mixture by SEC-MALS (Figure 13F). Only a relatively small amount of the mutant protein appeared to associate with IKK2 in a manner that could be analyzed and the size of the resultant complex was nearly twenty times the calculated combined molecular weights of NEMO and IKK_S

suggesting that mutation to proline of NEMO at residue 227 strongly induces even higher order oligomerization of resultant NEMO:IKK2 complexes. It is possible that the activation of IKK2/β protein kinase activity that results from such oligomerization is one basis for the disease pathology associated with this mutation in NEMO.

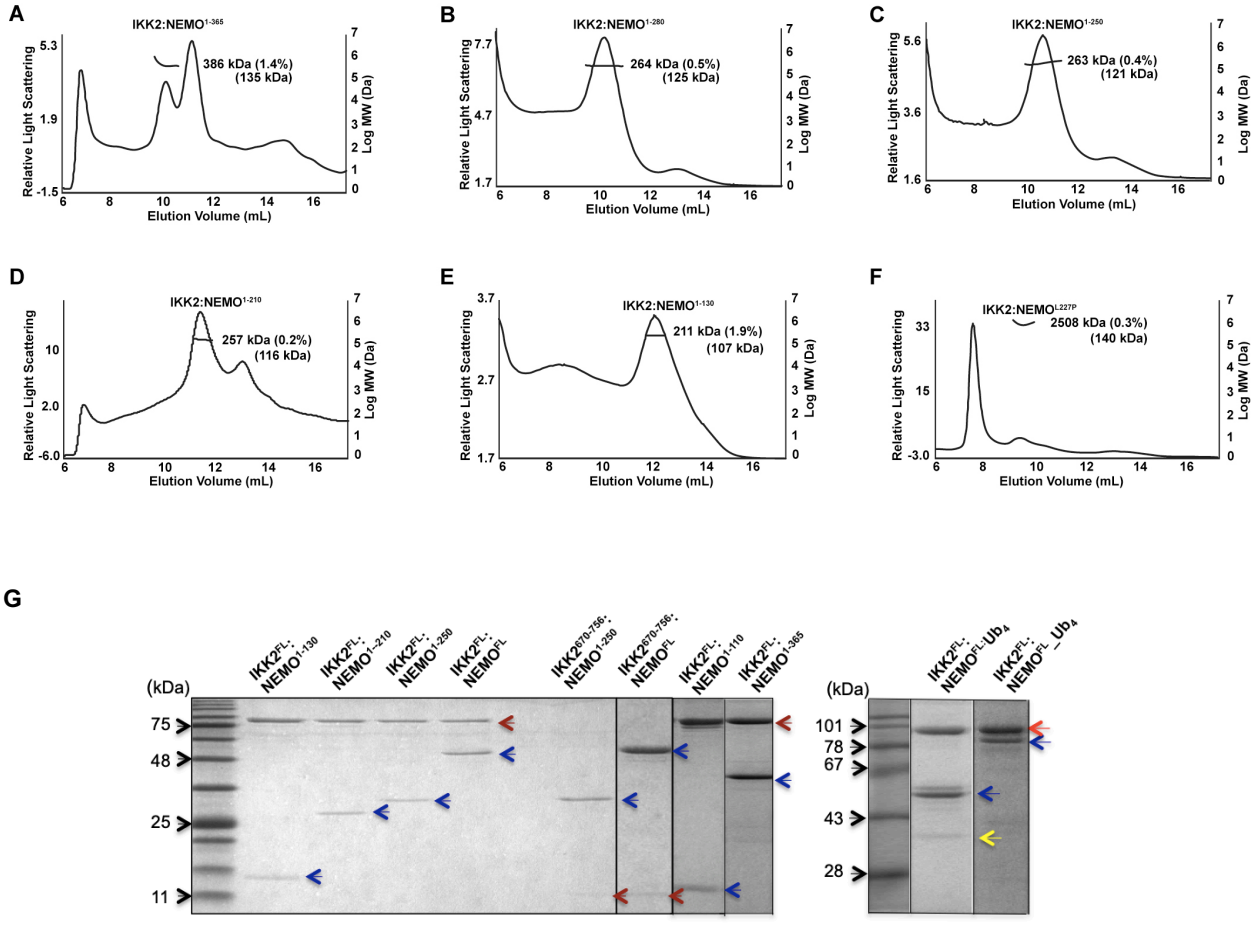

Figure 13. Solution analysis IKK2 in complex with mutant NEMO proteins.
SEC-MALS chromatograms of full length human IKK2/β protein in complex with A) $NEMO^{1-365}$, B) $NEMO^{1-280}$, C) $NEMO^{1-250}$, D) $NEMO^{1-210}$, E) $NEMO^{1-130}$, and F) $NEMO^{L227P}$. G) Coomassie stained SDS PAGE gel for various IKK2-NEMO complexes.

2.5 DISCUSSION

The IKK complex plays critical roles as an integrator of diverse cellular signaling inputs and as an inducer of select response gene expression via regulation of transcription factor NF-κB. However, despite many years of intensive investigation, the precise molecular mechanisms by which inactive IKK complexes switch to become catalytically active remain poorly understood. That the process culminates with phosphorylation at two serine residues within the activation segments of catalytic IKK subunits (serines 177 and 181 in human IKK2/β; 176 and 180 in human IKK1/α) is clear [63]. The nature and source of this catalytic subunit phosphorylation as well as the necessary role of the accessory NEMO protein subunit are, at best, only somewhat well understood.

One major impediment to the study of IKK activation has been a lack of high-resolution structural models of functional multisubunit complexes. Early characterization was limited to the observation that active IKK that was either purified as an endogenous complex from HeLa cells or reconstituted through co-expression of individual subunits in insect cells appeared as a high MW particle within the range of 700-900 kDa [56-58]. This high MW form of IKK was associated with its activated state until it was firmly established that both inactive and active forms of IKK appear as similarly large particles in size-exclusion chormatography and that IKK activation via activation segment phosphorylation was not associated with significant changes in size of the complex [60]. Detailed X-ray crystallographic analyses of nearly full-length IKK2/β proteins revealed that they form well-folded homodimers with a propensity to self-associate as higher order oligomers [59-61]. Critical questions that remain concern the nature and structure of the multisubunit

IKK complex and the mechanism by which it is able to become activated in response to diverse cellular stress signals.

To address these questions and in the absence of any structure for full-length NEMO, I focused our attention on its stability in solution. In light of the relatively well-folded structures of the catalytic subunit dimers, I assumed NEMO to be responsible for the observed large particle size of IKK in solution. This is consistent with original observations that in cells devoid of NEMO, IKK catalytic subunits were purified as roughly 300 kDa complexes [91]. Three major parts of NEMO, the KBD, CC1, and CC2, that have been studied by X-ray crystallography all appear as imperfect homodimeric coiled coils [74-80]. In order to improve understanding of the structure of full-length NEMO and its influence on multisubunit IKK complex in solution, I have carried out biophysical characterization via SEC, SEC-MALS, AUC, nanoDFS, and CD spectroscopy on purified full-length NEMO and a series of NEMO deletion and disease-associated point mutant proteins as well as various NEMO:IKK2 complexes.

My SEC-MALS and AUC sedimentation velocity experiments firmly establish that NEMO preferentially forms homodimers of ~100 kDa in solution. When one considers that the same full-length NEMO homodimers elute from analytical SEC at the same volume as globular proteins of >700 kDa, it seems clear that NEMO dimers do not exhibit a compact fold. This conclusion is further corroborated by our sedimentation velocity analysis of NEMO in solution that fits the ratio of the major axes of NEMO at >30. SEC-MALS analysis of NEMO deletion mutants revealed that they also form homodimers in solution, with the important caveat that when deletions are within defined structural elements that flank CC1 and CC2, aberrantly large and/or mixtures of higher molecular

weight oligomers were detected. Taken together, these observations lead us to conclude that rather than assembling as one long homodimer through the additive influence of three separate coiled coil regions in a long array, the NEMO homodimer is held together through a mutually regulatory dynamic association/competition between individual elements. On the basis of our observations, I hypothesize that NEMO residues 110-250, comprising the IVD and CC1, plays a critical role in this process by modulating the association of the flanking coiled coil CC2 element (Figure 14). The manner by which the IVD-CC1 region might accomplish this is not clear. However, in light of structural prediction and CD data that strongly support alpha-helical secondary structure for this segment as well as the increased thermal stability I observe for deletion proteins that contain the central region, I propose that the IVD exerts control over NEMO dimerization through flanking coiled coil regions, perhaps by competitively adopting its own unique helical homodimeric structure. In support of such a model, I note that many point mutations within this region are associated with disease phenotypes and my analysis of several of these mutant NEMO proteins revealed that they exhibit drastically altered solution behavior.

Analysis of assembled NEMO:IKK2 complexes in solution both by SEC-MALS and AUC clearly reveals that although its predominant state is a $NEMO_2$:$IKK2_2$ tetramer, it can also form higher order $(NEMO_2:IKK_2)_n$ oligomers. It is interesting that C-terminal deletions to NEMO do not appear to influence the ability of the multisubunit IKK heterotetramer to assemble so long as the KBD is preserved in NEMO. This might suggest that association of dynamic NEMO to IKK2/β dimers serves to attenuate whatever influence the IVD exerts on NEMO structure and dynamics. Of even more interest, however, is that the

combination of NEMO with IKK2/β does not appear to alter the solution oligomerization states for either of the separate proteins—both NEMO and IKK2/β remain as homodimers In the absence of additional knowledge concerning the surfaces employed by IKK2/β and, to a lesser degree, NEMO homodimers to induce oligomerization of multisubunit IKK, it is challenging to predict how NEMO exerts control over higher order oligomerization of IKK (Figure 15). It remains to be determined what, if any, functional significance is owed to higher order oligomerization of $NEMO_2$:$IKK2_2$ tetramers in the cell.

The significance of the observed structural plasticity of NEMO is evident from the involvement of various mutant forms of the protein in disease. As mentioned previously, NEMO is frequently mutated in two human disorders: Anhidrotic Ectodermal Dysplasia with Immunodeficiency (EDA-ID) and Incontinentia Pigmenti (IP). Male EDA-ID patients with hemizygous NEMO mutations retain residual NF-κB activation (hypomorphic mutations), whereas in female patients the NEMO mutation is always heterozygous resulting either in maintainence of residual NF-κB activation (EDA-ID) or its near abolition (IP) [19, 91-92], or in some cases constitutive activation of IKK2/β [93]. This suggests that specific mutations impact the control of IKK over NF-κB from particular signaling inputs [94]. This further reinforces the idea that NEMO responds to different signals in distinct manners which can be accomplished by modulation over the structural plasticity of NEMO by its modular coiled coil regions, many of which are capable of dimerization and association with other factors. I note that similar conclusions were drawn from a recently published study by Shaffer, *et al*. [95]. Our observation that many disease-causing NEMO mutant proteins display altered oligomerization states in solution

reinforces the idea that NEMO exerts its control over IKK activation by integrating diverse cellular signals to regulate higher order oligomerization of IKK complexes.

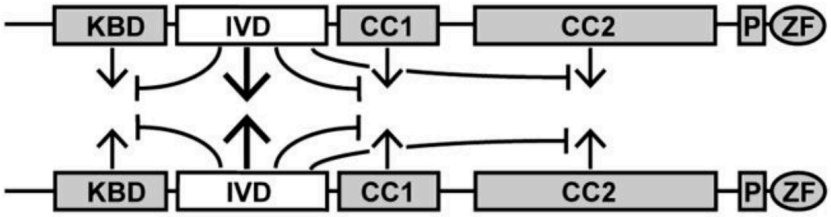

Figure 14. Schematic of the proposed role of NEMO IVD.
Schematic of the proposed role of NEMO IVD in influencing dimerization of flanking coiled coil regions of NEMO, which either on their own or through association with additional factors are capable of dimerization. Abbreviations for individual NEMO structural elements are the same as in Figure 1A and those elements of known structure are shaded grey.

A

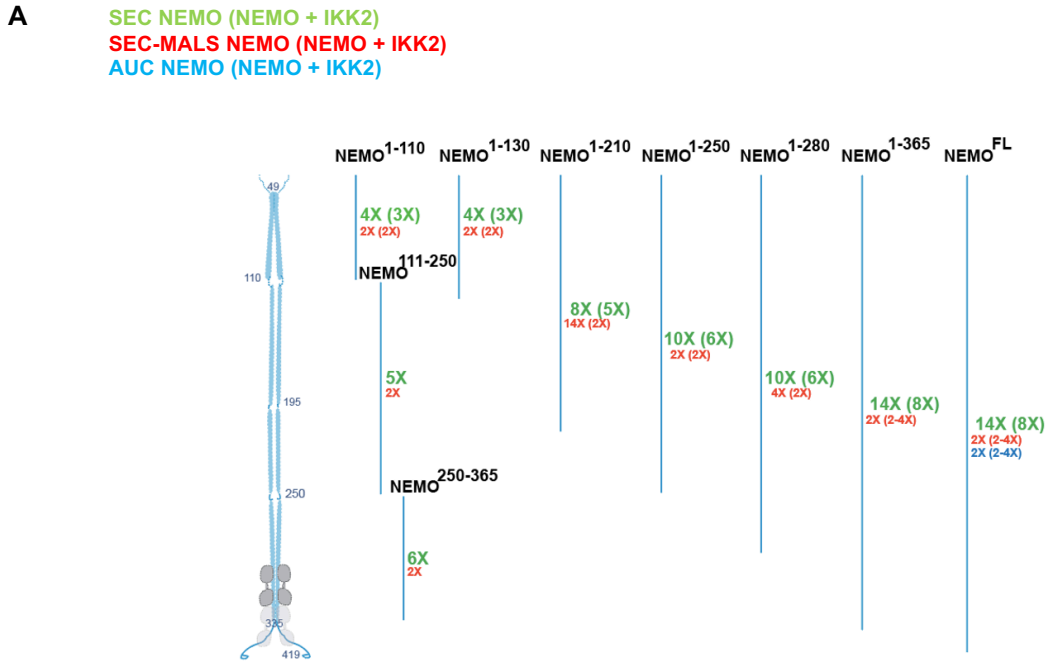

B

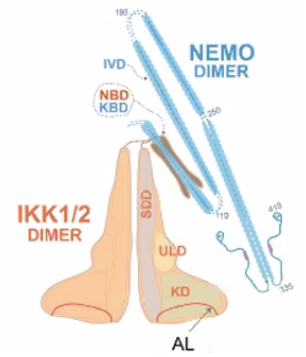

Figure 15. Schematic of predicted structure of IKK2-NEMO complex.
A) From SEC, NEMO itself exhibits an elongated larger sized shape as shown MW 14 times higher than a NEMO monomer but a complex with IKK2 exhibits 8 times higher than a IKK2-NEMO monomer. From AUC, NEMO itself is significantly an elongated dimer as shown a major axis ratio of 31.4 but IKK2-NEMO complex is shown a less elongated conformation as a major axis ratio of 27.2 (IKK2 itself,14.0). IKK2-NEMO complex does not exhibit even much more elongated shape than NEMO itself. B) Hypothetical model of IKK2-NEMO complex. When NEMO forms a complex with IKK2 through a primary interaction of KBD-NBD, NEMO might have auto-inhibited conformation through intramolecular or intermolecular interaction between subdomains that induce a kinky structure.

2.6 ACKNOWLEDGEMENTS

Chapter two, this research was supported by various grants from organizations including the National Institutes of Health *(*NIH*)* (CA141722), Tobacco-Related Disease Research Program (TRDRP), and American Association for Cancer Research (AACR).

Chapter two, in full, has been published for publication of the material as it may appear in BBA - Proteins and Proteomics, 2020, Myung Soo Ko; Tapan Biswas; Maria Carmen Mulero; Andrey A Bobkov; Gourisankar Ghosh; Tom Huxford. The dissertation/thesis author was the primary investigator and author of this paper.

CHAPTER THREE

3. Cytokine-induced Activation of IKK2/β occurs upon Ub-mediated interaction with a NEMO segment

3.1 ABSTRACT

Two key events associated with the canonical signaling, switch of the catalytic state of IKK2/β from inactive to active via AL phosphorylation is the most critical function of canonical signaling and non-covalent interaction between the linear Ub-chain and NEMO is essential for the AL phosphorylation of IKK2/β. However, how the interaction between the Ub-chain and NEMO lead to IKK2/β activation in the response to upstream events is still remained. In order to improve understanding of the process of IKK2/β activation induced through NEMO non-covalently linked to linear Ub-chains upon canonical signaling, this study was discovered a novel interaction of the adapter protein NEMO with IKK2/β regulated by its association with Ub-chains. The novel interaction between IKK2 and NEMO was shown as “second site" where Ub-chain binding stabilizes NEMO dimer leading to its conformational change resulting in the AL phosphorylation of IKK2. In vitro and In vivo studies, cell-permeable peptides of a short segment of NEMO targeting the novel interaction selectively inhibited NEMO-mediated IKK2 activation and consequently blocked NF-kB activation. These findings open a new dimension in search for a much-needed alternate for IKK regulation and NF-κB regulatory therapy.

3.2 INTRODUCTION

The transcriptional activity of the NF-κB family of proteins is directly controlled by actions of two distinct classes of protein factors- IκB kinases (IKK) and the IκB kinase inhibitors (IκB). In resting cells, NF-κB remains inhibited by IκB through the formation of stable NF-κB:IκB complexes [51]. This inhibition is relieved by IKK-mediated phosphorylation of IκB, and its subsequent degradation by the proteasome. There are two distinct IKK catalytic subunits- IKK1 (also known as IKKα) and IKK2/β, which are activated by two distinct signaling pathways leading to the degradation of two different classes of IκB inhibitors [18]. The canonical activation pathways activate IKK2/β and the non-canonical, IKK1/α. The activation of IKK2/β requires an adapter protein, NEMO (NF-κB essential modulator), whereas IKK1/α activation requires NF-κB inducing kinase (NIK) [54]. The kinase domain of IKK contains a pair of serine (Ser177 and Ser181 of IKK2/β) within the kinase 'activation loop' (AL) that undergoes phosphorylation in response to signaling [55-57]. This phosphorylation is essential for IKK to be catalytically active, thus marking IKK activation. The switch of the catalytic state of IKK2/β from inactive to active via AL phosphorylation is perhaps the most critical function of canonical signaling. Mutation of these two serine to phosphomimetic Asp/Glu or phospho-resistant Ala convert IKK2/β to constitutively active or inactive, respectively [18,25-28]. IKK1/α and IKK2/β share 40 % sequence identity and display a similar domain organization, where in addition to the kinase domain (KD) they contain a ubiquitin-like domain (ULD), and a long three-helical bundle domain (SDD) responsible for IKK dimerization (Figure 4) [32-33]. These three domains interact with each other forming a stable but somewhat flexible structural core. At the extreme C-termini of IKK1/2, a flexible segment of approximately 85 residues

strongly interacts with the N-terminus of NEMO, and this interaction is responsible for the formation of a heterotrimeric 'IKK complex', IKK1/α:IKK2/β:NEMO. How this rather poorly defined IKK complex receives canonical signaling for the activation of IKK2/β is still unknown. The precise role of IKK1/α within the heterotrimeric complex is also unclear although it is known that the NF-κB activation potential remains largely intact in cells devoid of IKK1/α.

Another key event associated with the canonical signaling is the synthesis of poly-ubiquitin chains of various types - linear (M1-linked), lysine 63-linked (K63), and mixed [1]. These chains are bound to adapter proteins including NEMO, covalently or non-covalently. NEMO displays non-covalent interaction with linear Ub-chain with high affinity, and K63-linked Ub-chain weakly [11, 51]. This non-covalent interaction between the linear Ub-chain and NEMO is essential for the AL phosphorylation of IKK2/β, irrespective of the nature of its covalent linkage to linear Ub-chain [14]. It is generally believed that another kinase TAK1 - bound to its adapter proteins TAB1 and TAB2 - directly phosphorylates the AL serines of IKK2/β in response to most, if not all, canonical signaling pathways. Like NEMO, TAB2 also interact with Ub-chain, thus bring the TAK1:TAB1/2 complex in close proximity to the IKK1/2:NEMO complex allowing IKK2/β activation [13-17]. This could constitute a primary mechanism of IKK2/β activation although certainly not universal since IKK2/β can be activated by the specific stimulus of the canonical pathways even in the absence of TAK1 [12-14,37]. It is possible that different stimuli of canonical IKK2/β activation pathways generate different poly-Ub chain variants that are covalently linked to different adapter molecules and render variations in kinetics and amplitudes of IKK2/β activity. Overall, the biochemical mechanism of IKK2/β activation and its regulation is

mostly unknown. In this report, I investigated the process of activation of IKK2/β induced upon canonical signaling through linear Ub-chains. Employing a suite of orthogonal experiments, I discovered a novel interaction of the adapter protein NEMO to IKK regulated by its association with Ub. Additionally, I unraveled a short segment of NEMO that mediates this interaction, and can function as a competitive antagonist in trans. These findings open a new dimension in search for a much-needed alternate for IKK regulation and NF-κB regulatory therapy.

3.3 MATERIALS AND METHODS

3.3.1 Recombinant Plasmid and Baculovirus Preparation

The full-length human IKK2/β cDNA clone was graciously provided by the laboratory of M. Karin (School of Medicine, UC, San Diego). For large-scale purification and in vitro biochemical assays, full-length human IKK2/β was cloned in pFastBacHTb (Invitrogen) vector within BamHI and NotI sites giving rise to an N-terminal hexa-Histidine tag followed by TEV protease recognition sequence. For site-directed mutagenesis, codons corresponding to S177 and S181 were mutated to G by the Quickchange mutagenesis protocol (Agilent) to generate the human IKK2EE clone. Codons corresponding to K44 was mutated to M by PCR with base changes incorporated in the oligonucleotide primers. Gene fragments corresponding to human IKK2WT 11-669 and IKK2EE 11–669 and IKK1WT 10-670 were amplified by PCR and subcloned into pFastBacHTa or pFastBacHTb. Recombinant baculovirus production, amplification, and titer optimization were carried out in Sf9 insect cell suspensions as described in Figure 5 [89].

Full-length human NEMO and deletion mutants ($NEMO^{250-365}$, $NEMO^{250-419}$, and $NEMO^{111-419}$) were subcloned individually into the NdeI and BamHI restriction sites of the pET15b vector in frame with an N-terminal hexahistidine tag. Methione-linked tetra ubiquitin chain was subcloned into the BamHI and NotI restriction sites of the pET24D vector giving rise to an N-terminal hexa-Histidine tag followed by TEV protease recognition sequence.

Glutathione S-transferases (GST)-NEMO was constructed by subcloning the full-length cDNA and deletion mutants ($NEMO^{241-350}$, $NEMO^{241-375}$, $NEMO^{241-283}$, $NEMO^{241-390}$, $NEMO^{241-419}$, and $NEMO^{111-419}$) into the BamHI and NotI sites of pGEX-4T2 (GE Healthcare Life Sciences) in frame with an N-terminal GST tag. Codons corresponding to Q384R385R386 or Q384R385R386S387P388P389 in N-terminal GST fused $NEMO^{241-419}$ backbone was mutated to G by PCR with base changes incorporated in the oligonucleotide primers.

For cellular assays, human IKK2 WT was cloned as a HA-tagged version into pRC or pCMV-HA (Clontech) vector. Generated several mutants (total 36; 23 single, 12 double and 1 triple) of human IKK2/β changed to A or G were prepared by PCR with base changes incorporated in the oligonucleotide primers. Human NEMOWT was cloned as a Myc-tagged version into pcDNA-3.1 (Invitrogen). Residues 384 to 386 or 384 to 389 of the NEMOWT in pcDNA-3.1 were mutated 3 G or 6 G by PCR with base substitutions incorporated in the oligonucleotide primers.

3.3.2 Cell Culture and Reagents

HeLa, HEK 293T, MEF, and RAW murine macrophage cells were maintained in Dulbecco's modified Eagle's medium (Invitrogen) supplemented with 10% fetal bovine

serum, 2 mM L-glutamine, penicillin (50 units/ml), and streptomycin (50 μg/ml). Glutathione agarose beads and Ni-NTA agarose beads were purchased from BioBharati LifeScience Pvt. Ltd (BBL). Mouse anti-HA antibody was purchased from BioLegend. Rabbit anti-NEMO, rabbit anti-IKK2, rabbit anti-His, rabbit anti-UB, rabbit anti-Myc, rabbit anti-γ-Actin, rabbit anti-ERK2 were purchased from BioBharati LifeScience Pvt. Ltd (BBL). Mouse anti p84 was purchased from GeneTex. Mouse anti-GST, rabbit anti-p65/RelA, and rabbit anti-IKBα were from Santa Cruz Biotechnology. Rabbit anti-P100/p52 was a gift from N. Rice (National Cancer Institute, Frederick, MD). Rabbit anti-Phospho-SAPK/JNK (Thr183/Tyr185), rabbit anti-SAPK/JNK, rabbit anti-Phospho-p38 MAPK (Thr180/Tyr182), rabbit anti-p38 MAPK, rabbit anti- Phospho-p44/42 MAPK (Erk1/2) (Thr202/Tyr204), and rabbit anti-Phospho-IKKα/β (Ser176/180) were purchased from Cell Signaling. The horseradish peroxidase - conjugated secondary antibodies against either rabbit or mouse IgG were from BioBharati or Cell Signaling. Mouse TNF-α was purchased from BioBharati LifeScience Pvt. Ltd (BBL). LPS was purchased from Sigma. Mouse LTβR was purchased from Abcam.

3.3.3 Peptides

Based on the affinity binding assay and cell based IKK activity assay, I identified a minimal sequence of 6 residues that possibly retains the NEMO biological effects in NEMO-mediated IKK2 activation. I, therefore, designed a 17 aa peptide based on this sequence conjugated to TAT sequence (NEMO Activation Peptide, $NEMO^{ActPep}$) and a mutant peptide changed to 6 glycine at the 6 targeting aa conjugated with TAT ($mNEMO^{ActPep}$). Peptides were synthesized by Bon Opus Biosciences. Peptides were characterized by matrix-assisted laser desorption ionization mass spectrometry and

analytical reverse phase high pressure liquid chromatography analysis. Peptides were dissolved in 1XPBS to stocks of between 2mM and 10mM.

3.3.4 Protein Expression and Purification

All His-tagged NEMO proteins were expressed in BL21 (DE3) cells. 1 L cultures in LB media with 100 ug/mL ampicillin were grown at 37°C to OD600 of 0.2 before induction with 0.2 mM isopropyl β-D-1-thiogalactopyranoside (IPTG) (BioBharati) and stirring at 150 rpm for 22°C for 16 hours. Cells were harvested by centrifugation at 3,000 x *g* for 10 minutes (Beckman Coulter) and cell pellets were lysed by sonication (VWR Scientific) on ice in 200 mL of lysis buffer (20 mM Tris-HCl pH 8.0, 300 mM NaCl, 10% w/v glycerol, 10 mM imidazole, 0.2% TritonX, 1 mM PMSF, and 5 mM β-mercaptoethanol). Lysates were clarified by centrifugation at 15,000 rpm for 45 minutes. Supernatants containing soluble proteins were then applied to a 1 mL Ni NTA-Agarose (BioBharati) column that was preequilibrated with lysis buffer. Bound proteins were washed with 25 mL wash buffer (lysis buffer with 30 mM imidazole) and eluted in 10 mL elution buffer (lysis buffer containing 250 mM imidazole).

Sf9 insect cells from 1 L suspension cultures were harvested by centrifugation at 3,000 x *g* for 10 minutes at 4°C and lysed by sonication in 100 mL of lysis buffer (25 mM Tris-HCl, pH 8.0, 200 mM NaCl, 10 mM imidazole, 10% w/v glycerol, 5 mM β-mercaptoethanol). The lysate was clarified by centrifugation at 18,000 rpm for 45 minutes at 4°C. Pre-equilibrated Ni NTA-Agarose resin was added at a ratio of 1 mL of resin slurry/liter of lysed cell culture and the mixture was incubated on a rotator at 4°C for 3 hours. The Ni beads were pelleted at 1,000 rpm for 2 minutes in a swinging bucket centrifuge rotor. Supernatant was carefully decanted and the protein-bound resin was

resuspended with wash buffer (lysis buffer containing 30 mM imidazole) and incubated at 4°C on a rotator for 2 minutes. The Ni beads were pelleted again and decanted (wash 1). This was repeated until the last wash fraction contained 0.01-0.1mg/mL of protein (Bio-Rad Protein Assay). Elution buffer (lysis buffer containing 250 mM imidazole) was added, and eluted fractions were collected and stored in -80°C.

Recombinant N-terminal GST tagged NEMO proteins were expressed in Escherichia coli Rosetta cells by growing cells to an A_{600} of 0.2 followed by induction with 0.2 mM isopropyl β-D-1-thiogalactopyranoside (IPTG) for 16 h at 22 °C. Cells were lysed with lysis buffer [25 mM Tris (pH 8.0), 300 mM NaCl, 0.1% (v/v) TritonX, 10% (v/v) glycerol, 1 mM ethylenediaminetetraacetic acid (EDTA), 1.0 mM PMSF, and 5 mM β-mercaptoethanol] and sonicated. The lysate was clarified by centrifugation at 15000 rpm for 45 minutes at 4 °C. The supernatant was loaded onto a Glutathione Sepharose resin column pre-equilibrated with lysis buffer at 4 °C. Protein was eluted with elution buffer [25 mM Tris (pH 8.0), 150 mM NaCl, 0.1% (v/v) TritonX, 10% (v/v) glycerol, 5 mM β-mercaptoethanol, and 10 mM glutathione]. Eluted fractions were collected and stored in -80°C.

3.3.5 Fraction by Size-Exclusion Chromatography

Purified individual full length His-tagged IKK2/β inactive mutant ($IKK2^{K44M}$), and deletion mutant active IKK2 ($IKK2^{11\text{-}669EE}$) and NEMOWT and Ub4 proteins as well as NEMO:Ub4 complexes were subjected to gel filtration with a Superose6 Increase 10/300 GL size-exclusion column (GE Healthcare) on an NGC™ Liquid Chromatography System (Bio-Rad). The column was equilibrated in a buffer with 25 mM Tris-HCl, pH 8.0, 250 mM

NaCl, 2 mM DTT, and 5% glycerol at a flow rate of 0.2 mL/min at 22°C. Peak fractions were collected and analyzed by Coomassie stained gels.

3.3.6 Whole Cell Extracts and Nuclear/Cytoplasmic Fractionations

HEK293T cells were cultured in DMEM supplemented with 10% (v/v) fetal bovine serum (FBS) and 1% (v/v) penicillin/streptomycin/glutamine. Then, cells at 70-80% confluence were transiently transfected with empty, HA-IKK2WT, or HA-IKK2 mutant plasmids using polyethylenimine (PEI, PolySciences). After being transfected for 48 hours, cells were harvested. To prepare whole cell extracts, cells were lysed in RIPA buffer [20 mM Tris-HCl (pH 8.0), 200 mM NaCl, 1% (v/v) Triton X-100, 2 mM DTT, 5 mM 4-nitrophenyl phosphate di(tris) salt, 2 mM sodium orthovanadate, 1 mM PMSF, and protease inhibitor cocktail] for 1 hour at 4 °C. Then, cells were centrifuged at 13000 rpm for 20 minutes at 4 °C, and supernatants containing the whole cell protein extracts were measured by the Bradford assay to determine the total amount of protein.

To prepare nuclear and cytoplasmic protein extracts, HeLa, MEF, and RAW murine macrophage cells were lysed in the buffer containing 10 mM HEPES (pH 7.9), 1.5 mM $MgCl_2$, 10 mM KCl, 0.5 mM DTT, 0.05% (v/v) NP-40, and protease inhibitor cocktail for 10 minutes on ice and spun at 3000 rpm at 4 °C for 10 minutes. The supernatant containing the cytoplasmic fraction was measured by the Bradford assay to determine the total amount of protein. Pellets were resuspended in the nuclear extract buffer (420mM NaCl, 25mM Tris pH7.5, 10% glycerol, 0.2mM EDTA, 1mM DTT, 0.5mM PMSF, 1X protease inhibitor cocktail) once and then subjected to three lysis cycles (freeze at −80 °C and thaw at 37 °C). Finally, samples were centrifuged at 13000 rpm at 4 °C for 20 minutes, and supernatants containing the soluble nuclear fraction were measured by the Bradford

assay to determine the total amount of protein. Nuclear and cytoplasmic extracts were aliquoted and kept at −80 °C.

3.3.7 Cell Culture/Stimulation and Peptide Treatment

Hela, MEF, RAW murine macrophages were cultured in Dulbecco's MEM containing 10% fetal bovine and 2 mM L-glutamine serum supplemented with penicillin and streptomycin, at 37°C in a humidity incubator with 5% CO_2. RAW murine macrophage cells were seeded and allowed to adhere for 24 hours then treated with wild type or mutant peptide at different concentrations 60 min before the LPS challenge (100 ng/ml). After 2 hours nuclear and cytoplasmic extracts were collected. Hela and MEF cells seeded for 24 hours then treated with wild type or mutant peptide at different concentrations 60 min before the TNFα challenge (10 ng/ml) for 15 minutes and then nuclear and cytoplasmic extracts were collected. After MEF cells were treated with wild type or mutant peptide at different concentrations 1 hour before the LTβR challenge (300 ng/ml). After 24 hours whole cell extracts were collected and aliquoted and kept at −80 °C for further experiments.

3.3.8 Western Blot Analysis

An equal amount of protein from cell extracts was separated by SDS-polyacrylamide gels and transferred to polyvinylidene fluoride (PVDF) membranes (Millipore, Bedford, MA, USA). The membrane was blocked with 5% bovine serum albumin (BSA) for 1 hour at room temperature and then the membrane was incubated with the primary antibodies overnight at 4°C. Antibodies for IKK2, His, HA, Myc, NEMO, GST, UB, IκBα, phosphor-specific IKK2, p65/RelA, p84, γ-Actin, p100/52, phospho-ERK, phospho-JNK, phospho-p38, ERK, JNK, and P38 were used for detecting multiple

specific protein targets. After binding of an appropriate secondary antibody coupled to horseradish peroxidase, the immunoreactive bands were visualized by enhanced chemiluminescence substrate.

3.3.9 In-Vitro Trans Auto-Phosphorylation Kinase Assay

Full-length His-tagged IKK2/β mutant ($IKK2^{K44M}$) was incubated with catalytic active IKK2/β truncated form ($IKK2^{11-669EE}$), $NEMO^{WT}$, and Ub4 at 30 °C in the presence of 20 mM ATP in a reaction buffer containing 20 mM Tris-HCl pH 7.5, 100 mM NaCl, 2 mM DTT, 1 mM Na3VO4, 10 mM NaF, 20 mM β-glycerophosphate. Reactions were halted at the indicated times by adding SDS loading buffer and heating the sample at 95°C for 5 min. Samples were resolved on 8% SDS-PAGE and analyzed by western blot using antibody against phospho-Ser181 of IKK2/β.

3.3.10 In-Vitro GST Pull-Down Assay from Recombinant Protein

Glutathione-agarose beads equilibrated with the binding buffer (25mM Tris-HCl, pH 7.5, 150 mM NaCl, 1 mM EDTA, 0.2% NP40, 5% glycerol). Recombinant purified N-terminal GST fused NEMO proteins were mixed with recombinant purified IKK2/β proteins in the absence or presence of Ub4. The mixtures were added to Glutathione-agarose beads in GST binding buffer. The mixtures were incubated for 2 hours at 4°C. GST- fusion protein complexes bound to glutathione-agarose beads were washed four times with the binding buffer. Proteins bound to beads were resuspended in SDS loading buffer, resolved by SDS-PAGE, and analyzed by western blot.

3.3.11 In-Vitro Pull-Down Assay from Whole Cell Extract

Proteins of HEK293T cells transfected with full length human IKK2 WT or mutants were extracted using lysis buffer (50 mM Tris-HCl, pH 7.4, 200 mM NaCl, 1 mM EDTA, 1%

NP40, 10% glycerol, 0.1mM PMSF, 1X protease inhibitor cocktail). After centrifugation at 16,000 *g* for 20 minutes, the supernatants were adjusted to the binding buffer (25mM Tris-HCl, pH 7.5, 150 mM NaCl, 1 mM EDTA, 0.2% NP40, 5% glycerol) and these whole-cell extracts were incubated with Escherichia coli expressed GST fusion NEMO in the absence of presence of Ub4 bound to glutathione-agarose beads. After gentle shaking for 2 hours at 4°C, the beads were centrifuged at 500 *g* for 2 minutes and washed four times in the binding buffer. Proteins bound to beads were resuspended in SDS loading buffer, resolved by SDS-PAGE and analyzed by immunoblotting.

For peptide In-vitro pull-down assay, proteins of HEK293T cells expressing full length human IKK2 WT were extracted using the same lysis buffer above. The whole cell lysates were mixed with Escherichia coli expressed GST fused NEMO, $NEMO^{ActPep}$, or $mNEMO^{ActPep}$ at different concentrations in the absence of presence of Ub4 and incubated for 2 hours at 4°C. The beads were then washed four times in the binding buffer. Proteins bound to beads were resuspended in SDS loading buffer, resolved by SDS-PAGE and analyzed by western blot.

3.3.12 Cell Based In-Vitro Kinase Activity Assay

HEK293T cells were cultured in DMEM supplemented with 10% (v/v) fetal bovine serum (FBS) and 1% (v/v) penicillin/streptomycin/glutamine. Then, cells were transiently transfected with empty, HA-IKK2 WT or individual mutant, or co-transfected with Myc-NEMO WT, 3G, or 6G mutant plasmids using polyethylenimine PEI (PolySciences) following the manufacturer's protocol. After being transfected for 48 hours, cells were harvested and lysed in the RIPA buffer for 1 hour at 4 °C. Then, cells were centrifuged at 13000 rpm for 15 minutes at 4 °C, and supernatants containing the whole cell protein

extracts were measured by the Bradford assay to determine the total amount of protein. Proteins were added SDS loading buffer and heating the sample at 95°C for 5 minutes. Samples were resolved on 10% SDS-PAGE and analyzed by immunoblot using antibody against phospho-Ser181 of IKK2 (Cell Signaling Technology) and antibodies-HA and -Myc were used for loading controls. Protein expression was normalized by IKK2 WT.

3.3.13 Electrophoretic Mobility Assays

Electrophoretic mobility shift assays (EMSAs) were performed as previously described [135]. Briefly, IgkB probe was radio-labeled and incubated with the proteins under study for 20 minutes at room temperature in binding buffer [10 mM Tris-HCl (pH 7.5), 10% (v/v) glycerol, 1% (v/v) NP-40, 1 mM EDTA, and 0.1 mg/mL salmon sperm DNA]. Samples were run in TGE buffer (24.8 mM Tris base, 190 mM glycine, and 1 mM EDTA) at 200 V for 1 hour, and the gel was dried. In the supershift reactions, all proteins and p65/RelA antibody were incubated simultaneously for 20 min in the binding buffer in the presence of the probe under study. The amount of protein was quantified by the Bradford assay. Protein complexes were analyzed by native electrophoresis on a 4% (w/v) nondenatured polyacrylamide gel. EMSA analysis with quantitative densitometry and signal intensity was quantitated using ImageJ software. EMSAs were performed in triplicate.

3.3.14 *In Vivo* Studies

3.3.14.1 LPS-induced Shock and Peptide Administration

All animal protocols were approved by the Institutional Animal Care and Use Committee (IACUC) of UCSD. 2 to 3-week-old C57B/L male mice were purchased Jackson Laboratories (Bar Harbor, ME, United States). After LPS-induced shock was

tested by intraperitoneal injection of 1.2mg (60mg/kg) bodyweight LPS and monitored for survival, the animals were grouped into different treatment groups. $NEMO^{ActPep}$ or $mNEMO^{ActPep}$ (40mg/kg) was dissolved in 1XPBS and administered by subcutaneous injection in a volume of 100 µl.

3.3.14.2 Plasma Analysis

Each mouse was subcutaneous (SC) injected with the $NEMO^{ActPep}$ or $mNEMO^{ActPep}$ 800 ug/mouse (total 40 mice) 1 hour prior to LPS treatment (1.2 mg/mouse), mice were euthanized at 4 time points (after 0, 1, 2 and 6 hours). Whole blood was removed via 27-gauge needle from the abdominal aorta and centrifuged at 2,000 × *g* for 2 min in EDTA-coated tubes. The plasma was prepared in cold immediately from the blood and used for testing concentration of cytokine (IL-1b, IL-2, IL-6, IL-8, IL-10, IP-10, TNFa, MCP-1, MIP1 and MIP2) expression by specific solid-phase sandwich enzyme-linked immunosorbent assay (ELISA) in accordance to the manufacturer's instructions (Meso Scale Diagnostics, LLC).

The numbers of lymphocyte and neutrophil were counted in circulating blood and tissues. Each mouse was Injected with the $NEMO^{ActPep}$ or $mNEMO^{ActPep}$ one time or 5 successive days. After mice were sacrificed, the plasma was used for testing cytokine expression and lymphocyte numbers (B and T cell) and myeloid cell (macrophage and neutrophil) numbers.

3.3.15 Statistical analysis

Assay values from $NEMO^{ActPep}$ peptides-induced inhibition of NF-kB are expressed as mean ± S.E. Statistical analysis was performed using analyzed using unpaired *t*-test.

All p-values were reported as two-sided; no adjustments were made for multiple comparisons. *P* value < 0.05 was considered statistically significant in all analyses.

3.4 RESULT and DISCUSSION

3.4.1 AL of IKK2/β undergo phosphorylation in the presence of NEMO and Ub4

My rationale is that the second site interaction between IKK2/β and NEMO in the presence of Ub4 induces the conformational alteration of AL from a closed to an open state allowing its phosphorylation by IKK2/β or other kinases. To this end, first of all, I examined kinetics of phosphorylation of the AL of full length kinase dead (KD) IKK2/β K44M (IKK2^{K44M}) mutant by an active truncated IKK2/β$^{11\text{-}669EE}$. In this case, IKK2/β^{K44M} mutant acts as a substrate where the AL is mostly unphosphorylated. The AL of inactive IKK2/β is unphosphorylated, which must undergo conformational change into an 'open state' to be targeted by an active kinase [60,63-64]. If interaction between the sensor region of IKK2/β and the NEMO:Ub4 complex induces conformational change of the AL, the rate of phosphorylation will be significantly greater in the presence of the NEMO:Ub4 complex than its absence. I monitored phosphorylation by western blot using phospho-Ser181-specific antibody. As expected, Figure 16 is shown that active IKK2/β$^{11\text{-}669EE}$ barely phosphorylates the AL of IKK2/β^{K44M} mutant. Phosphorylation of the AL was significantly enhanced in the presence of NEMO which underwent further enhancement when Ub4 was added. I also showed that Ub4 alone could not enhance phosphorylation in the absence of NEMO.

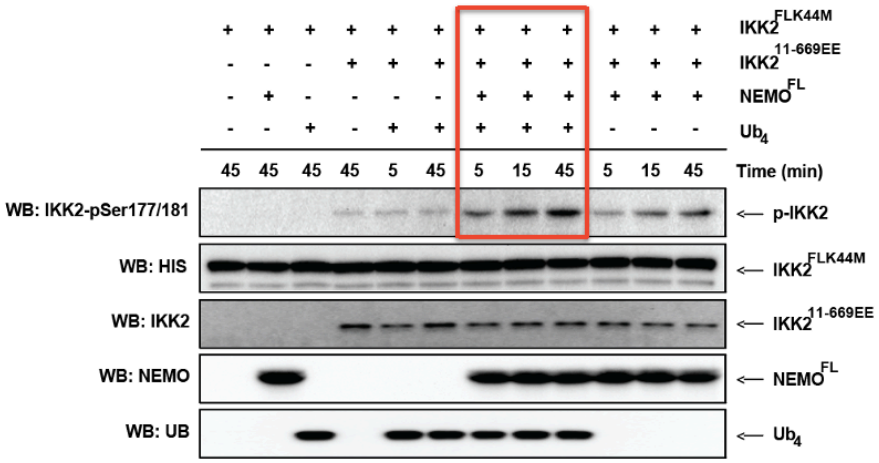

Figure 16. In vitro reconstitution of IKK2 trans auto-phosphorylation.
A catalytically inactive (K44M) and C-terminally truncated IKK2 (lanes 1–12) and mixtures of that enzyme with a catalytically active full-length version (lanes 4–12), NEMO (lanes 2 & 7–12), and Ub4 (lanes 3 & 5–9) were incubated with Mg-ATP for the time periods indicated and then probed via Western blot with anti-phosphoSer181 antibody.

A

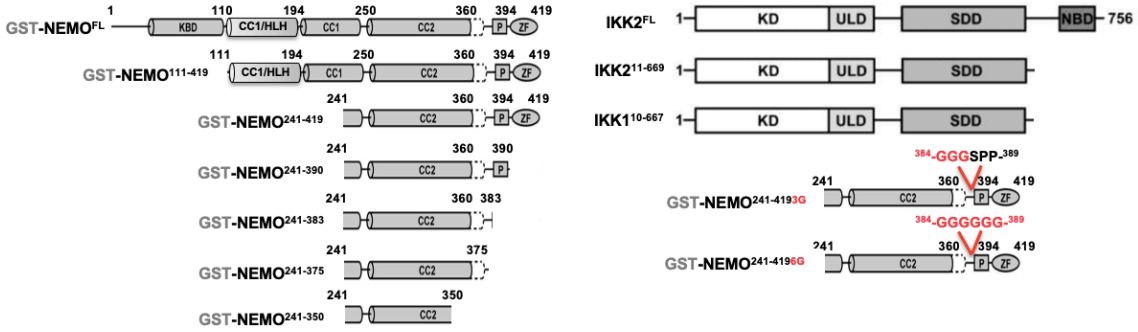

B

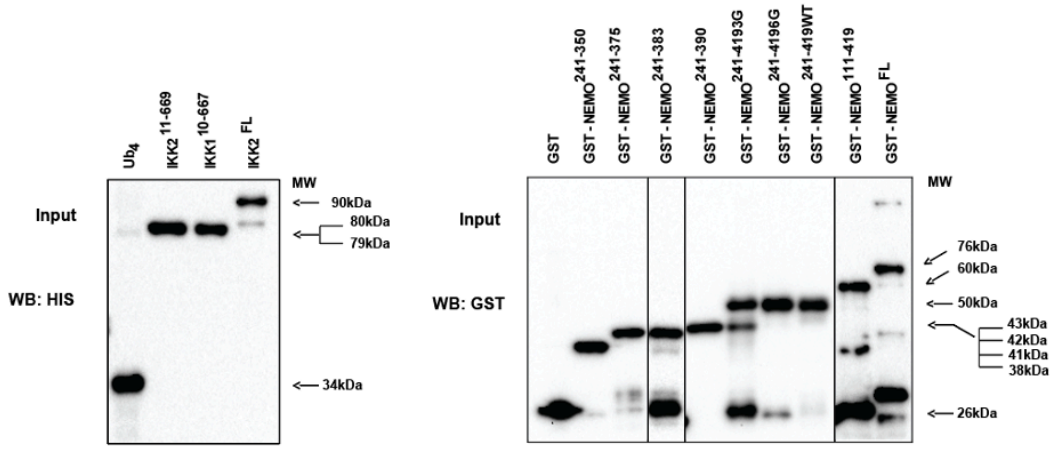

Figure 17. GST affinity pull down assay: Input.

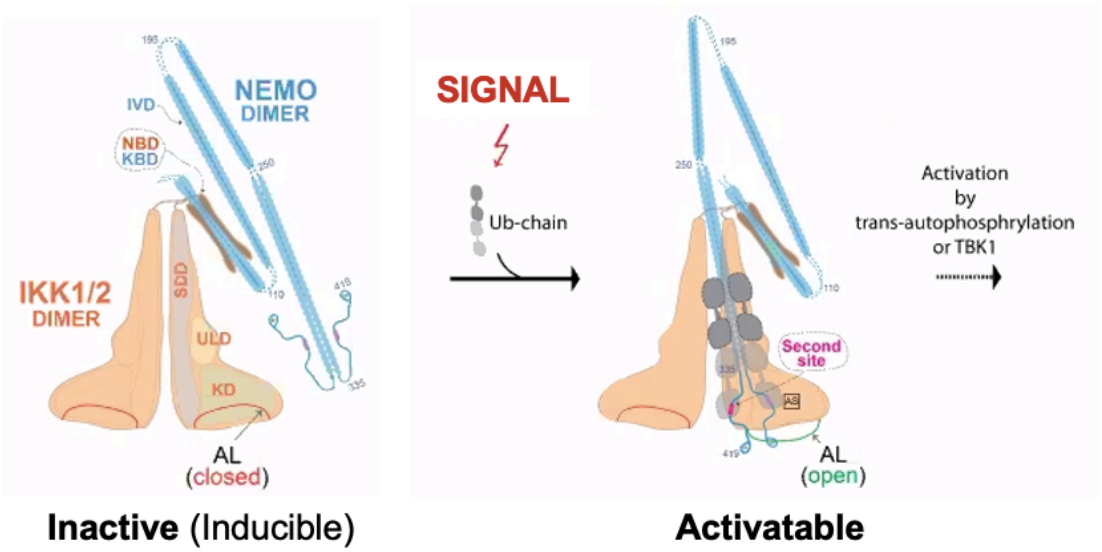

Figure 18. A schematic model of IKK2/β activation by NEMO in association with an unanchored Ub-chain during canonical NF-κB signaling.
For simplicity only a single of possible multiple units of IKK1:IKK2:$NEMO_2$ complex is depicted; A similar model could be true for IKK2:IKK2:$NEMO_2$ complex. In addition to the known NBD-KBD interaction, a NEMO C-terminal segment (purple) interacts with a separate region of SDD of IKK and triggers open conformation of the activation loop for phosphorylation.

3.4.2 Linear Ub-chain induces interaction between NEMO and IKK2/β through a second site.

The mechanism of an obligatory role of NEMO in IKK2/β activation is unknown. To dissect the mechanism, I put forth a plausible model (Figure 18) that is consistent with current biological and biochemical data. I hypothesized that a separate segment of NEMO, in addition to its C-terminal first 110 residues that is involved in a 'high-affinity interaction' with NBD of IKK [72-73,128], makes a transient contact with a segment of IKK2/β distant from its NBD. I also propose that binding of poly-Ub-chain to NEMO enables this transient NEMO-IKK2/β interaction through a secondary site(s) and induces a conformational change of the AL of IKK2/β from a closed to an open conformation, which allows AL serines (Ser177 and 181) to be accessible for phosphorylation by IKK2/β and/or other upstream kinases such as TAK1. The association of linear Ub-chain to NEMO or an adapter protein could be either covalent or non-covalent.

To test the model, I generated mutants of NEMO lacking its 'high-affinity interaction' segment i.e. N-terminal kinase binding domain (KBD), and assessed their interaction with IKK2/β or its mutant lacking NBD using affinity pull-down experiments both in presence and absence of a linear polyubiquitin chain. The linear Ub chain (Ub4) is generated by fusing 4 Ub moieties N- to C-termini. This Ub4 chain was shown in vitro to be more than sufficient for activation since an M1-linked Ub2 (di-Ub) is known to trigger efficient NF-κB activation in the cell [99]. NEMO proteins, full-length and truncated, were expressed as GST-fusion proteins in *E. coli* host (Figure 17B).

NEMO forms head-to-head dimers (Figure 17A) on its own with its multiple coiled segments, thus linkage of GST with a flexible linker is unlikely to cause any aberrant phenotype with either the full-length or deletion mutants.

IKK2/β proteins were expressed as 6X-His-fusion in Sf9 insect cells. The full-length NEMO and the full-length IKK2/β displayed strong interaction as expected to be mediated through NBD and KBD, and the presence of Ub4 did not make any discernible difference in this already highly stable bond (Figure 19). The affinity pull-down experiments additionally revealed an interaction between a truncated IKK2/β ($IKK2^{11\text{-}669}$ lacking NBD) with both the full-length NEMO and KBD-deleted NEMO ($NEMO^{111\text{-}419}$) that was strikingly enhanced in presence of Ub4. This was consistent with my model which is the presence of a second interaction (Figure 19). Surprisingly, GST-$NEMO^{111\text{-}419}$ failed to pull down full-length IKK2/β in the presence of Ub4. However, the same NEMO construct was effective in contacting $IKK2^{11\text{-}669}$ in the presence of Ub4.

To further understand why $NEMO^{111\text{-}419}$ failed to interact with $IKK2^{FL}$, I reasoned perhaps this construct assumes an altered conformation preventing Ub4 binding. I performed size-exclusion chromatography and made complexes of NEMO:Ub4 with four different NEMO constructs full length and three truncated mutants, 111-419 which removed KBD, 250-419 which removed additional domain IVD, and 250-365 only containing CC2 domain. All NEMO constructs containing the Ub binding domain (CC2) interact with Ub4 but both $NEMO^{FL}$ and $NEMO^{111\text{-}419}$ bind Ub4 poorly compared to $NEMO^{250\text{-}419}$ and $NEMO^{250\text{-}365}$ (Figure 20). It seems that NEMO IVD may engage in weak interaction with Ub binding domain (CC2/UBAN) but disengages when NBD and KBD

interact in the native complex. This might cause that the presence of unbound the NBD of IKK2 prevents the proper contact to NEMO.

To further define the interaction, I proceeded to test if segment(s) of NEMO mediating this second interaction with IKK2/β is located upstream or downstream of its Ub-chain binding domain. A GST affinity pull-down assay with truncated NEMO ($NEMO^{241-419}$; lacking the KBD and a large segment following it) and both full-length and truncated IKK2/β showed interaction with near equal efficiency to that of $NEMO^{111-419}$ in presence of Ub4 but not in its absence (Figure 21). Overall, these data suggest that NEMO and IKK2/β interact through a 'second interaction site' in M1-Ub-chain dependent manner.

In canonical pathway, a high affinity primary interaction between IKK1/α:NEMO or IKK2/β:NEMO that forms IKK1:2:NEMO complex but NEMO-mediated IKK2/β phosphorylation activates IKK complex [65-67]. Thus, I wondered how NEMO plays a role associated with each kinase through a second interaction site. This possibility of the second site interaction was tested between truncated $IKK1^{10-667}$ devoid of NBD and NEMO. NEMO could also interact with IKK1/α but weaker than with IKK2/β (Figure 21). Since a primary binding interaction between NBD of IKK1/α and KBD of NEMO has no effects on IKK2/β activation through canonical pathway and IKK1/α activation does not require NEMO in non-canonical pathway [65-67], this new interaction in IKK1/α:NEMO in the presence of Ub4 might not facilitate IKK activation in canonical pathway.

To identify if a specific region of NEMO C-terminus mediates the interaction with IKK2/β through a second site, I stepwise generated multiple truncation mutants of NEMO targeting c-terminal NEMO domains in addition of $NEMO^{241-419}$ based on my hypothetical

model, - $NEMO^{241-390}$ lacking of zinc finger domain, $NEMO^{241-375}$ lacking of proline-rich segment and CC domain following this, and $NEMO^{241-350}$ only containing CC2/Ub binding domain, all as GST fusion proteins. Affinity pull-down experiments in the presence of Ub4 indicates that $NEMO^{241-390}$ binds IKK2/β similarly as $NEMO^{241-419}$ suggesting that the Zn-finger region is not necessary for the second interaction (Figure 22). However, the interaction is lost with both $NEMO^{241-350}$ and $NEMO^{241-375}$. This suggested that a segment encompassing residues 376 to 390 is essential for Ub4-dependent IKK2/β binding (Figure 22B). Analysis of the conservation of amino acid sequences within this region, and a comparison study with distant homologs such as Drosophila NEMO that is missing 10 residues prior to residue 384 and further 6 residues 384-389 are identical on four other species, suggested that a short segment spanning residues 384 to 389 might constitute the secondary interaction motif (Figure 22C). Affinity pull-down experiments with GST-$NEMO^{241-383}$ indicated that it is not capable of interacting with IKK2/β even in the presence of Ub4 and this tallies with my postulation (Figure 22D).

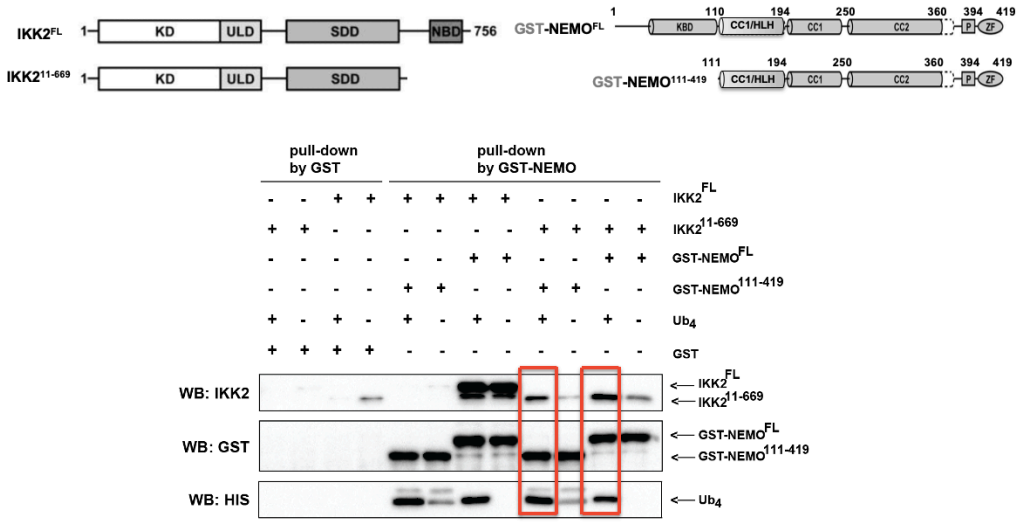

Figure 19. A GST pull-down assay showing NEMO interacting with IKK2/β using a second interaction site.

The assay was performed using IKK2/β fragments derived from baculovirus infected Sf9 cells. This interaction is enhanced in presence of Ub4.

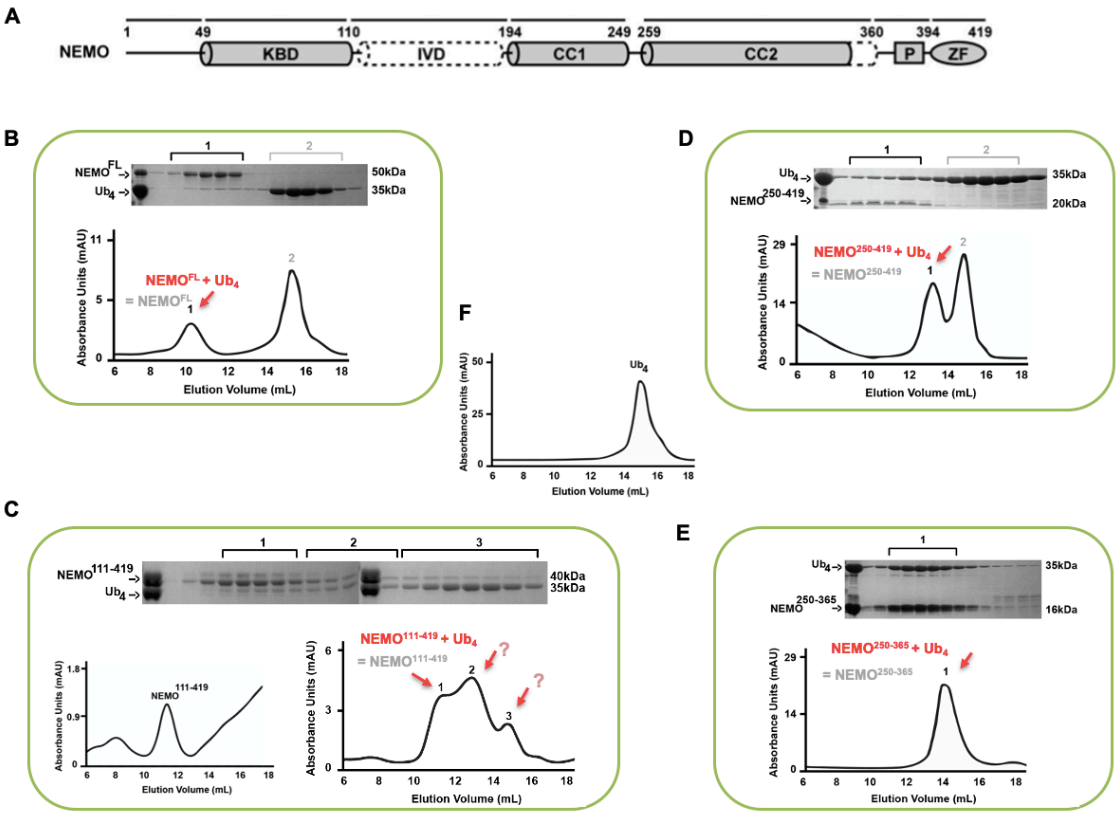

Figure 20. Analytical-scale size exclusion chromatography (SEC) chromatograms of complexes of NEMO:Ub4.

A) Two-dimensional structural diagram of human NEMO protein. B) $NEMO^{FL}$:Ub4 complex C) $NEMO^{111-419}$:Ub4 complex D) $NEMO^{250-419}$:Ub4 complex E) $NEMO^{250-365}$:Ub4 complex F)Ub4.

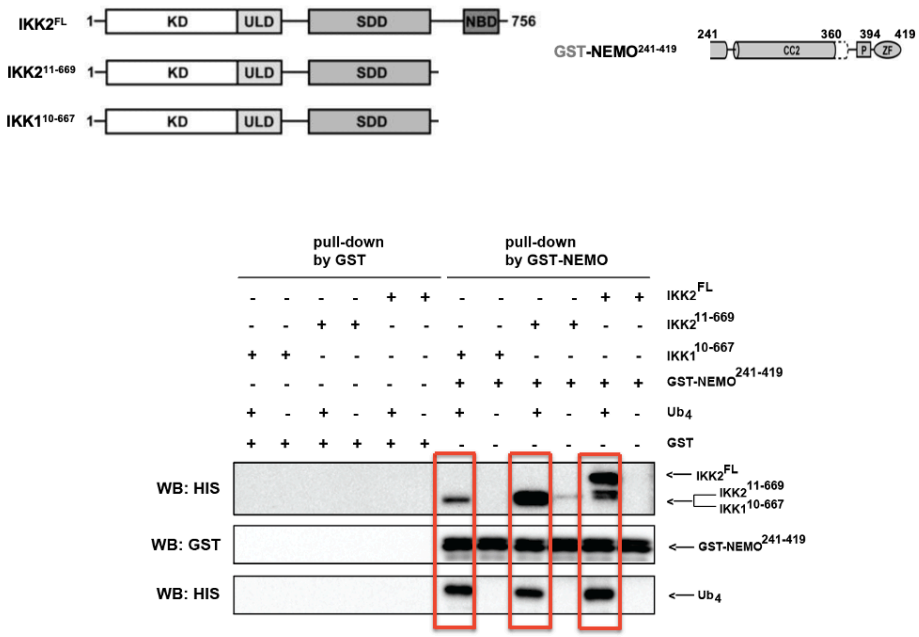

Figure 21. A GST pull-down assay showing Ub-chain (signal)-dependent interaction between NEMO and IKK2/β or IKK1/α.
A GST pull-down assay showing NEMO$^{241-419}$ is sufficient to interact with IKK2/β. Additionally, this fragment can also interact with IKK1/α.

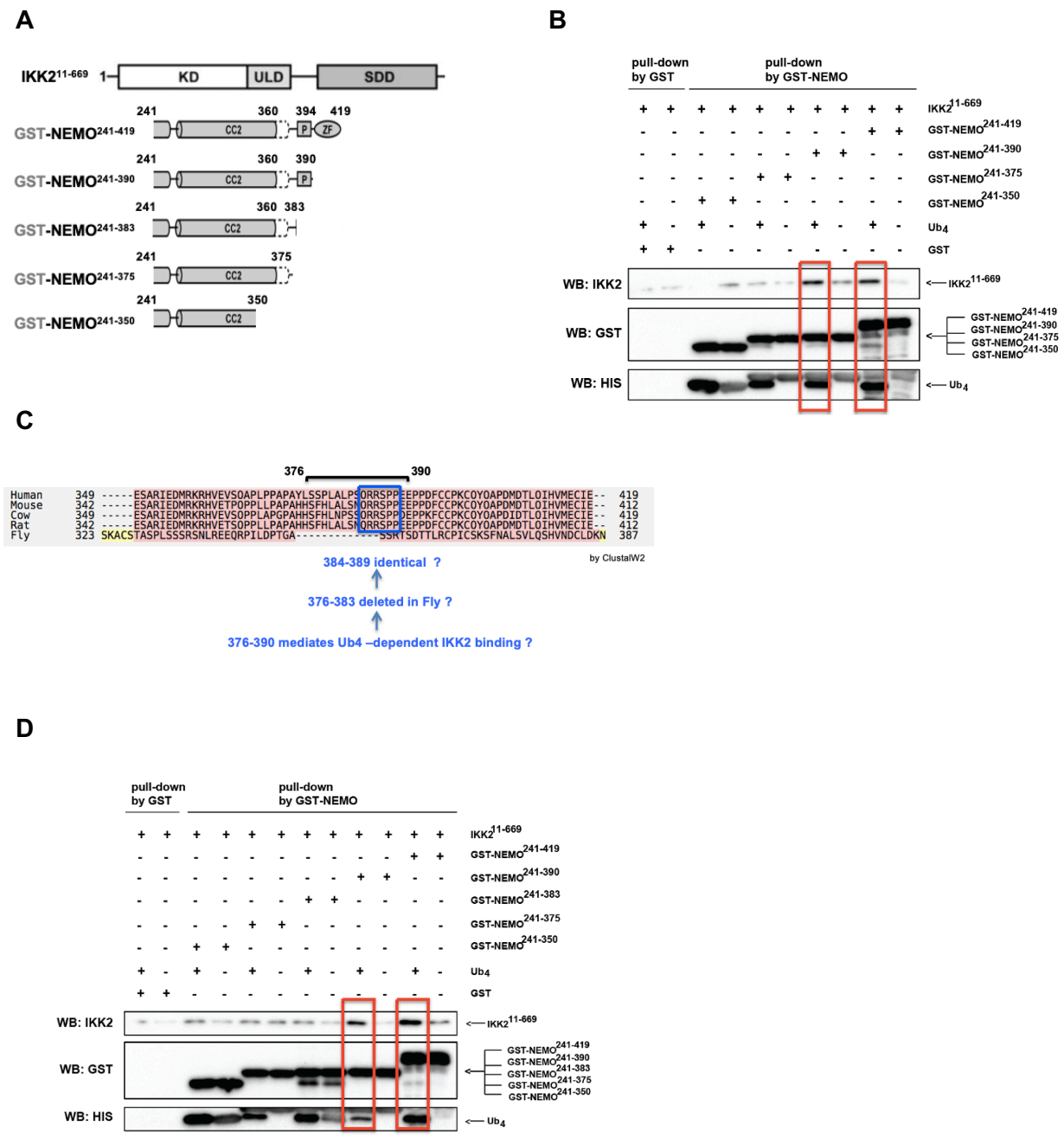

Figure 22. GST pull-down assays showing NEMO residues 384-389 is essential for 'second site' interaction with IKK2/β.

A) Cartoon for GST-fused NEMO constructs and IKK2/β B) and D) GST affinity pull down assay C) NEMO amino acid alignment from five different species by ClustalW2.

3.4.3 A short peptide segment immediately upstream of the Zn-finger domain of NEMO is essential for IKK2/β activation

Comparison of NEMO sequences revealed that residues spanning from 384 to 389 are highly conserved barring drosophila (Figure 22C). To further confirm if this segment is important, I generated two mutants in NEMO$^{241-419}$ background all six residues of 384-389 segment or the first three residues were mutated to glycine (NEMO^{6G} and NEMO^{3G}, respectively) and expressed as GST-fusion proteins. Affinity pull-down experiments showed that the interaction of GST-NEMO$^{241-419\ 3G}$ or GST-NEMO$^{241-419\ 6G}$ mutants to IKK2/β in the presence of Ub4 is almost abolished (Figure 23) suggesting the possible significance of this short segment in IKK2 activation.

I next generated identical mutants in full length background. These mutants were expressed in mammalian cells to monitor their potential to activate IKK2/β. Earlier studies established that when overexpressed, IKK2/β is partly autoactivated, and this activation is further enhanced (hyperactivation) in the presence of wt NEMO [12,18,60-61]. I found that this hyperactivation of wt HA-IKK2 is observed in presence of wt Myc-NEMO but severely diminished in the presence of Myc-NEMO^{6G} or Myc-NEMO^{3G} mutant (Figure 24). These results confirmed an important role of the 6-residues of 384-389 segment of NEMO in IKK2/β activation.

I wanted test if the peptide in isolation could act as a competitor of Ub-dependent interaction between NEMO and IKK2/β. To further validate this, I made a peptide spanning residues 375 and 391 and named it NEMO Activation Peptide (NEMO^{ActPep}). This peptide was covalently linked these peptides with a HIV-TAT peptide (TAT-NEMO^{ActPep}). A corresponding mutant peptide with residues 384QRRSPP389 altered to

384GGGGGG389 (mNEMO^{ActPep}) is used as a control (Figure 25). I performed affinity pull down using extracts of 293 cells transfected with plasmids harboring HA-IKK2. I mixed the extract with His-Ub4 and GST-NEMO$^{241-419WT}$ bound to beads in the absence or presence of increasing concentration of wt or mutant peptide. As expected, GST-NEMO was able to pull down HA-IKK2 in the presence of Ub4. However, this interact was disrupted at higher concentrations of wt peptide. The mutant peptide failed to block the NEMO-IKK2 interaction. Neither peptide made any difference in Ub4 binding to NEMO binding. These experiments indicate that the wt peptide but not the mutant competed out wt NEMO for its Ub4-dependent interaction to IKK2/β (Figure 26). Together, these results suggest a direct, signal-induced interaction of NEMO (through NEMO^{ActPep} segment) to IKK2/β (at a second site) that is essential for IKK2/β activation.

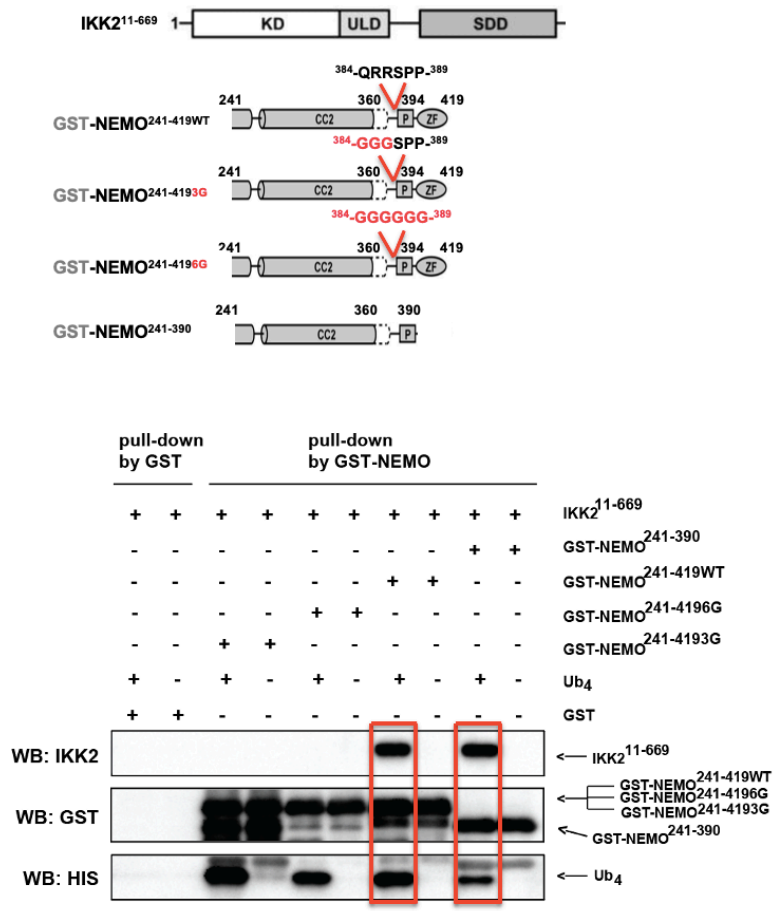

Figure 23. A GST pull-down assay confirming a short segment of NEMO spanning residues 384QRRSPP389 being essential for interaction with IKK2/β.
All six or the first three residues of the 384-389 patch were mutated to glycine in 6G and 3G mutant.

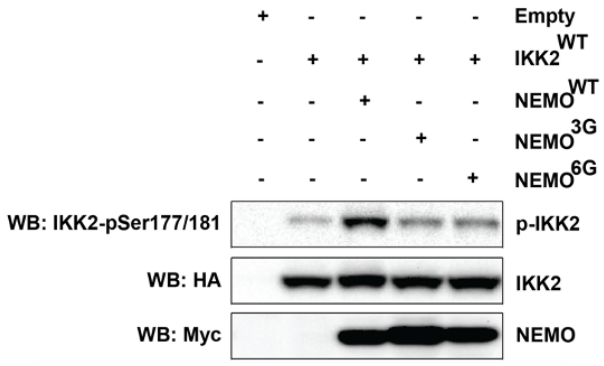

Figure 24. Mutant NEMO fail to induce IKK2/β activation in cells.
Western blot analysis of IKK2 AL phosphorylation of extract prepared from 293 cells transfected with IKK2 expression vector along with NEMO expression vectors. In the absence of NEMO, levels of IKK2 AL phosphorylation is low which is enhanced if wt $NEMO^{wt}$ is coexpressed. NEMOFL6G mutant is more defective than 3G mutant although appears to be less defective due to higher expression.
$NEMO^{3G}$: LPSQ384GR385GR386GEEP.
$NEMO^{6G}$: LPSQ384GR385GR386GS387GP388GP389GEEP

A

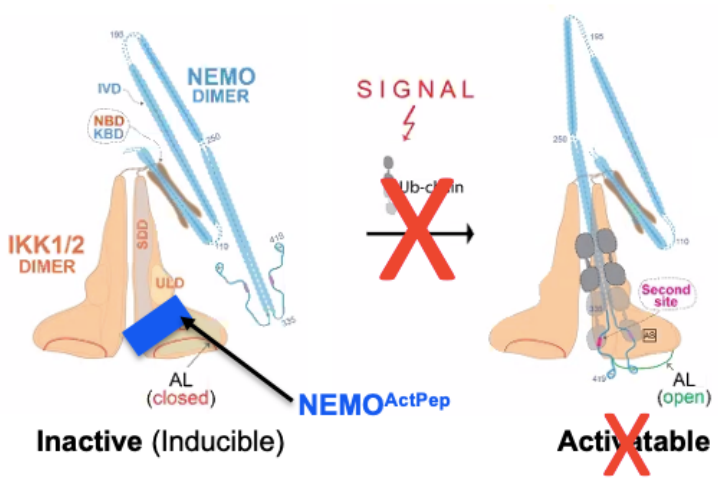

B

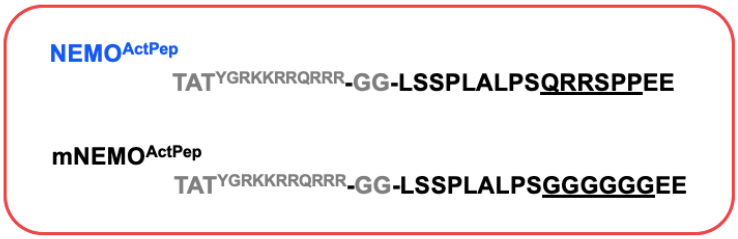

Figure 25. Development of cell permeable "NEMO Activation Peptide" (NEMO^{ActPep}). A)The segment of NEMO spanning residues 384QRRSPP389 can act either as an inhibitor or activator of IKK2 in isolation, referred this peptide as to NEMO^{ActPep}. B)Sequences of NEMO^{ActPep} and mutant NEMO^{ActPep} (mNEMO^{ActPep}).

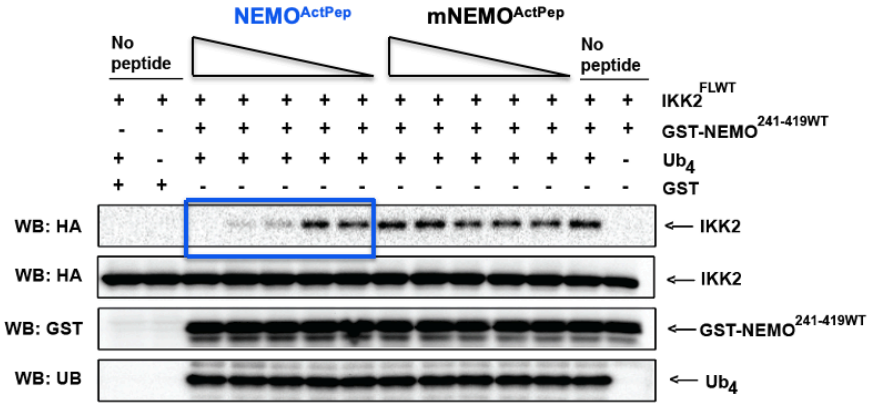

Figure 26. Inhibition of interaction between IKK2 and NEMOΔKBD by NEMO^{ActPep} but not mNEMO^{ActPep} *in vitro*.
HeLa cell extract containing HA-IKK2 was mixed with GST-NEMO$^{241-419}$ (lacking high affinity IKK2 interaction domain) in presence of linear tetra-ubiquitin chain (from right lanes, 2-12 &14). Only in presence of Ub4 IKK2 and NEMOΔKBD interacts (lane 2 from right). The interaction is blocked in the presence increasing conc. of NEMO^{ActPep} but not mNEMO^{ActPep}.

A

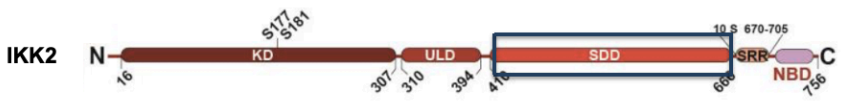

T381A, T383A, T385A, Q438A, K441AE442A, N445A, Q448AQ449A, M452A, M455A, M456A, M455AM456A, R460A, S463A, M468A, M552A, M468AK469A, E569A, P551AP552A, P551GP552G, R554AK555A, R554GK555GQ556G, E565A, D561AD562A, R572A, Q588A, R592A, L595A, Q599A, E602A, R606A, Y609AT610A, K614A, V617A

B

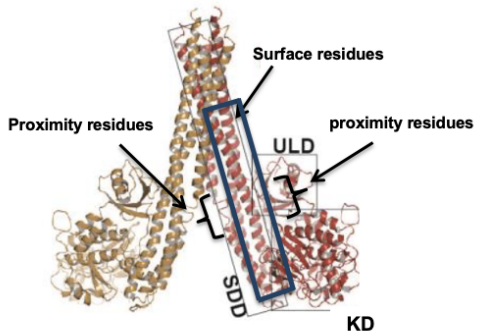

(Polley et al.,2013, 2016)

C

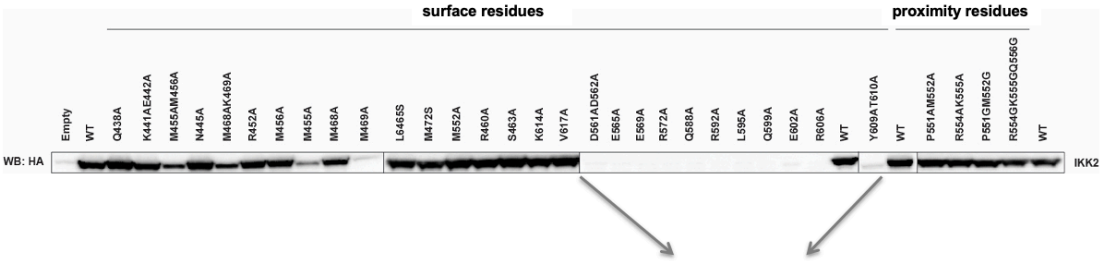

All mutants in this region were not expressed in HEK293T cells caused by disrupting its proper folding and stability

Figure 27. Identification of the IKK2/β docking site for the NEMO short segment through a second site.

A) and B) generated several mutants (total 36; 23 single, 12 double and 1 triple) of IKK2/β where surface residues were changed to Ala or Gly. C)Map of the IKK2 docking site for a new interaction in IKK2-NEMO All mutants in this region were not expressed in HEK293T cells caused by disrupting its proper folding and stability.

3.4.4 Identification of the IKK2/β docking site for the NEMO^{ActPep}

Since truncated IKK2/β proteins encompassing only the KD or KD along with ULD appear to be structurally unstable and thus inactive, I reasoned that the segment of SDD juxtaposed to KD-ULD provides the structural integrity and likely plays an important role in IKK2/β activation [60]. I postulate that this segment is a likely candidate to mediate Ub-dependent interaction with NEMO^{ActPep} as discussed above.

To test this possibility, I targeted several residues within the SDD. Few residues located in close proximity to SDD were also selected. Altogether I generated 36 mutants (23 single, 12 double, and 1 triple; Figure 27) rationally designed with information from previous structural and biochemical studies of IKK2/β. Most of these residues are located within the large triple-helical domain abutting the kinase and ULD domains. Since different IKK2/β mutants express differently with some showing very little or no expression perhaps because of structural instability due to mutations but few other mutants are shown overexpression seemed to be constitutive active forms [60], their levels were normalized to the wt level (Figure 27C and Figure 28).

The activities of these IKK2/β mutants were assessed by western blot with phospho-S181-specific antibody of extracts from HEK293 cells transfected with wt or mutant IKK2/β expression plasmids along with a NEMO expression plasmid. As discussed earlier, IKK2/β mutant(s) defective in enhancing AL phosphorylation in the presence of wt NEMO in transfection-based assay is considered to be defective in IKK2/β activation. Only three mutants, K441A, E442A, and N445A showed significantly reduced level of AL phosphorylation as compared to the wt IKK2/β (Figure 28). All three mutants

expressed similarly to the wt and the mutation sites are mapped on the surface of SDD, implying that the activation defect is unlikely due to a global structural distortion.

To further test if these mutants are defective in $NEMO^{241-419}$ binding, I performed GST pull-down experiments in which *E. coli* expressed GST-$NEMO^{241-419}$ was mixed with whole cell extracts of HEK293 cells expressing IKK2/β mutants from transfected plasmids, both in the presence or absence of *E. coli* expressed Ub4. All three of these mutants showed defective binding, whereas a control mutant Q438A that display no defect in AL phosphorylation showed wt binding (Figure 29).

Surprisingly, some mutants displayed higher levels of AL phosphorylation than the wt IKK2/β, alluding to the likely constitutively active phenotype of these mutants. I refer the $NEMO^{ActPep}$ binding site on IKK2 as IKK2 docking site. Figure 30 depict a model of how $NEMO^{ActPep}$ might be contacting the docking site.

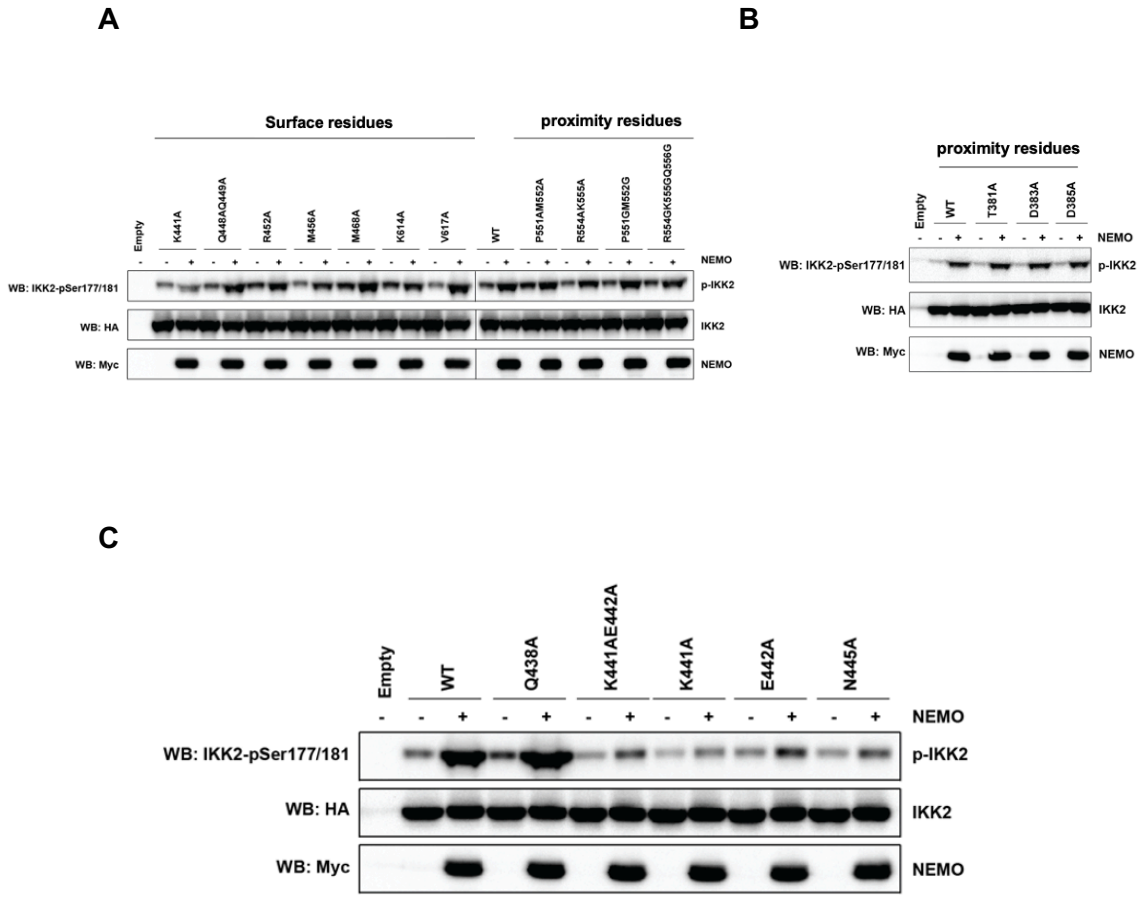

Figure 28. IKK2/β residues critical for IKK2/β AL phosphorylation.
A) and B) All mutants expressed in HEK293T cells were selected to examine NEMO-mediated IKK2/β activation C) Western blot analysis showing IKK2/β mutants defective in AL phosphorylation. only five mutants at residues K441A, E442A, and N445A showed defective NEMO-mediated IKK2 AL phosphorylation compared to the wild type.

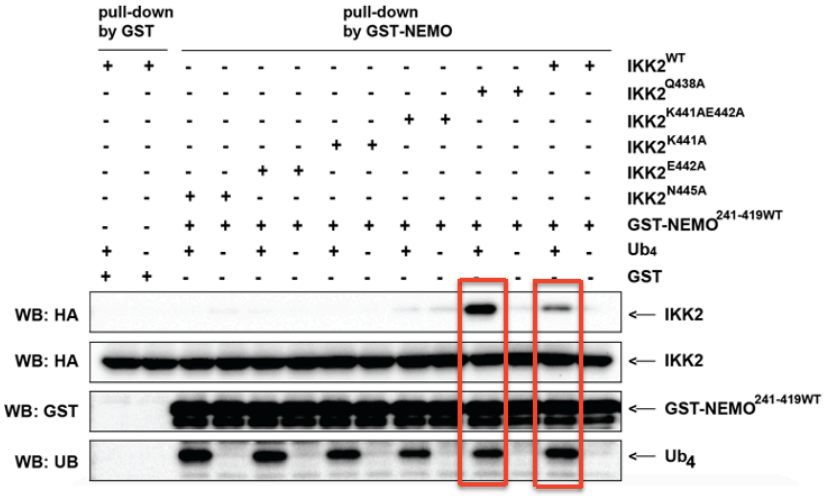

Figure 29. IKK2/β docking site interacting with NEMO$^{\text{short segment of 6 residues}}$.
GST pull down assay with mammalian cell extract and purified GST-NEMO and Ub4 showing binding only with WT IKK2 but not to the IKK2 K441, E442, and N445A mutants.

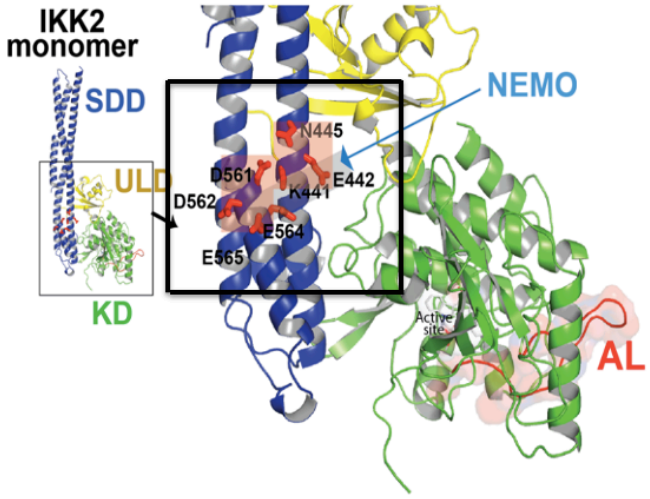

Figure 30. A model of signal-dependent interaction between NEMO and IKK2/β.
In addition to K441, E442 and N445, D561, D562, E564 and E565 could be important and together these residues might form a charged surface for interacting with highly charged NEMO^{384QRRSPP389}.

3.4.5 NEMO^{ActPep} blocks IKK2/β activation in cell

Aberrant IKK activation is associated with various human diseases including cancer and inflammatory diseases [25, 50, 63]. Despite tremendous efforts, IKK inhibitors have been failed in clinical trials mostly due to toxicity [45,141]. For more effective “drug like compounds” but keeping basal NF-kB activity and reducing potential toxic side effect [72], I developed cell-permeable peptides spanning residues NEMO 375-391 named NEMO Activation Peptide (NEMO^{ActPep}) selectively inhibiting NEMO-mediated IKK2 activation by blocking a second site interaction through canonical pathways.

I was intrigued by the ability of a short NEMO segment in weakly interacting and activating IKK2/β. Thus, I explored potential of this short segment peptide as a modulator. HeLa S3 cells were pre-treated with TAT-NEMO^{ActPep} or a mutant version TAT-mNEMO^{ActPep} (as a control) 1 hour prior to stimulation with 10 ng TNF-α for 15 min. NF-κB activation was measured by EMSA using nuclear extracts and IgkB site as the probe in the cell-extract (Figure 31A). Even at 10 μM NEMO^{ActPep} the shifted band was partially reduced and at 20uM the wt peptide nearly abolished NF-κB activation; however, the reduction was not noticeable with the mutant peptide. I further verified IKK2 activation by measuring AL phosphorylation, IκBα degradation, and RelA nuclear localization. As expected, wt peptide was able to block IKK2 phosphorylation, IκBα degradation and nuclear localization of RelA (Figure 31C). Mutant peptide showed no such effect and neither peptide affected DNA binding of the transcription factor Oct-1 [72].

I next tested if the effect is universal, RAW murine macrophages cells were used to monitor the properties of an effective inhibitor as described above. Indeed, DNA binding and RelA nuclear localization were inhibited due to failure of IKK2 activation and IκBα

degradation. Again, the mutant peptide failed to show any effect (Figure 32). I also tested the effect of these peptides on MEF cells by EMSA and IKK2 activation. TAT-NEMO^{ActPep} but not TAT-mNEMO^{ActPep} inhibited IKK/NF-κB activation in response to TNF-α (Figure 33). These results suggest that the peptide prevents IKK activation, and consequently block IκBα degradation, nuclear localization of RelA, and its DNA-binding.

While a trigger by TNF-a or LPS NEMO-mediated IKK2 phosphorylation is indispensable for the activation of NF-κB through the canonical pathway, a trigger by LTβR NIK-mediated IKK1 phosphorylation regulates NF-κB signaling through the non-canonical pathway where IKK1 activation leads to processing of p100 and generation of the NF-κB subunit p52 [4,44,65]. However, affinity binding assay showed that NEMO$^{241-419}$ could interact with IKK1 in the presence of Ub4 through a second site (Figure 21). To clarify the role of IKK1 in the new interaction with NEMO, I also tested the effect of the peptide on IKK1 activation by measuring processing of p100 to p52 to assess the specificity of the peptide towards IKK2 vs IKK1 (Figure 34A). Neither the WT nor the mutant peptide were able to block p52 processing suggesting that NEMO^{ActPep} is functional only in canonical NF-κB activation pathways.

Since, MAP kinases such as ERK, JNK and p38 are involved in another signaling pathway that plays a critical role in inflammation through activation of NF-κB [27,116]. To further show specificity of the peptide, I tested if MAPK activation by TNF-α is affected by the inhibitor by monitoring activation of JNK, Erk2 and p38. As expected all three MAP kinases are activated by TNF-α but no effect of either the wt or mutant peptide was found on these MAP kinases (Figure 34B).

A

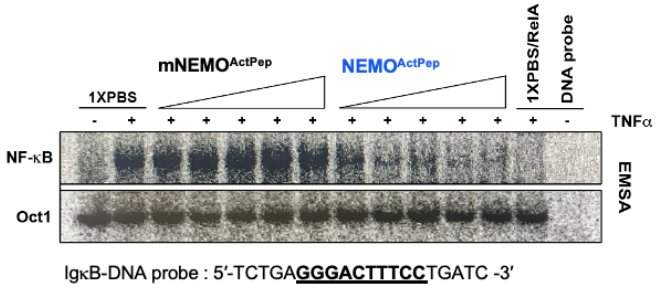

B

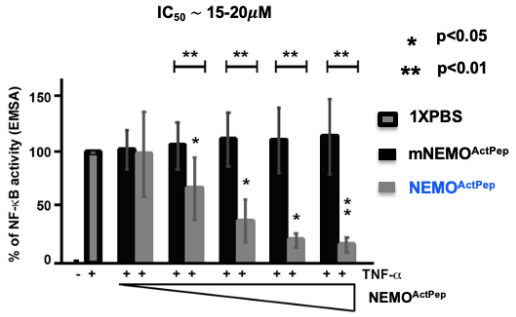

C

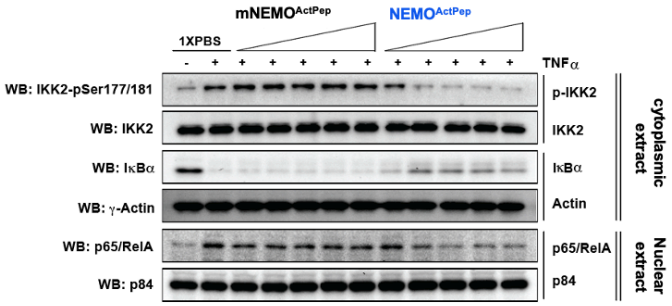

Figure 31. NEMO^{Actpep} was able to block IKK2-NF-kB activation pathway in HeLa.
Effect of NEMO^{ActPep} and mNEMO^{ActPep} on A) p65 (RelA) DNA binding using EMSA B) IC_{50} of ~ 15-20 μM on NEMO^{Actpep} inhibition of NF-kB activation C) IKK phosphorylation, IκBα degradation, RelA nuclear localization in HeLa cells by WB using specific antibodies. IKK2, γ-Actin, and α-p84 Ab denote loading control in total and nuclear extracts, respectively. Data between different groups were compared by unpaired t-test. *, $p < 0.05$. **, $p < 0.01$.

A

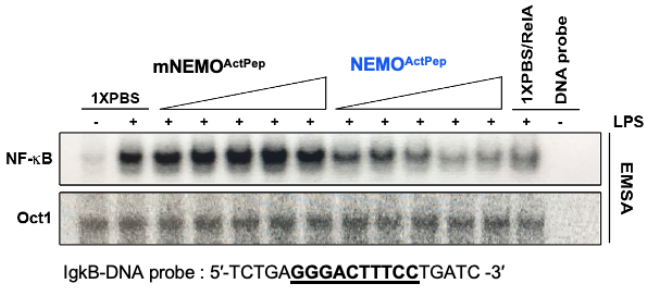

B

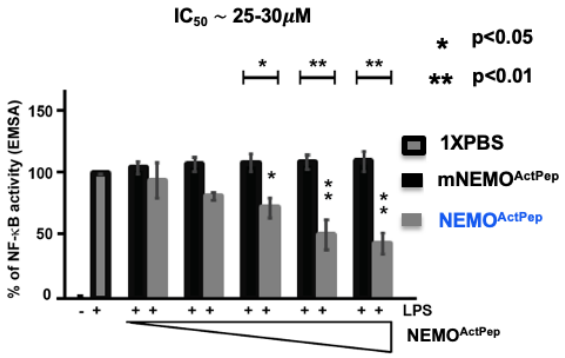

C

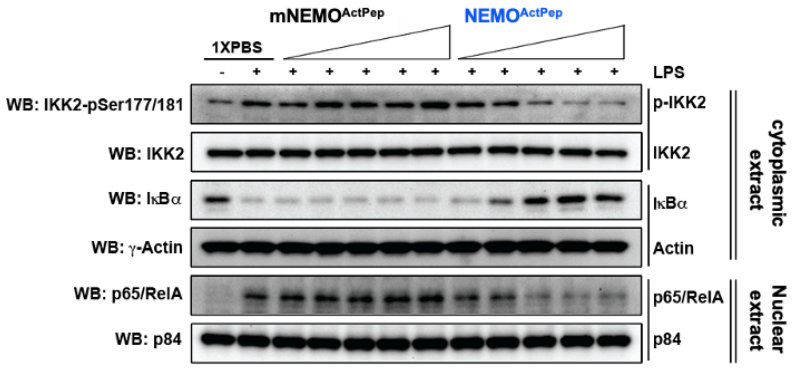

Figure 32. NEMO^{Actpep} also blocked LPS-induced IKK2-NF-kB activation in macrophage RAW cells.

Effect of NEMO^{ActPep} and mNEMO^{ActPep} on A) p65 (RelA) DNA binding using EMSA B) IC_{50} of ~ 25-30 μM on NEMO^{Actpep} inhibition of NF-kB activation C) IKK phosphorylation, IκBα degradation, RelA nuclear localization in RAW murine macrophage cells by WB using specific antibodies. IKK2, γ-Actin, and α-p84 Ab denote loading control in total and nuclear extracts, respectively. Data between different groups were compared by unpaired t-test. *, $p < 0.05$. **, $p < 0.01$.

A

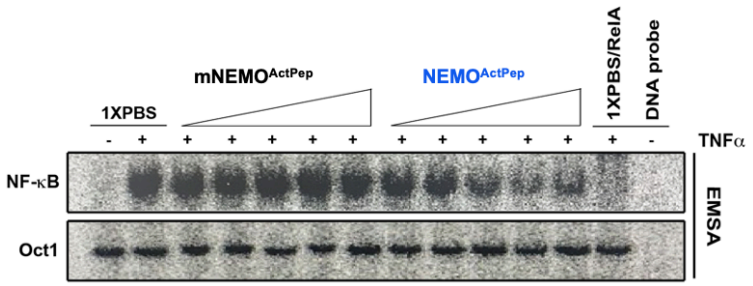

B

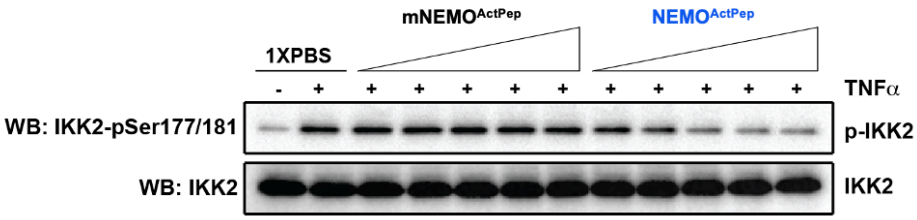

Figure 33. NEMO^{Actpep} also blocked TNFa-induced IKK2-NF-kB activation in MEF cells. Effect of NEMO^{ActPep} and mNEMO^{ActPep} on A) p65 (RelA) DNA binding using EMSA B) IKK phosphorylation in MEF cells by WB using specific antibody. IKK2 Ab denote loading control.

A

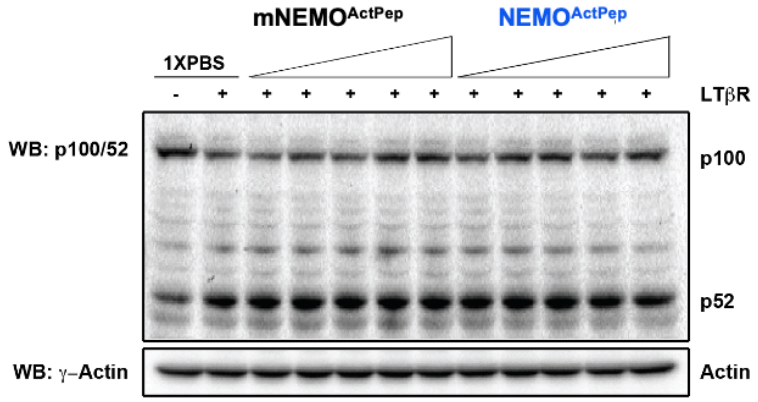

B

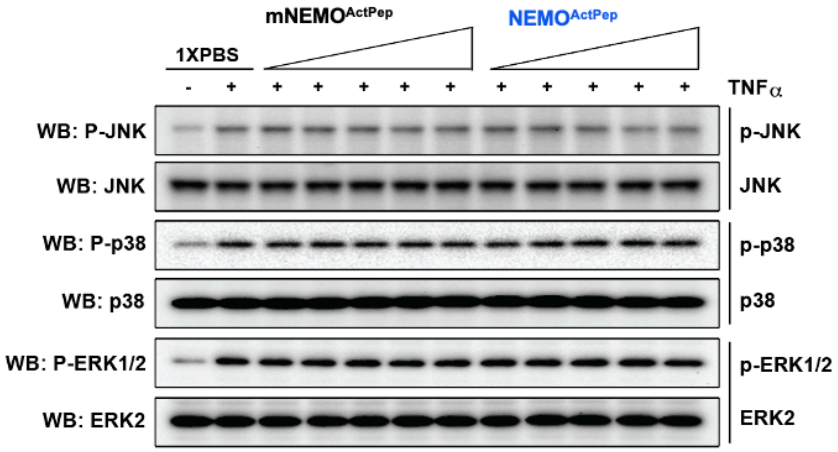

Figure 34. NEMO^{ActPep} is specific only in canonical NF-κB activation pathways.
A) Effect of NEMO^{ActPep} on the LTβR-induced NF-kB activation on non-canonical pathway by WB using specific antibodies. B) Effect of NEMO^{ActPep} and mNEMO^{ActPep} on MAP kinase activation by TNFa by WB using specific antibodies. γ-Actin, ERK, JNK, and p38 Ab denote loading control in total extracts, respectively.

3.4.6 NEMO^{ActPep} protects mice from LPS challenge

I next investigated the effect of NEMO^{ActPep} in vivo, collaborating with School of Medicine. I wished to investigate if NEMO^{ActPep} can protect mice from the cytokine storm. I determined the minimum LPS dosage that is lethal to mice [142]. Mice of body weight approximately 20g when challenged with ~1.2 mg of LPS died within 24 to 96 hours. Thus, I challenged mice with this dose of LPS 1 hour after injection with 800 μg (40mg/kg) of NEMO^{Actpep} or mNEMO^{ActPep} and scored viability. All 5 mice pretreated with NEMO^{ActPep} survived during the entire course of the experiment (sacrificed after ten days); however, all 5 mice pre-treated with mNEMO^{ActPep} died within 4 days (Figure 35).

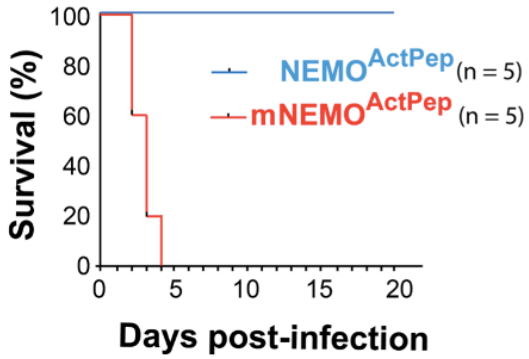

Figure 35. Survival plot of mice treated with NEMO^{ActPep} (blue) and mNEMO^{ActPep} (red) 1 hr prior to injection of LPS.
NEMO^{ActPep} were administrated subcutaneously into each mouse. Each mouse was injected 800μg/100μL of NEMO^{ActPep}.

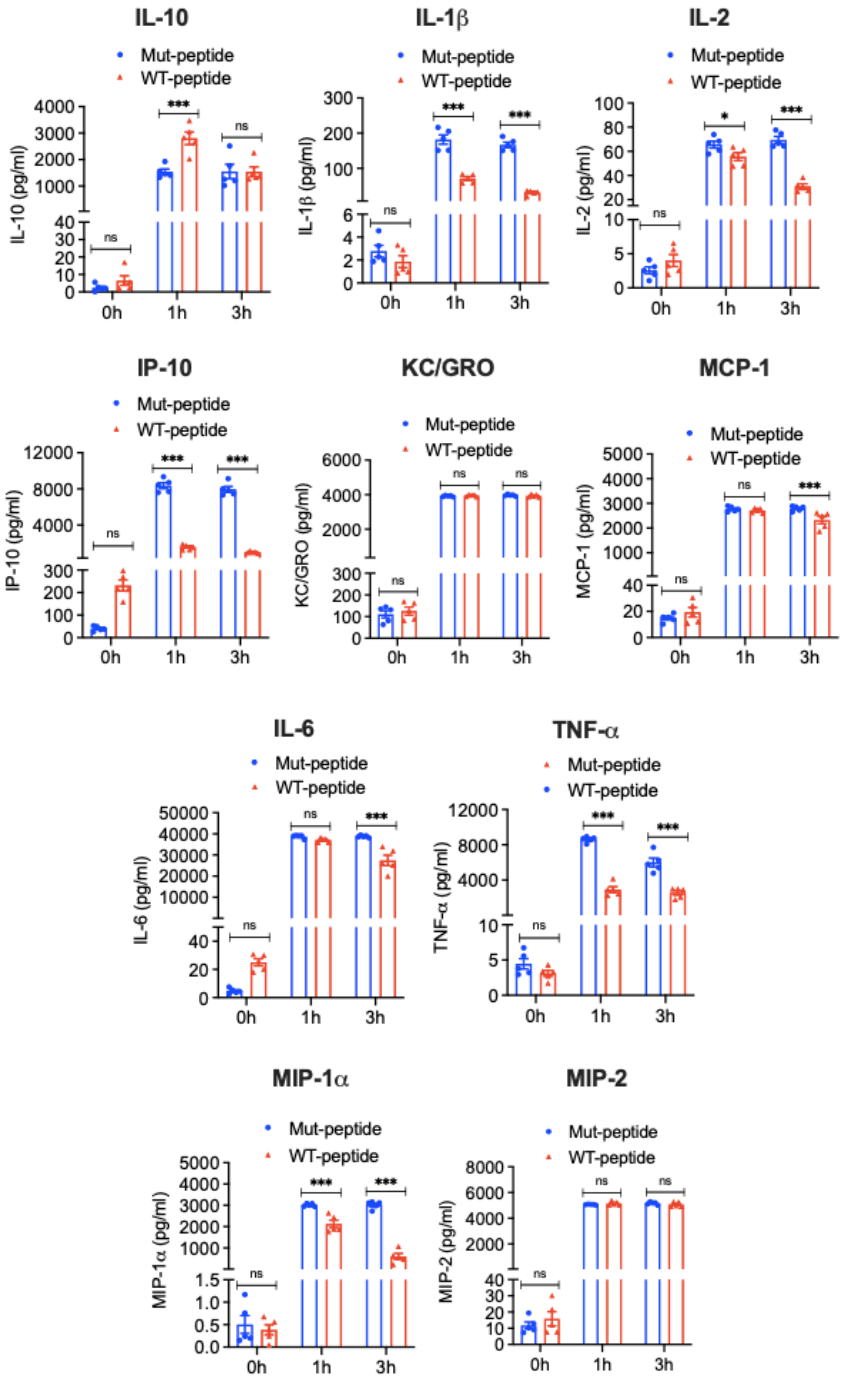

Figure 36. NEMO^{ActPep} blocked cytokine storm upon LPS treatment.
Expression of IL-1β, IL-2, IL-6, IL-10, KC/GRO, IP-10, TNF-α, MCP-1, MIP1 and MIP2 in plasma of mice measured by ELISA. Data between different groups were compared by unpaired t-test. *, $p < 0.05$. **, $p < 0.01$. ***, $p < 0.001$.

3.4.7 NEMO^{ActPep} selectively blocks cytokine storm in LPS-induced inflammatory response of mouse plasma

NF-κB activity is required for maximal transcription of many cytokines, including tumor necrosis factor-α (TNF-α), interleukin-1 (IL-1), IL-6, and IL-8, which are thought to be important in the generation of acute inflammatory responses [136-137]. However, excessive cytokine-mediated inflammation is likely to be crucial in the pathogenesis of a variety of disease states [136-140]. In order to clarify the NEMO^{ActPep} role of NF-κB in LPS-induced inflammatory response, mice were challenged with LPS treatment at 0, 1, and 3 hours after peptide injection to check the inflammatory level by cytokine expression. The ELISA results were observed that compared with the mice treated with mutant NEMO^{ActPep}, NEMO^{ActPep} showed that the expressions of inflammatory factors IL-1β, TNF-α, IL-2, IP-10, and MIP1 were significantly decreased 1-3 hours after LPS challenge. However, by 3 hours after LPS the levels of IL-6 and MCP-1 were reduced only to a small extent. The LPS-induction of KC/GRO and MIP-2 in both treatment groups remained unaffected after LPS. In contrast, the LPS-induction of IL-10 was not reduced, but rather exhibited modest elevation 1 hour after LPS challenge then by 3 hours went down and kept the same level as mutant NEMO^{ActPep} treatment (Figure 36). It appears that NEMO^{ActPep} selectively inhibits levels of cytokine in LPS challenge mice.

3.5 SUMMARY of the STUDY

The IkB Kinase (IKK) complex is a signaling hub that integrates many diverse cell signaling inputs and transmits them to downstream effectors including the NF-kB family transcription factors [51]. Two key events associated with IKK regulation towards NF-kB activation through the canonical signaling are that switch from inactive to active via AL phosphorylation in IKK2 is the most critical function of canonical signaling and non-covalent interaction between the linear Ub-chain and NEMO is essential for the AL phosphorylation of IKK2 [11,14,26,51,70,80]. The end result of this process is the inducible control over select response gene expression via transcription factor NF-κB [51,56,58].

However, aberrant NF-κB transcriptional activity plays pivotal roles in a large number of human pathologies, including a variety of cancers and chronic inflammatory diseases [25,68-69]. Therefore, there has been a large increase in studies aimed at identifying and testing drugs or small molecule inhibitors that would specifically block NF-κB activation in inflammatory diseases and cancer [25, 83,92-94].

In this study, I describe an in vivo and in vitro systems to test the inhibitory effects of the novel inhibitor of NEMO Activation Peptide ($NEMO^{ActPep}$) on IKK-NF-κB activation. A novel interaction between IKK2-NEMO was discovered as showing “a new second site" where Ub-chain binding stabilizes NEMO dimer leading to its conformational change resulting in the AL phosphorylation of IKK2. In vitro and In vivo studies, cell-permeable peptides of a short segment of NEMO targeting this second site selectively inhibited NEMO-mediated IKK2 activation by blocking the second site interaction but neither the WT nor the mutant peptide were able to block other signaling pathways by IKK1 and MAP

kinases activation. Furthermore, $NEMO^{ActPep}$ protected mice from LPS challenge and selectively blocked cytokine storm in LPS-induced mouse inflammatory response. Thus, this peptide inhibiting NF-kB activation may be an effective approach to the treatment of inflammatory diseases.

Although we still need to investigate if $NEMO^{ActPep}$ could be more active in spiteful cells than in normal cells, it is promising that this peptide controls NF-κB activation without any effects on other signaling pathways as shown neither the WT nor the mutant peptide were able to block through non-canonical and MAPK signaling pathways.

In addition, for selectively targeting specific NF-κB signaling component in a particular disease, one may expect to minimize side-toxicity and avoid wide suppression of innate immunity [15, 25-26,45, 72,143]. It should also consider that excessive and prolonged NF-κB inhibition can be harmful due to its important role in innate immunity [45,51,143]. Inhibition of NF-κB activation should be transient and highly reversible to avoid long-term immunosuppression [7,143].

Drugs targeting the IKK-NEMO interaction may be clinically important for the regulation of inflammation. The $NEMO^{ActPep}$ is only 6 amino acids long, so one should expect to design as a drug-like compound that disrupt the NEMO-IKK interaction, which may possibly maintain a low level of NF-kB activity that may be required to avoid potential toxic side effects and manage long-term immunotherapy treatment. I conclude that $NEMO^{ActPep}$ is a potent inhibitor of NF-κB and NF-κB-regulated gene products and may be a valuable new drug candidate for the treatment of inflammation and cancer.

3.6 ACKNOWLEDGEMENTS

Chapter three, this research was supported by various grants from organizations including the National Institutes of Health *(*NIH*)* (CA141722), Tobacco-Related Disease Research Program (TRDRP), and American Association for Cancer Research (AACR).

CHAPTER FOUR

4. DISCUSSION

In Ubiquitin (Ub)–proteasome pathway [170], a protein targeted for degradation is first modified by covalent attachment of Ub, a highly conserved polypeptide of 76 amino acids. Ubiquitination is a three-step process. First, Ub is activated by a Ub-activating enzyme (E1); the activated Ub is then transferred to a Ub carrier protein (E2, also referred to as Ub-conjugating enzyme [Ubc]); finally, Ub is conjugated to a protein substrate by forming an isopeptide bond between the C-terminal glycine residue of Ub and the ε-amino group of one or more lysine residues of the protein substrate. This conjugation step often requires a Ub protein ligase (E3). Multiple molecules of Ub can be ligated to a protein substrate to form multi-Ub chains, which are then recognized by a large ATP-dependent protease (molecular mass ~2000 kDa) know as 26S proteasome [170].

Signal-induced activation of the transcription factor NF-κB requires inactivation of IkBa that is a well characterized example of coupling between phosphorylation and ubiquitination. Ubiquitination of IkBa is regulated by its site-specific phosphorylation at S32 and S36, residues required for the signal-induced phosphorylation and degradation of IkBa in vivo. Chen [171], in 1996, reported the identification of a large, multisubunit kinase (molecular mass ~700 kDa) that phosphorylates IκBα at S32 and S36. The activity of this kinase requires the Ub-activating enzyme (E1), a specific Ub carrier protein (E2) of the Ubc4/Ubc5 family, and Ub but not requires E3. This ubiquitination event in the kinase complex is a prerequisite for specific phosphorylation of IκBα [171], which serves a novel regulatory function that does not involve proteolysis. Since multiubiquitination of

protein substrates usually requires an E3, the IκBα kinase complex probably contains an E3 activity or other proteins in cells can act as E3. Thus, the identity of this E3 and the target of ubiquitination remained to be determined.

Over several decades the IkB kinase responsible for the initial and critical step of NF-kB activation has been started to be the subject of intense interest and many kinases had been proposed as candidates. In earlier studies, CHUK (Component of Inhibitor of Nuclear Factor Kappa B Kinase Complex) was described serine-threonine kinase of unknown function, in yeast tow-hybrid screen for NIK-interacting proteins [180]. In 1997, however, CHUK was identified as an activator of a NF-kB dependent reporter gene when overexpressed [179]. Regnier reported that a catalytically inactive mutant of CHUK suppresses NF-kB activation induced by TNF and IL-1 stimulation as well as by TRAF2, TRAF6, and NIK overexpression. CHUK associates with both NIK and IkBa in mammalian cells. CHUK phosphorylates IkBa on serines 32 and 36, and this phosphorylation is strongly enhanced by NIK costimulation. These findings demonstrate that CHUK is an IkBa kinase that directly associates with and is activated by NIK. Additionally, Didonato tested cell extracts for the presence of a protein kinase activity that is activated by tumor-necrosis factor (TNF) and phosphorylates IkBa at S32/36. He found that such an activity was detected in extracts of TNF-treated HeLa cells and its substrate specificity and kinetics of activation correlated well with those of IkBa phosphorylation in living cells. He purified this activity and determined a partial peptide sequence for one of its components. Molecular cloning and functional analysis identified this subunit as a protein kinase whose associated IkB kinase activity was rapidly stimulated by proinflammatory cytokines. This activity was inhibited upon dephosphorylation with protein phosphatase 2 (PP2A). Thus,

he demonstrated that this is protein kinase IKKα, is critical for NF-kB activation in response to proinflammatory cytokines. Although many kinases have been proposed as candidates, but only CHUK IKKα, which referred to as IKK1, had the characteristics expected of a cytokine-inducible IkB kinase. Strikingly, in another lab, Mercurio identified IKK1 and he also observed an additional component which is the closely related kinase IKK2 as interacting components of the IKK signalsome, a multiprotein signaling complex that regulates NF-kB activation in response to proinflammatory cytokines [181]. He identified that IKK1 and IKK2 are functional kinases within the IKK signalsome that mediate IkB phosphorylation and NF-kB activation. As a protein complex containing multiple interacting components, including a RelA kinase, the IKK signalsome containing IKK1 and IKK2 had the potential to integrate the diverse signaling pathways known to activate NF-kB in different cell types and channel them toward selective gene expression.

In Michael Karin lab, in 1998, they purified the IKK complex to homogeneity from human cell lines by using a monoclonal antibody against IKK1 [182]. Surprisingly, they observed that IKK was composed of similar amounts of IKK1, IKK2 and two other polypeptides, for which they obtained partial sequences. These polypeptides were differentially processed forms of a third subunit, which was called NEMO. Molecular cloning and sequencing indicated that NEMO was composed of several potential coiled-coil motifs. NEMO interacted preferentially with IKK2 and was required or the activation for the IKK complex. Moreover, NEMO carboxy-terminal truncation mutant that still bound IKK2 blocked the activation of IKK and NF-kB. Reduced NEMO expression resulted in deceased IKK activation and its complete absence abolished IKK and NF-kB activation altogether. Although IKK activity was absolutely dependent on IKK1/2 dimerization,

NEMO was shown unlikely to function as a chaperone or a co-factor that stabilized IKK1-IKK2 dimers. In vitro, NEMO stably interacted with IKK2 and not with IKK1, it was likely that once recruited into the complex NEMO also interacted with IKK1.

NEMO has been shown to participate in ubiquitin-mediated NF-κB signalling by either being ubiquitinated or interacting with the polyubiquitin chains of the other signalling components [176]. It was shown that ubiquitin forms diverse polychains through isopeptide bond between the Gly76 of a distal ubiquitin molecule and one of seven lysines (K6, K11, K27, K29, K33, K48, or K63) located within a proximal ubiquitin, and distinct functions have been attributed to the different lysine linkages [173]. Recently, a novel form of polyubiquitin linkage was introduced into the NF-κB signalling paradigm, where ubiquitin chains were connected with a peptide bond between Gly76 of one ubiquitin and Met1 of another ubiquitin [172,177]. It was shown that NEMO linear ubiquitination is required for efficient NF-κB activation induced by TNFα, which may also depend on the specific recognition of linear polyubiquitin by NEMO [177]. Consequently, linear ubiquitin chain formation is a key early event in the activation of the pathway. Later on, people identified that the IKK complex does not contain an E3 activity, but the ubiquitination of NEMO with linear ubiquitin chains is performed by the E3-ligase linear ubiquitin chain assembly complex (LUBAC) [176]. LUBAC consists of the proteins HOIP, HOIL-1L, and Sharpin, which HOIP and HOIL-1L belong to the RBR class of E3-ligases [6]. Even though both HOIP and HOIL-1L have an RBR domain, HOIP is the catalytic subunit of the complex [174-175]. The linear ubiquitin chain-forming activity and specificity of LUBAC is completely embedded within HOIP, which is the only E3 ligase that is known to build linear ubiquitin chains.

The formation of linear ubiquitin chains on NEMO by LUBAC requires the “priming” of the first ubiquitin on a NEMO lysine and ubiquitin chain formation on the ubiquitin N terminus, two reactions with different chemistries. Currently, it is unknown how this dual target specificity is regulated and how the molecular mechanisms involved in this process have not been fully elucidated. Furthermore, the role of NEMO linear ubiquitination in transducing signals to the cytoplasmic IKK complex, facilitating sequential activation of IKK in the NF-κB signaling pathways remained to be determined. This study provides a key into understanding molecular events leading to IKK activation, how specific signals selectively activate IKK2 within an IKK complex, with the help of pathway-specific modulator, NEMO.

The NEMO regulatory subunit plays a critical role in the assembly of the IKK complex and is thought to link the IKK complex to upstream activators by mechanisms that remain to be defined. First of all, to address what structural changes occur in NEMO when it interacts with IKK2, I performed biophysical characterizations on purified full-length NEMO and a series of NEMO deletion and disease-associated point mutants as well as various IKK2:NEMO complexes. NEMO exists as an elongated homodimer in solution with propensity to form oligomers and further is held together through a mutually regulatory dynamic association/competition between individual elements. Published papers showed that different regions of NEMO exert distinct functions. For example, the amino terminus is necessary for interaction with the IKKs [74], whereas the carboxy terminus of NEMO is required for binding to ubiquitin or the deubiquitinase CYLD or for the oligomerization of NEMO [34]. From the analysis of the solution behavior of NEMO truncated fragments, I specifically observed a distinct function in a region defined

intervening domain residues between 110-194 and the IVD controls over NEMO dimerization through flanking coiled coil regions, perhaps by competitively adopting its own unique helical homodimeric structure and my analysis of several of these mutant NEMO proteins revealed that they exhibit drastically altered solution behavior.

Over many years, published reports demonstrated that glycerol gradient ultracentrifugation analysis provided the composition of the IKK complex observed its heterogeneous composition under near-physiological conditions. IKK complex assembly has been previously characterized mainly by gel filtration in 293T, yeast, and HeLa cells, and several groups observed the formation of a large complex (700–900kDa) most of the time under conditions of overexpression [27, 65, 86, 96]. Probably, the molecular mass measurement of the IKK complex by gel filtration is erroneous mainly because of the abnormal hydrodynamic properties of NEMO. Indeed, whereas the calculated molecular mass of the NEMO subunit is 50kDa, I observed NEMO expressed in Escherichia coli is eluted as a 700-kDa protein corresponding by SEC. Similar abnormal behavior was observed with tight NEMO–IKK2 heterocomplexes which display an erroneous molecular mass as higher than 1200 kDa on gel filtration, probably caused by NEMO. I demonstrate that, in contrast, by SEC-MALS and AUC my data suggest that purified recombinant IKK2–NEMO complexes do not undergo a significant change but it is clear that adding NEMO to IKK2 strengthens the propensity of IKK2 oligomerization. Transient oligomerization of IKK2 in a conformation that promotes trans auto-phosphorylation would naturally direct and amplify the activity of any signaling kinase functioning directly upstream of IKK2 to quickly generate a pool of catalytically active IKK2, consistent with the rapid amplification of IKK2 phosphorylation that is observed in vivo [88,91,136]. The

introduction of mutations within the oligomerization interfaces observed in the IKK2 X-ray crystal structure is sufficient to disrupt activation suggests that small molecules designed to interfere with oligomerization through these interfaces should function as specific inhibitors of IKK2 [60]. Therefore, the crucial role for oligomerization of NEMO in the assembly and function of the IKK complex is reflected in the fact that the IKK complex can be activated by enforced oligomerization of NEMO [52,62,96]. Moreover, I observed that C-terminal deletions to NEMO do not appear to influence the ability of the multisubunit IKK heterotetramer to assemble so long as the KBD is preserved in NEMO. This might suggest that association of dynamic NEMO to IKK2 dimers serves to attenuate whatever influence the IVD exerts on NEMO structure and dynamics. In the absence of additional knowledge concerning the surfaces employed by IKK2/β and, to a lesser degree, NEMO homodimers to induce oligomerization of multisubunit IKK, it is challenging to predict how NEMO exerts control over higher order oligomerization of IKK. It remains to be determined what, if any, functional significance is owed to higher order oligomerization of $NEMO_2$:$IKK2_2$ tetramers in the cell.

The first protein kinase A (PKA) structure solved was in an active and phosphorylated state. The structure showed that a phospho-residue in the activation segment interacts with a pocket of positively charged residues on the surface of the kinase (Knighton et al., 1991). The earliest inactive structures showed that an unphosphorylated activation loop could adopt a variety of conformations that were different from protein kinase A and, in some cases, even exhibited disorder in the crystal structures [100,144-146]. A lot of people paid too much attention to the global conformation of the kinase, such as how the small lobe is positioned relative to the large

lobe and how the nucleotide binding site is “open.” Brad, in early 2000s, identified a larger region than what was previously defined (DFG.....APE) [100]. In order to make it clear that this was a bigger region than previously defined activation loops. Sometimes people used to call them the "T loop" because this region contains a phosphorylated Threonine residue in PKA. Brad started calling this the "activation segment". Now people call it "activation loop" again but it has been redefined to contain all of these sequences. Brad's insight, which came from his study of the structures of known kinases in their active and inactive states back in 2002 and his study of a particularly interesting SR protein kinase in yeast called Sky1p that was constitutively active without requirement for any activating factor, was that positioning of residues within this segment was the key for determining whether a kinase is active or not. By comparing the activation segments from currently available active protein kinase structures, several structural features characteristic of the active state were defined [100] and also showed that certain regions of the activation segment exhibit significant conformational diversity. These issues include, for instance, how activation loop conformation works together with active site residues, how phosphorylation induces an active conformation in some kinases, and why it is not required in others.

The human IKK2 x-ray crystal structure determined in 2013 [60]. The Kinase domain (KD) exhibits all of the sequence and structural features typical of a functional catalytic KD in its active conformation, which is similar to protein kinase A. Residues from the catalytic loop, the phosphate binding site, and the magnesium binding loop occupy the positions of an ordered catalytic center that can catalyze the phosphoryl transfer reaction. For example, the K44–E61 pair contributed by beta-strand β3 and alpha-helix

αC is properly oriented to form a salt bridge, the DFG tripeptide residues of the Mg^{2+} binding loop (DLG in IKK2) occupy their "active" positions, the catalytic base D145 is poised for catalysis, and the beta-sheet formed by strands β6 and β9 contains three hydrogen bonds, a signature feature of all active kinases. Furthermore, the KD within the IKK2 crystal structure also exhibits the constellation of buried hydrophobic residues that form the "spine" of an active protein kinase [60,100]. Moreover, the x-ray structure of two different subunits of IKK2/β revealed two different conformations [100, 147]. One of the subunits was fully phosphorylated where the other was not. Thus, I wanted to investigate the solution confirmation of AL in it inactive and active states. K44 in KD of IKK2 contacts the phosphate of ATP which is essential for catalytic activity of IKK2/β. Both K44M mutant and wt IKK2/β were expressed as truncated form (11-669) in baculovirus. The AL of wt IKK2/β but not K44M undergoes phosphorylation due to overexpression. K44M could not underwent trans autophosphorylation. This is consistent with all phospho-modification induced protein kinases that the AL conformations of IKK2/β are different between modified and unmodified AL. For the modification of AL serines/thronine/tyrosines different kinases use different mechanism.

In IKK2 activation through canonical pathway, moreover, the association with NEMO to IKK2 can help IKK2 readily activated in response to early signaling events including receptor-mediated signalsome assembly and poly-ubiquitin chain formation. As shown in my in-vitro trans autophosphorylation, kinetics of phosphorylation of the AL of full length kinase dead (KD) IKK2/β K44M mutant by an active truncated $IKK2^{11-669}$ underwent conformational change into an 'open state' to be targeted by an active kinase and further when interaction between the sensor region of IKK2/β and the NEMO:Ub4

induced conformational change of the AL, the rate of phosphorylation was significantly greater in the presence of the NEMO:Ub4 complex than NEMO with the absence of Ub4. Phosphorylation by protein kinases is recognized as a critical mechanism by which virtually every activity of eukaryotic cells is regulated, including proliferation, gene expression, metabolism, motility, membrane transport, and apoptosis. Perhaps, In this process to inactive IKK2 becoming inactivate to activate states, phosphorylation can occur in 1 second for altering metabolic rate, have kinetics spanning hours that are both reversible and highly coordinated for orchestrating complex with proteins “helper” in physiological processes, and act as a means of signal amplification**,** and the activation of a single kinase molecule can result in the phosphorylation of many proteins that can be itself or other proteins [2,3,8,10]. Although the overall fold of protein kinases is conserved, differences in the core sequence and flanking regions between kinases can also allow each kinase to respond to a unique set of signals to turn their activity on or off. However, the precise mechanism by which NEMO prepares IKK2 for activation remains unclear, though it is apparently passive as the ability of NEMO to interact with IKK2 remains unchanged throughout the process of NF-κB induction. It is apparent that the dependence upon NEMO for IKK2 activation can be circumvented by increasing the IKK2 concentration either in vitro or by its overexpression in transfected cells. This is why transfected IKK2–NEMO complexes are active while endogenous IKK2–NEMO remain inactive unless first induced by a pro-inflammatory stimulus [32]. Furthermore, defining the structure is still remined but it could be possible that the linear bound NEMO might stabilize interaction between IKK2 and NEMO then enhances IKK activation. I suggest that early signaling events involving poly-ubiquitin chains allow NEMO to permit rapid,

transient oligomerization of IKK2, which leads directly to activation of the kinase catalytic activation via *trans* auto-phosphorylation. Such rapid binding and dissociation could then allow IKK2 activity to become amplified efficiently through activation loop *trans* auto-phosphorylation of neighboring transient assemblages.

While NF-κB activation by most canonical signaling pathways remains mostly intact in the absence of the IKK1/α subunit, NEMO is an essential component for receiving and transducing canonical signaling in association with IKK2. However, what is much less well understood is a critical event in IKK activation by proinflammatory cytokines is the generation of 'linear (Met1)' and/or 'lysine 63 (Lys63)' linked polyubiquitin chains (Ub-chains) which interact non-covalently with NEMO, and trigger phosphorylation of IKK2/β AL. To this end, I investigated that binding of a linear Ub-chain to NEMO stabilizes the CC2-LZ dimer of NEMO, and the stabilized CC dimer of NEMO interacts with SDD of IKK2/β on a surface located opposite to the AL. This NEMO:Ub interaction with IKK2 induces allosteric conformational changes in the AL of the IKK2/β kinase domain (KD) from a 'closed' to an 'open' state. The 'open' AL of a kinase in an IKK-dimer could access the active site of a kinase in another dimer to get phosphorylated in trans. Thus, I refer to this NEMO:Ub-IKK2 interface of NEMO as 'second site". To determine whether the Ub-bound NEMO could interact with IKK through the second site in vitro I performed in vitro affinity pull down assay using recombinant IKK1, IKK2, NEMO, and Ub4. I observed that both IKK2 and IKK1 interact with NEMO in the presence of Ub4 but IKK1 has weaker interaction than IKK2. This observation seems to be agreed the previous report using NBD peptide represented that the vitro affinity assay revealed the distinct differences in

affinity of the IKKs for NEMO as blocking the IKK*2* interaction required higher concentrations of NBD peptide than that which inhibited IKK*1* [72-73].

The ability to block the interaction in vitro led me question whether the NEMO Activation Peptide could be delivered to cells to disrupt NF-*κ*B signaling. I generated the peptide ($NEMO^{ActPep}$) encompassing residues 384-389 of NEMO and tested IKK2 activation. To accomplish this, I utilized the ability of an expanding list of small naturally occurring or synthetic peptides to traverse cell membranes [148]. These peptides are named CPPs and coupling of bioactive cargo such as an inhibitory peptide to a CPP allows cellular uptake of the otherwise refractory cargo [148]. I therefore generated a fusion consisting of the NEMOActPep (376-389) with a CPP named TAT that is one of the most widely used and best-characterized CPPs [148]. Remarkably this TAT-$NEMO^{ActPep}$ fusion peptide rapidly entered HeLa, MEF, RAW murine macrophage cells and blocked both TNF- and LPS-induced NF-*κ*B activation, and consistent with my in vitro interaction studies, a mutant version of peptide containing QRRSPP→GGGGGG mutations did not block NF-*κ*B signaling. The most exciting feature of the $NEMO^{ActPep}$ is its ability to function in vivo. This was first demonstrated in mouse models in LPS acute inflammation where subcutaneous injection of the peptide, respectively blocked inflammation. These accumulated in vitro and in vivo studies of the $NEMO^{ActPep}$ confirm my hypothesis that dissecting specific molecular interactions within the IKK complex identifies targets for the development of potentially effective therapeutic strategies. Nevertheless, while the $NEMO^{ActPep}$ serves as a convincing “proof of principle” for this approach, much remains to be accomplished before reagents targeting this domain can be brought to clinical trials. we need to obtain a full understanding of the pharmacokinetics

and potential toxicity of the $NEMO^{ActPep}$ and we must establish the effects of long-term treatment. However it is possible that the $NEMO^{ActPep}$ will serve as a model for the future development of new generations of inhibitors such as small molecules or peptidomimetics designed to insert into the IKK binding groove of NEMO.

Cyclic adenosine monophosphate (cyclic AMP) is a ubiquitous cellular second messenger that controls gene expression through protein kinase A mediated phosphorylation of the constitutively DNA bound transcription factor, the cyclic AMP response element binding protein [149]. In cells, elevation of cyclic AMP through the use of adenylyl cyclase (AC) activators, phosphodiesterase (PDE) inhibitors, synthetic cyclic AMP analogs, or β-adrenergic receptor agonists has been shown to inhibit the production of proinflammatory genes [149], such as tumor necrosis factor-α (TNF-α) and tissue factor 1 (TF1), whose expression is positively regulated by the transcription factor, nuclear factor kappa B NF-κB [150].

IKK activation is the initial “switch” for triggering NF-κB activation. The literature does not report on cAMP effects on non-canonical NF-κB activation, which is quite remarkable considering the important role of this cascade in B cells, wherein cAMP/NF-κB crosstalk was initially reported. Hence, all effects described probably concern IKK2 [150]. Neumann et al. [151] were the first to propose that inhibition of NF-κB in activated T cells by the adenylyl cyclase activator forskolin or prostaglandin E2 (PGE2) was the result of elevation of intracellular IκB levels by cAMP. Since then, this mechanism has been reported in a variety of cell types, using different stimuli to activate both NF-κB and cAMP signaling cascades [152-154]. Conversely, dopamine signaling via the Gi-coupled D4 receptor inhibited IκB expression, probably by reducing [cAMP]i [154], indicating that

it is a mechanism that can act in two directions. Whereas the augmentation of cellular IκB levels by cAMP inducers appears to be a common mechanism, some groups did not find cAMP-mediated effects at this level of the NF-κB signaling cascade [155-156]. It should be noted, however, that many investigators did not perform a kinetic analysis of IκB expression levels, which might confound some of the conclusions. In fact, only a few studies have reported rapid inhibition of IκB degradation due to blocking of IKK activity by cAMP [155-156]. In one study, it was shown that the neurotransmitter serotonin, via the cAMP-inducing 5HT1 receptor, could induce PP2A phosphatase activity, which in turn led to IκB dephosphorylation and inhibition of its degradation [168]. This observation indicates that effects on IκB phosphorylation do not necessarily reflect cAMP-mediated targeting of the IKK kinase. Most studies, however, did not find effects of cAMP at the level of early stimulus-induced IκB degradation, but instead reported enhanced levels of resynthesized IκB [9]. In a few studies, both mechanisms were operative [157]. The mechanisms at the basis of the elevated expression of resynthesized IκB remain largely unresolved. There is some evidence that cAMP enhances IκB resynthesis at the transcriptional level [158]. Other studies rather indicated that increased IκB levels are the result of stabilization at the protein level, but where precisely cAMP intersects the IκB degradation cascade (i.e. via interfering with IκB ubiquitinylation, or by decreasing proteasomal activity) was not addressed [162-163]. Interestingly, in J774 murine macrophages, cAMP activated IKK, resulting in NF-κB activation instead of inhibition [162]. The cAMP effects on IKK activity were inhibited by the PKA inhibitor H89. However, cAMP also induced protein kinase C (PKC) activity, which might explain the discrepant results. Activation of IKK by cAMP was recently also demonstrated in acute lymphoblastic leukemia cells [167]. The fact that the

role of cAMP is often supported solely by the use of pharmacological cAMP/PKA activators/inhibitors, the selectivity of which is disputable, is indeed an important obstacle in the interpretation of many of the reported studies [167]. The idea that cAMP and/or PKA would enhance NF-κB transactivation via posttranslational modification of Rel proteins appears to be in conflict with the widely.

The cAMP/cAMP-dependent protein kinase (PKA) pathway and the mitogen-activated protein kinase (MAPK) cascades modulate common processes in the cell and multiple levels of cross-talk between these signalling pathways have been described. Indeed, cAMP has been shown to block the MEKK/JNK cascade [159], the p38 MAPK [164] and PI3 K [165], which all stimulate NF-κB transactivation. These kinases that have a well-documented link to the NF-κB pathway are various members of the large mitogen-activated protein kinase family (MAPK) including Jun-N-terminal kinase, JNK, and p38 [164]. Both kinases are also triggered by stimuli that activate NF-κB (such as TNFα), as adapter proteins lead to a branching of the signaling towards different downstream pathways. The mutual influences of these kinases and NF-κB are pleiotropic. p38 and related kinases are known to be cofactors in NF-κB activation [162], whereas there is a rather counteracting relationship between NF-κB and JNK [169]. Further members of the kinase family, which activate or regulate NF-κB include protein kinase C (PKC) [164] and Akt triggered by PI3K [165]. However, it is important to note that the effect of a signaling molecule on NF-κB often strictly depends on the cell type or the micro-environment and that even opposite effects can occur in distinct cell types. This has been reported for instance for the influence of Akt on NF-κB, which is activating in cell types such as epithelial cells, but can be inhibitory in macrophages [166]. Moreover, inhibitors of multiple

signaling pathways can inhibit proinflammatory cytokine production following TNF-α stimulation, highlighting that important crosstalk between these multiple pathways is essential for altering the normal homeostatic state of the microglial cell to a classically activated phenotype.

To this end, I like to examine how NEMO^{Actpep} affects TNF-α-induced cell activation through signaling intermediaries of the NF-κB and MAPK pathways. I observed that NEMO^{ActPep} inhibited IKK2-NFkB activation with a does dependent manner but all three MAP kinases are activated by TNF-α but no effect of either the WT or mutant peptide. Taken together, in this study I suggest the inhibitory effects of NEMO^{ActPep} on induction of NF-kB activation in cells and demonstrate that these actions of NEMO^{ActPep} inhibits IKK2-NF-kB activation through unique mechanism which is IKK2 activation via canonical pathway. This peptide inhibits the activity of the IKK complex, and consequently inflammatory gene expression in the stimulated different cells. I have demonstrated that NEMO^{ActPep} inhibits IKK-2 activity selectively, compared with at least other kinases including those in the MAP kinase inflammatory pathways such as p38, JNK and ERK. Furthermore, this selectivity can be maintained in TNF-a stimulated cells. The demonstrated selectivity of NEMO^{ActPep} validates its use as a pharmacological tool to dissect the effects of IKK-2 inhibition on the activation of the NF-kB pathway in a cell-based system.

This study is the first report of the role of the NEMO in the molecular mechanisms by which the binding of ubiquitin to NEMO controls IKK activation between a second interaction in IKK complex through cell signaling networks and how defects in this process underlie the pathogenesis. To harness the potential of the pleiotropic IKK signal

transducer as a drug target in numerous types of inflammatory diseases, diabetes, and cancers, it is critical to understand how its activity is directed to different signaling axes and cellular functions and the degree to which these are insulated from or connected with each other. The present work identifies NEMO as a key molecule and provides a framework for future investigations.

Bibliography

[1] Abbott, D.W., Yang, Y., Hutti, J.E., Madhavarapu, S., Kelliher, M.A., and Cantley, L.C. (2007) Coordinated regulation of Toll-like receptor and NOD2 signaling by K63-linked polyubiquitin chains. Mol. Cell. Biol. 27, 6012–6025.

[2] Acharyya, S., Villalta, S.A., Bakkar, N., Bupha-Intr, T., Janssen, P.M., Carathers, M., Li, Z.W., Beg, A.A., Ghosh, S., Sahenk, Z., et al. (2007) Interplay of IKK/NF-kappaB signaling in macrophages and myofibers promotes muscle degeneration in Duchenne muscular dystrophy. J. Clin. Invest. 117, 889–901.

[3] Blonska, M., Shambharkar, P.B., Kobayashi, M., Zhang, D., Sakurai, H., Su, B., and Lin, X. (2005) TAK1 is recruited to the tumor necrosis factor-alpha receptor 1 complex in a receptor-interacting protein (RIP)-dependent manner and cooperates with MEKK3 leading to NF-kappaB activation. J. Biol. Chem. 280, 43056–43063.

[4] Bonizzi, G., Bebien, M., Otero, D.C., Johnson-Vroom, K.E., Cao, Y., Vu, D., Jegga, A.G., Aronow, B.J., Ghosh, G., Rickert, R.C., et al. (2004) Activation of IKKalpha Target genes depends on recognition of specific kappaB binding sites by RelB:p52 dimers. EMBO J. 23, 4202–4210.

[5] Cardone, G., X. Yan, R. S. Sinkovits, J. Tang, and T. S. Baker. (2013) Three-dimensional reconstruction of icosahedral particles from single micrographs in real time at the microscope. J. Struct. Biol. 183:329-341.

[6] Cohen, S., Achbert-Weiner, H., and Ciechanover, A. (2004) Dual effects of IkappaB kinase beta-mediated phosphorylation on p105 fate: SCF(beta- TrCP)-dependent degradation and SCF(beta-TrCP)-independent processing. Mol. Cell. Biol. 24, 475–486.

[7] Courtois, G., and Gilmore, T. D. (2006) Mutations in the NF-kappaB signaling pathway: implications for human disease. Oncogene 25, 6831–6843.

[8] Cusson-Hermance, N., Khurana, S., Lee, T.H., Fitzgerald, K.A., and Kelliher, M.A. (2005) Rip1 mediates the Trif-dependent toll-like receptor 3- and 4-induced NF-kB activation but does not contribute to interferon regulatory factor 3 activation. J. Biol. Chem. 280, 36560–36566.

[9] De Bosscher, K., Vanden Berghe, W., and Haegeman, G. (2006) Cross-talk between nuclear receptors and nuclear factor kappaB. Oncogene 25, 6868– 6886.

[10] Delhase, M., Hayakawa, M., Chen, Y., and Karin, M. (1999) Positive and negative regulation of IkappaB kinase activity through IKKbeta subunit phosphorylation. Science 284, 309–313.

[11] Deng, L., Wang, C., Spencer, E., Yang, L., Braun, A., You, J., Slaughter, C., Pickart, C., and Chen, Z.J. (2000) Activation of the IkappaB kinase complex by TRAF6 requires a dimeric ubiquitin-conjugating enzyme complex and a unique polyubiquitin chain. Cell 103, 351–361.

[12] DiDonato JA, Hayakawa M, Rothwarf DM, Zandi E, Karin M (1997) A cytokine-responsive IkB kinase that activates the transcription factor NF-kB. Nature 388, 548–554.

[13] Fong, A., Zhang, M., Neely, J., and Sun, S.C. (2002) S9, a 19 S proteasome subunit interacting with ubiquitinated NF-kappaB2/p100. J. Biol. Chem. 277, 40697–40702.

[14] Fukushima, T., Matsuzawa, S., Kress, C.L., Bruey, J.M., Krajewska, M., Lefebvre, S., Zapata, J.M., Ronai, Z., and Reed, J.C. (2007) Ubiquitin-conjugating enzyme Ubc13 is a critical component of TNF receptor-associated factor (TRAF)-mediated inflammatory responses. Proc. Natl. Acad. Sci. USA 104, 6371–6376.

[15] Hacker, H., and Karin, M. (2006) Regulation and function of IKK and IKK- relate kinases.Sci. STKE 2006, re13.

[16] Hacker, H., Redecke, V., Blagoev, B., Kratchmarova, I., Hsu, L.C., Wang, G.G., Kamps, M.P., Raz, E., Wagner, H., and Hacker, G., et al. (2006) Specificity in Toll-like receptor signalling through distinct effector functions of TRAF3 and TRAF6. Nature, 439, 204–207.

[17] Harhaj, E.W., Maggirwar, S.B., and Sun, S.C. (1996) Inhibition of p105 processing by NF-kappaB proteins in transiently transfected cells. Oncogene 12, 2385–2392.

[18] Hayden, M.S., and Ghosh, S. (2008) Shared principles in NF-kB signaling. Cell 132, 344–362.

[19] Fagraeus, A. (1948) Antibody production in relation to the development of plasma cells. Acta Medica Scandinavica, March

[20] Hollister, J. R., Shaper, J. H., and Jarvis, D. L. (1998) Stable expression of Mammalian beta 1,4 galactosyltransferase extends the N-glycosylation pathway in insect cells. Glycobiology 8, 473–480.

[21] Ishimaru, N., Kishimoto, H., Hayashi, Y., and Sprent, J. (2006) Regulation of naive T cell function by the NF-kappaB2 pathway. Nat. Immunol. 7, 763–772.

[23] Janssens, S., Tinel, A., Lippens, S., and Tschopp, J. (2005) PIDD mediates NF-kappaB activation in response to DNA damage. Cell 123, 1079–1092.

[24] Jarvis DL, Weinkauf C, Guarino LA. (1996) Immediate early baculovirus vectors for Foreign gene expression in transformed or infected insect cells. Protein Expr. Purif.

8, 191–203.

[25] Karin, M. (2006) Nuclear factor-kappaB in cancer development and progression. Nature 441, 431–436.

[26] Karin M, Ben-Neriah Y. (2000) Phosphorylation meets ubiquitination: the control of NF-κB activity. Annu Rev Immunol 18, 621–663.

[27] Li, J., Ma, J., Wang, K.S., Mi, C., Wang, Z., Piao, L.X., Xu, G., Li, X.L., Lee, J.J., And Jin, X. (2016) Baicalein inhibits TNF-α-induced NF-κB activation and expression of NF-κB-regulated target gene products. Oncology Reports, 36, 2771-2776

[28] Lawrence, T., Bebien, M., Liu, G.Y., Nizet, V., and Karin, M. (2005) IKKalpha limits macrophage NF-kappaB activation and contributes to the resolution of inflammation. Nature 434, 1138–1143.

[29] Lee, T.H., Shank, J., Cusson, N., and Kelliher, M.A. (2004) The kinase activity of Rip1 is not required for tumor necrosis factor-alpha-induced IkappaB kinase or p38 MAP kinase activation or for the ubiquitination of Rip1 by Traf2. J. Biol. Chem. 279, 33185–33191.

[30] Lo YC, Lin SC, Rospigliosi CC, Conze DB, Wu CJ, et al. (2009) Structural basis for recognition of diubiquitins by NEMO. Mol Cell 33, 602–615.

[31] Manning, G., Whyte, D. B., Martinez, R., Hunter, T. & Sudarsanam, S. The protein kinase complement of the human genome. Science 298, 1912 (2002).

[32] Huxford, T., Huang, D.B., Malek, S., and Ghosh, G. (1998) The Crystal Structure of the IκBα/NF-κB Complex Reveals Mechanisms of NF-κB Inactivation. Cell, 95, 759-770

[33] Huxford, T., Hoffmann, A., and Ghosh, G. (2011) Understanding the logic of IkB:NF-kB regulation in structural terms. Curr Top Immunol. 349, 1-24.

[34] Rahighi, S., Ikeda, F., Kawasaki, M., Akutsu, M., and Suzuki, N.(2009) Specific recognition of linear ubiquitin chains by NEMO is important for NF-kB activation. Cell. 136,1098–1109.

[35] Rushe, M., Silvian, L., Bixler, S., Chen, L.L., and Cheung. A. (2008) Structure of a NEMO/IKK- associating domain reveals architecture of the interaction site. Structure 16, 798–808.

[36] Tseng, Y. S., Gurda, B. L., Chipman, P., R. McKenna, S., Afione, J. A., Chiorini, N., Muzyczka, N. H., Olson, T. S., Baker, J., and Agbandje-McKenna, M. (2015) Adeno-Associated Virus serotype 1 (AAV1)- and AAV5-antibody complex structures reveal

evolutionary commonalities in parvovirus antigenic reactivity. J. Virol. 89, 1794 807.

[37] Xia, Z.P., Sun, L., Chen, X., Pineda, G., and Jiang, X. (2009) Direct activation of protein kinases by unanchored polyubiquitin chains. Nature 461, 114–119.

[38] Sen, R. and Baltimore, D. (1986) Multiple nuclear factors interact with the immunoglobulin enhancer sequences. Cell. 46, 705–716.

[39] Shakhov, A. N., Collart, M., Vassalli, A.P., Nedospasov, S. A., and Jongeneel, C. V. (1990) kB–type enhancers are involved in lipopolysaccharide-mediated transcriptional activation of the tumor necrosis factor gene in primary macrophages. J Exp Med. 17, 35–47.

[40] Hoffmann, A. and Roeder, R. G. (1991) Purification of his-tagged proteins in non-denaturing conditions suggests a convenient method for protein interaction studies. Nucleic Acids Res.19, 6337–6338.

[41] Pasparakis M., Luedde T., and Schmidt-Supprian, M. (2006) Dissection of the NF-kappaB signaling cascade in transgenic and knockout mice. Cell Death Differ. 13, 861-872.

[42] Kober-Hasslacher M., Oh-Strauß, H., Kumar, D., Soberon, V., Diehl, C., Lech, M., Engleitner, T., Katab, E., Fernández-Sáiz, V., Piontek, G., Li, H., Menze, B., Ziegenhain, C., Enard, W., Rad, R., Böttcher, J.P., Anders, H.J., Rudelius, M., and Schmidt-Supprian, M.J. (2020) c-Rel gain in B cells drives germinal center reactions and autoantibody production. Clin Invest. 130, 3270-3286.

[43] Schmid, J.A, and Birbach, A. (2008) IkappaB kinase beta (IKKbeta/IKK2/IKBKB)-a key molecule in signaling to the transcription factor NF-kappaB. Cytokine Growth Factor Rev. 19, 157-165.

[44] Gupta, A.S., Biswas, D.D., Brown, S.N., Mockenhaupt, K., Marone, M., Hoskins, A., Siebenlist, U., Kordula, T.J. (2019) A detrimental role of RelB in mature oligodendrocytes during experimental acute encephalomyelitis. Neuroinflammation. 16, 161-174.

[45] Dejardin, E. (2006) The alternative NF-kappaB pathway from biochemistry to biology: pitfalls and promises for future drug development. Biochem Pharmacol. 72,1161-1179.

[46] Ding, Y., He, P., and Li, Z. (2020) MicroRNA – 9119 regulates cell viability of Granulosa cells in polycystic ovarian syndrome via mediating Dicer expression. Mol Cell Biochem. 465,187-197.

[47] Khan, S.Z., Gasperino, S., and Zeichner, S.L. (2019) Nuclear Transit and HIV LTR

Binding of NF-κB Subunits Held by IκB Proteins: Implications for HIV-1 Activation. Viruses. 11, 1162-1176.

[48] Nenci, A., Becker, C., Wullaert, A., Gareus, R., Van Loo, G., Danese, S., Huth, M., Nikolaev, A., Neufert, C., Madison, B., Gumucio, D., Neurath, MF., and Pasparakis, M. (2007) Epithelial NEMO links innate immunity to chronic intestinal inflammation. Nature. 446, 557-561.

[49] Galle-Treger, L., Hurrell, B.P., Lewis, G., Howard, E., Jahani, P.S., Banie, H., Razani, B., Soroosh, P., and Akbari, O.J. (2020) Autophagy is critical for group 2 Innate lymphoid cell metabolic homeostasis and effector function. Allergy Clin Immunol. 145, 502-517.

[50] Awasthee, N., Rai, V., Chava, S., Nallasamy, P., Kunnumakkara, A.B., Bishayee, A., Chauhan, S.C., Challagundla, K.B., and Gupta, S.C. (2018) Targeting IκappaB kinases for cancer therapy. Semin Cancer Biol. 56, 12-24.

[51] Hayden, M. S., and Ghosh, S. (2008) Shared principles in NF-κB signaling, Cell 132, 344-362.

[52] Mulero, M. C., Huxford, T., and Ghosh, G. (2019) NF-κB, IκB, and IKK: Integral components of immune system signaling, Adv. Exp. Med. Biol. 1172, 207-226.

[53] Scheidereit, C. (2006) IκB kinase complexes: gateways to NF-κB activation and transcription, Oncogene 25, 6685-6705.

[54] Huxford, T., and Ghosh, G. (2009) A structural guide to proteins of the NF-κB signaling module, Cold Spring Harb. Perspect. Biol. 1, a000075.

[55] Chen, Z. J., Parent, L., and Maniatis, T. (1996) Site-specific phosphorylation of IκBα by a novel ubiquitination-dependent protein kinase activity, Cell 84, 853-862.

[56] DiDonato, J. A., Hayakawa, M., Rothwarf, D. M., Zandi, E., and Karin, M. (1997) A cytokine- responsive IκB kinase that activates the transcription factor NF-κB, Nature 388, 548-554.

[57] Mercurio, F., Zhu, H., Murray, B. W., Shevchenko, A., Bennett, B. L., Li, J., Young, D. B., Barbosa, M., Mann, M., Manning, A., and Rao, A. (1997) IKK-1 and IKK-2: cytokine-activated IκB kinases essential for NF-κB activation, Science 278, 860-866.

[58] Zandi, E., Rothwarf, D. M., Delhase, M., Hayakawa, M., and Karin, M. (1997) The IκB kinase complex (IKK) contains two kinase subunits, IKKα and IKKβ, necessary for IκB phosphorylation and NF-κB activation, Cell 91, 243-252.

[59] Xu, G., Lo, Y. C., Li, Q., Napolitano, G., Wu, X., Jiang, X., Dreano, M., Karin, M., And Wu, H. (2011) Crystal structure of inhibitor of κB kinase β, Nature 472, 325-

330.

[60] Polley, S., Huang, D. B., Hauenstein, A. V., Fusco, A. J., Zhong, X., Vu, D., Schröfelbauer, B., Kim, Y., Hoffmann, A., Verma, I. M., Ghosh, G., and Huxford, T. (2013) A structural basis for IκB kinase 2 activation via oligomerization-dependent trans auto-phosphorylation, PLoS Biol. 11, e1001581.

[61] Liu, S., Misquitta, Y. R., Olland, A., Johnson, M. A., Kelleher, K. S., Kriz, R., Lin, L. L., Stahl, M., and Mosyak, L. (2013) Crystal structure of a human IκB kinase β asymmetric dimer, J. Biol. Chem. 288, 22758-22767.

[62] Hauenstein, A. V., Rogers, W. E., Shaul, J. D., Huang, D. B., Ghosh, G., and Huxford, T. (2014) Probing kinase activation and substrate specificity with an engineered monomeric IKK2, Biochemistry 53, 2064-2073.

[63] Delhase, M., Hayakawa, M., Chen, Y., and Karin, M. (1999) Positive and negative regulation of IκB kinase activity through IKKβ subunit phosphorylation, Science 284, 309-313.

[64] Nolen, B., Taylor, S., and Ghosh, G. (2004) Regulation of protein kinases; controlling activity through activation segment conformation, Mol. Cell 15, 661-675.

[65] Polley, S., Passos, D. O., Huang, D. B., Mulero, M. C., Mazumder, A., Biswas, T., Verma, I. M., Lyumkis, D., and Ghosh, G. (2016) Structural Basis for the activation of IKK1/α, Cell Rep. 17, 1907- 1914.

[66] Senftleben, U., Cao, Y., Xiao, G., Greten, F. R., Krahn, G., Bonizzi, G., Chen, Y., Hu, Y., Fong, A., Sun, S. C., and Karin, M. (2001) Activation by IKKα of a second, evolutionary conserved, NF-κB signaling pathway, Science 293, 1495-1499.

[67] Xiao, G., Harhaj, E. W., and Sun, S. C. (2001) NF-κB-inducing kinase regulates the processing of NF-κB2 p100, Mol. Cell 7, 401-409.

[68] Rudolph, D., Yeh, W. C., Wakeham, A., Rudolph, B., Nallainathan, D., Potter, J., Elia, A. J., and Mak, T. W. (2000) Severe liver degeneration and lack of NF-κB activation in NEMO/IKKγ-deficient mice, Genes Dev. 14, 854-862.

[69] Schmidt-Supprian, M., Bloch, W., Courtois, G., Addicks, K., Israël, A., Rajewsky, K., and Pasparakis, M. (2000) NEMO/IKK gamma-deficient mice model incontinentia pigmenti, Mol. Cell 5, 981-992.

[70] Chen, J., and Chen, Z. J. (2013) Regulation of NF-κB by ubiquitination, Curr. Opin. Immunol. 25, 4-12.

[71] Rothwarf, D. M., Zandi, E., Natoli, G., and Karin, M. (1998) IKKγ is an essential regulatory subunit of the IκB kinase complex, Nature 395, 297-300.

[72] May, M. J., D'Acquisto, F., Madge, L. A., Glockner, J., Pober, J. S., and Ghosh, S. (2000) Selective inhibition of NF-κB activation by a peptide that blocks the interaction of NEMO with the IκB kinase complex, Science 289, 1550-1554.

[73] May, M. J., Marienfeld, R. B., and Ghosh, S. (2002) Characterization of the IκB-kinase NEMO binding domain, J. Biol. Chem. 277, 45992-46000.

[74] Barczewski, A. H., Ragusa, M. J., Mierke, D. F., and Pellegrini, M. (2019) The IKK-binding domain of NEMO is an irregular coiled coil with a dynamic binding interface, Sci. Rep. 9, 2950.

[75] Rushe, M., Silvian, L., Bixler, S., Chen, L. L., Cheung, A., Bowes, S., Cuervo, H., Berkowitz, S., Zheng, T., Guckian, K., Pellegrini, M., and Lugovskoy, A. (2008) Structure of a NEMO/IKK-associating domain reveals architecture of the interaction site, Structure 16, 798-808.

[76] Bagnéris, C., Ageichik, A. V., Cronin, N., Wallace, B., Collins, M., Boshoff, C., Waksman, G., and Barrett, T. (2008) Crystal structure of a vFlip-IKKγ complex: insights into viral activation of the IKK signalosome, Mol. Cell 30, 620-631.

[77] Rahighi, S., Ikeda, F., Kawasaki, M., Akutsu, M., Suzuki, N., Kato, R., Kensche, T., Uejima, T., Bloor, S., Komander, D., Randow, F., Wakatsuki, S., and Dikic, I. (2009) Specific recognition of linear ubiquitin chains by NEMO is important for NF-κB activation, Cell 136, 1098-1109.

[78] Lo, Y. C., Lin, S. C., Rospigliosi, C. C., Conze, D. B., Wu, C. J., Ashwell, J. D., Eliezer, D., and Wu, H. (2009) Structural basis for recognition of diubiquitins by NEMO, Mol. Cell 33, 602-615.

[79] Yoshikawa, A., Sato, Y., Yamashita, M., Mimura, H., Yamagata, A., and Fukai, S. (2009) Crystal structure of the NEMO ubiquitin-binding domain in complex with Lys 63-linked di-ubiquitin, FEBS Lett. 583, 3317-3322.

[80] Fujita, H., Rahighi, S., Akita, M., Kato, R., Sasaki, Y., Wakatsuki, S., and Iwai, K. (2014) Mechanism underlying IκB kinase activation mediated by the linear ubiquitin chain assembly complex, Mol. Cell. Biol. 34, 1322-1335.

[81] Saito, K., Kigawa, T., Koshiba, S., Sato, K., Matsuo, Y., Sakamoto, A., Takagi, T., Shirouzu, M., Yabuki, T., Nunokawa, E., Seki, E., Matsuda, T., Aoki, M., Miyata, Y., Hirakawa, N., Inoue, M., Terada, T., Nagase, T., Kikuno, R., Nakayama, M., Ohara, O., Tanaka, A., and Yokoyama, S. (2004) The CAP-Gly domain of CYLD associates with the proline-rich sequence in NEMO/IKKγ, Structure 12, 1719-1728.

[82] Cordier, F., Grubisha, O., Traincard, F., Veron, M., Delepierre, M., and Agou, F. (2009) The zinc finger of NEMO is a functional ubiquitin-binding domain, J. Biol. Chem. 284, 2902-2907.

[83] Smahi, A., Courtois, G., Rabia, S. H., Döffinger, R., Bodemer, C., Munnich, A., Casanova, J. L., and Israël, A. (2002) The NF-κB signalling pathway in human diseases: from incontinentia pigmenti to ectodermal dysplasias and immune-deficiency syndromes, Hum. Mol. Genet. 11, 2371-2375.

[84] Agou, F., Ye, F., Goffinont, S., Courtois, G., Yamaoka, S., Israël, A., and Veron, M. (2002) NEMO trimerizes through its coiled-coil C-terminal domain, J. Biol. Chem. 277, 17464-17475.

[85] Drew, D., Shimada, E., Huynh, K., Bergqvist, S., Talwar, R., Karin, M., and Ghosh, G. (2007) Inhibitor κB kinase β binding by inhibitor κB kinase γ, Biochemistry 46, 12482-12490.

[86] Tegethoff, S., Behlke, J., and Scheidereit, C. (2003) Tetrameric oligomerization of IκB kinase γ (IKKγ) is obligatory for IKK complex activity and NF-κB activation, Mol. Cell. Biol. 23, 2029-2041.

[87] Shaul, J. D., Farina, A., and Huxford, T. (2008) The human IKKβ subunit kinase domain displays CK2- like phosphorylation specificity, Biochem. Biophys. Res. Commun. 374, 592-597.

[88] Chaturvedi, S. K., Ma, J., Brown, P. H., Zhao, H., and Schuck, P. (2018) Measuring macromolecular size distributions and interactions at high concentrations by sedimentation velocity, Nat. Commun. 9, 4415.

[89] Micsonai, A., Wien, F., Kernya, L., Lee, Y. H., Goto, Y., Refregiers, M., and Kardos, J. (2015) Accurate secondary structure prediction and fold recognition for circular dichroism spectroscopy, Proc. Natl. Acad. Sci. USA 112, E3095-3103.

[90] Cole, C., Barber, J. D., and Barton, G. J. (2008) The Jpred 3 secondary structure prediction server, Nucleic Acids Res. 36, W197-201.

[91] Yamaoka, S., Courtois, G., Bessia, C., Whiteside, S. T., Weil, R., Agou, F., Kirk, H. E., Kay, R. J., and Israël, A. (1998) Complementation cloning of NEMO, a component of the IκB kinase complex essential for NF-κB activation, Cell 93, 1231-1240.

[92] Smahi, A., Courtois, G., Vabres, P., Yamaoka, S., Heuertz, S., Munnich, A., Israël, A., Heiss, N. S., Klauck, S. M., Kioschis, P., Wiemann, S., Poustka, A., Esposito, T., Bardaro, T., Gianfrancesco, F., Ciccodicola, A., D'Urso, M., Woffendin, H., Jakins, T., Donnai, D., Stewart, H., Kenwrick, S. J., Aradhya, S., Yamagata, T., Levy, M., Lewis, R. A., and Nelson, D. L. (2000) Genomic rearrangement in NEMO impairs NF-κB activation and is a cause of incontinentia pigmenti. The International Incontinentia Pigmenti (IP) Consortium, Nature 405, 466-472.

[93] Döffinger, R., Smahi, A., Bessia, C., Geissmann, F., Feinberg, J., Durandy, A.,

Bodemer, C., Kenwrick, S., Dupuis-Girod, S., Blanche, S., Wood, P., Rabia, S. H., Headon, D. J., Overbeek, P. A., Le Deist, F., Holland, S. M., Belani, K., Kumararatne, D. S., Fischer, A., Shapiro, R., Conley, M. E., Reimund, E., Kalhoff, H., Abinun, M., Munnich, A., Isräel, A., Courtois, G., and Casanova, J. L. (2001) X-linked anhidrotic ectodermal dysplasia with immunodeficiency is caused by impaired NF-κB signaling, Nat. Genet. 27, 277-285.

[94] Zilberman-Rudenko, J., Shawver, L. M., Wessel, A. W., Luo, Y., Pelletier, M., Tsai, W. L., Lee, Y., Vonortas, S., Cheng, L., Ashwell, J. D., Orange, J. S., Siegel, R. M., and Hanson, E. P. (2016) Recruitment of A20 by the C-terminal domain of NEMO suppresses NF-κB activation and autoinflammatory disease, Proc. Natl. Acad. Sci. USA 113, 1612-1617.

[95] Fusco, F., Pescatore, A., Conte, M. I., Mirabelli, P., Paciolla, M., Esposito, E., Lioi, M. B., and Ursini, M. V. (2015) EDA-ID and IP, two faces of the same coin: how the Same IKBKG/NEMO mutation affecting the NF-κB pathway can cause Immunodeficiency and/or inflammation, Int. Rev. Immunol. 34, 445-459.

[96] Hauenstein, A. V., Xu, G., Kabaleeswaran, V., and Wu, H. (2017) Evidence for M1-Linked polyubiquitin-mediated conformational change in NEMO, J. Mol. Biol. 429, 3793-3800.

[97] Shaffer, R., DeMaria, A. M., Kagermazova, L., Liu, Y., Babaei, M., Caban-Penix, S., Cervantes, A., Jehle, S., Makowski, L., Gilmore, T. D., Whitty, A., and Allen, K. N. (2019) A central region of NF-κB essential modulator is required for IKKβ-induced conformational change and for signal propagation, Biochemistry 58, 2906-2920.

[98] Park, P., Kang, H., Sanderson, T.M., Bortolotto, Z.A., Georgiou, J., Zhuo, M., Kaang, B.K., and Collingridge, G.L. (2018) The Role of Calcium-Permeable AMPARs in Long-Term Potentiation at Principal Neurons in the Rodent Hippocampus. Front Synaptic Neurosci. 10, 42.

[99] Kensche, A., Pötschke, S., Hannig, C., Dürasch, A., Henle, T., and Hannig, M. (2020) Efficacy of mouthrinses with bovine milk and milk protein isolates to accumulate casein in the in situ pellicle. Clinical Oral Investigations,19.

[100] Nolen, B., Talor, S., and Ghosh, G. (2004) Regulation of protein kinases; controlling activity through activation segment conformation, Mol Cells. 15, 661-675.

[101] Weake, V. M., and Workman, J. L. (2010) Inducible gene expression: diverse regulatory mechanisms. 11, 426-437.

[102] Zeitlinger, J., Stark, A., Kellis, M., Hong, J. W., Nechaev, S., Adelman, K., Levine, M., and Young, R.A. (2007) RNA polymerase stalling at developmental control genes in the Drosophila melanogaster embryo. Nat Genet, 39, 1512-1516.

[103] De Nadal, E., and Posas, F. (2010) Multilayered control of gene expression by

stress-activated protein kinases. EMBO J. 29, 4-13.

[104] Ribatti, D., Crivellato, E., and Vacca, A. (2006) The contribution of Bruce Glick to the definition of the role played by the bursa of Fabricius in the development of the B cell lineage. Clin Exp Immunol. 145, 1-4.

[105] Lin, Y.C., Jhunjhunwala, S., Benner, C., Heinz, S., Welinder E., Mansson, R., Sigvardsson, M., Hagman, J., Espinoza, C. A., Dutkowski, J., Ideker, T., Glass, C.K., and Murre, C. (2010) A global network of transcription factors, involving E2A, EBF1 and Foxo1, that orchestrates B cell fate. Nature Immunology 11, 635-U109.

[106] Tonegawa, S. (1983) Somatic generation of antibody diversity. Nature. 302, 575-581.

[107] Nemazee D. (2017) Mechanisms of central tolerance for B cells. Nature Reviews Immunology. 17, 281-294.

[108] Zhang, Y., Fear, D.J., Willis-Owen, S. A. G., William O. Cookson, W. O., and Moffatt, M.F. (2016) Global gene regulation during activation of immunoglobulin class switching in human B cells. Scientific Reports, 6, 37988.

[109] Dullaers, M., Bruyne, R.D., Ramadani, F., Gould, H.J., Gevaert, P., and Lambrecht, B.N. (2016) The who, where, and when of IgE in allergic airway disease. The Journal of allergy and clinical immunology 129, 635–645.

[110] Nemazee, D. (2017) Mechanism of central tolerance for B cells. Nature Reviews Immunology. 17, 281-294.

[111] Wu, L. C. and Zarrin, A. A. (2014) The production and regulation of IgE by the immune Nature Reviews Immunology. 14, 247-259.

[112] Celebrating 25 years of NF-κB. (2011) nature immunology, 12, 681.

[113] Brockman, J.A., Scherer, D.C., McKinsey, T.A., Hall, S.M., Qi, X., Lee, W.Y., and Ballard, D.W. (1995) Coupling of a signal response domain in IκB to multiple pathways for NF-κB activation. Mol. Cell. Biol. 15, 2809-2818.

[114] DiDonato, J.A., Mercurio, F., Rosette, C., Wu-li, J., Suyang, H., Ghosh, S., and Karin, M. (1996) Mapping of the inducible IκB phosphorylation sites that signal its ubiquitination and degradation. Mol. Cell. Biol. 16, 1295-1304.

[115] Brown, K., Gerstberger, S., Carlson, L., Franzoso, G., and Siebenlist, U. (1995) Control of IκBα proteolysis by site-specific, signal-induced phosphorylation. Science. 267, 1485-1491.

[116] Liu, Z.-G., Hu, H., Goeddel, D.V., and Karin, M. (1996) Dissection of TNF receptor

1 effector functions JNK activation is not linked to apoptosis, while NF-κB activation prevents cell death. Cell. 87, 565-576.

[117] Lee, F.S., Hagler, J., Chen, Z.J., and Maniatis T. (1997) Activation of the IκBα kinase complex by MEKK1, a kinase of the JNK pathway. Cell. 88, 213-222.

[118] Laplantine, E., Fontan, E., Chiaravalli, J., Lopez, T., Lakisic, G., Ve´ron, M., Agou, F., and Israe¨l, A. (2009) NEMO specifically recognizes K63-linked poly-ubiquitin chains through a new bipartite ubiquitin-binding domain. The EMBO Journal, 28, 2885–2895.

[119] Hershko, A., and Ciechanover, A. (1998) The ubiquitin system. Annu Rev Biochem, 67, 425–479.

[120] Deshaies, R. J., and Joazeiro, C.A. (2009) RING domain E3 ubiquitin ligases. Annu Rev Biochem, 78, 399–434.

[121] Berndsen, C. E., and Wolberger, C. (2014) New insights into ubiquitin E3 ligase mechanism. Nat Struct Mol Biol, 21, 301–307.

[122] Sun, S.C. (2008) Deubiquitylation and regulation of the immune response.Nat Rev Immunol, 8, 501–511.

[123] Liu, S., and Chen, Z.J. (2011) Expanding role of ubiquitination in NF-κB signaling. Cell Res, 21, 6–21.

[124] Iwai, K. (2012) Diverse ubiquitin signaling in NF-κB activation. Trends Cell Biol, 22: 355–364.

[125] Husnjak, K, and Dikic, I. (2012) Ubiquitin-binding proteins: decoders of ubiquitin-mediated cellular functions. Annu Rev Biochem, 81, 291–322.

[126] Hu, H., and Sun, S.C. (2016) Ubiquitin signaling in immune responses. Cell research, 26, 457–483.

[127] Chen, Z. J., Parent, L. and Maniatis, T. (1996) Site-specific phosphorylation of IκBα by a novel ubiquitination-dependent protein kinase activity. Cell, 84, 853–862.

[128] Lo, Y. C., Lin, S.C., Rospigliosi, C.C., Conze, D.B., Wu, C.J., Ashwell, J.D., Eliezer, D., and Wu, H. (2009) Structural basis for recognition of diubiquitins by NEMO. Mol. Cell, 33, 602–615.

[129] Rahighi, S. Ikeda, F., Kawasaki, M., Akutsu, M., Suzuki, N., Kato, R., Kensche, T., Uejima, T., Bloor, S., Komander, D., Randow, F., Wakatsuki, S., and Dikic, I. (2009) Specific recognition of linear ubiquitin chains by NEMO is important for NF-κB activation. Cell, 136, 1098–1109.

[130] Ea, C. K., Deng, L., Xia, Z. P., Pineda, G. and Chen, Z. J. (2006) Activation of IKK by TNFα requires site-specific ubiquitination of RIP1 and polyubiquitin binding by NEMO. Mol. Cell, 22, 245–257.

[131] Wu, C. J., Conze, D. B., Li, T. Srinivasula, S. M. and Ashwell, J. D. (2006) Sensing of Lys 63-linked polyubiquitination by NEMO is a key event in NF-κB activation. Nature Cell Biol., 8, 398–406.

[132] Heyninck, K., Kreike, M. M. and Beyaert, R. (2003) Structure-function analysis of the A20-binding inhibitor of NF-κB activation, ABIN-1. FEBS Lett., 536, 135–140.

[133] Wagner, S. Carpentier, I., Rogov, V., Kreike, M., Ikeda,F., Lohr, F., Wu., C-J., Achwell, J.D., Dotsch, V., Dikic, I., and Beyaert, R. (2008) Ubiquitin binding mediates the NF-κB inhibitory potential of ABIN proteins. Oncogene, 27, 3739–3745.

[134] Husnjak, K. & Dikic, I. (2012) Ubiquitin-binding proteins: decoders of ubiquitin-mediated cellular functions. Annu. Rev. Biochem., 81, 291–322.

[135] Mulero, M.C., Shahabi, S., Ko, M.S., Schiffer, J.M., Huang, D.B., Wang, V.Y., Amaro, R.E., Huxford, T., and Ghosh, G. (2018) Protein Cofactors Are Essential for High-Affinity DNA Binding by the Nuclear Factor κB RelA Subunit. Biochemistry, 57, 2943-295.

[136] Kany, S., Vollrath, J.T., and Relja, B. (2019) Cytokines in Inflammatory Disease, Int. J. Mol. Sci., 20, 6008-6039

[137] Suzuki, K., Nakaji, S., Yamada, M., Totsuka, M., Sato, K., and Sugawara, K. (2002) Systemic inflammatory response to exhaustive exercise. Cytokine kinetics. Exerc Immunol Rev., 8, 6-48.

[138] Cytokines induced neutrophil extracellular traps formation: implication for the inflammatory disease condition

[139] Keshari, R.S., Jyoti, A., Dubey, M., Kothari, N., Kohli, M., Bogra, J., Barthwal, M.K., and Dikshit, M. (2012) Cytokines induced neutrophil extracellular traps formation: implication for the inflammatory disease condition. PLoS One. 10, e48111.

[140] Volpin, G., Cohen, M., Assaf, M., Meir, T., Katz, R., and Pollack, S. (2014) Cytokine levels (IL-4, IL-6, IL-8 and TGFβ) as potential biomarkers of systemic inflammatory response in trauma patients. Int Orthop., 38, 1303-1309.

[141] Freitas, R.H.C.N., and Fraga, C.A.M. (2018) NF-κB-IKKβ Pathway as a Target for Drug Development: Realities, Challenges and Perspectives. Curr DrugTargets, 19,1933-1942.

[142] Alermo, M.P., Aves-Rosa, F., Rubel, C., Fernandez, G.C., Fernandez-Alonso, G., Alberto, F., Rivas, M., & Isturiz, M. (2000) Pretreatment of mice with lipopolysaccharide (LPS) or IL-1β exerts dose-dependent opposite effects on Shiga toxin-2 lethality. Clin Exp Immunol,119, 77–83.

[143] Baud, V., & Karin, M. (2009) Is NF-κB a good target for cancer therapy? Hopes and pitfalls. Nat Rev Drug Discov, 8, 33-40.

[144] Knighton, D.R., J.H. Zheng, J.H., Ten, L.F., Ashford, V.A., N.H. Xuong, N.H., Taylor, S.S., and J.M. Sowadski. (1991) Crystal structure of the catalytic subunit of cyclic adenosine monophosphate-dependent protein kinase, Science, 253, 407-414.

[145] De Bondt, H.L., Rosenblatt, J., Jancarik, J., Jones, H.D., Morgan, D.O., and Kim, S.H. (1993) Crystal structure of cyclin-dependent kinase 2. Nature, 363, 595-602.

[146] J. Goldberg, A.C. Nairn, J. KuriyanStructural basis for the autoinhibition of Calcium /calmodulin-dependent protein kinase I, Cell, 84 (1996), pp. 875-887.

[147] Xu, G., Lo, Y.C., Li, Q., Napolitano, G., Wu, X., Jiang, X., Dreano, M., Karin, M., and Wu. H. (2011) Crystal structure of inhibitor of kappaB kinase beta. Nature, 472, 325-330.

[148] Solt, L.A., and May, M.J. (2008) The IκB kinase complex: master regulator of NF-κB signaling. Immunol Res. 42, 3–18.

[149] McKnight, G.S. (1991) Cyclic AMP second messenger systems. Curr Opin Cell Biol 3, 213–217.

[150] Vallabhapurapu, S., and Karin M (2009) Regulation and function of NF-kappaB transcription factors in the immune system. Annu Rev Immunol 27, 693–733.

[151] Norrdin, R.W., Jee, W.S., and High, W.B. (1990)The role of prostaglandins in bone in vivo. Prostaglandins Leukot Essent Fatty Acids, 41, 139–149.

[152] Fraser, C.C. (2008) G protein-coupled receptor connectivity to NF-kappaB in inflammation and cancer. Int Rev Immunol, 27, 320–350.

[153] Wu, X., Mahadev, K., Fuchsel, L., Ouedraogo, R., Xu, S.Q., and Goldstein, B.J. (2007) Adiponectin suppresses IkappaB kinase activation induced by tumor Necrosis factor-alpha or high glucose in endothelial cells: role of cAMP and AMP Kinase signaling. Am J Physiol Endocrinol Metab, 293, 1836–1844.

[154] Dobashi, K, Asayama, K, and Shirahata, A. (2003) Differential effects of cyclic AMP On induction of nitric oxide synthase in 3T3–L1 cells and brown adipocytes. Free Radic Biol Med, 35, 94–101.

[155] Wall, E,A, Zavzavadjian, J.R., Chang, M.S., Randhawa, B., Zhu, X., Hsueh, R.C., Liu, J., Driver, A., Bao, X.R., Sternweis, P.C., Simon, M.I., and Fraser, I.D. (2009) Suppression of LPS-induced TNF-alpha production in macrophages by cAMP is mediated by PKA-AKAP95–p105. Sci Signal 2, 28

[156] Shinaga, H., Jono, H., Lim, J.H., Komatsu, K., Xu, X., Lee, J., Woo, C.H., Xu, H., Feng, X.H., Chen, L.F., Yan, C., and Li, J.D. (2009) Synergistic induction of nuclear factor-kappaB by transforming growth factor-beta and tumour necrosis factor-alpha is mediated by protein kinase A-dependent RelA acetylation. Biochem J 417(2):583–591

[157] Farmer, P., and Pugin, J. (2000) beta-adrenergic agonists exert their “anti-inflammatory” effects in monocytic cells through the IkappaB/NF-kappaB pathway. Am J Physiol Lung Cell Mol Physiol 279(4):L675–L682

[158] Spooren, A., Kooijman, R., Lintermans, B., Van Craenenbroeck, K., Vermeulen, L., Haegeman, G., and Gerlo, S. (2010) Cooperation of NFkappaB and CREB to induce synergistic IL-6 expression in astrocytes. Cell Signal 22, 871–881

[159] Chio, C.C., Chang, Y.H., Hsu, Y.W., Chi, K.H., and Lin, W.W. (2004) PKA-dependent activation of PKC, p38 MAPK and IKK in macrophage: implication in the induction of inducible nitric oxide synthase and interleukin-6 by dibutyryl cAMP. Cell Signal 16, 565–575.

[160] Davies, S.P., Reddy, H., Caivano, M., and Cohen, P. (2000) Specificity and mechanism of action of some commonly used protein kinase inhibitors. Biochem J 351, 95–105

[161] Ho, H.Y., Lee, H.H., and Lai, M.Z. (1997) Overexpression of mitogen-activated protein kinase kinase kinase reversed cAMP inhibition of NF-kappaB in T cells. Eur J Immunol, 27,222–226

[162] Fraser, D.A., Arora, M., Bohlson, S.S., Lozano, E., and Tenner, A.J. (2007) Generation of inhibitory NFkappaB complexes and phosphorylated cAMP response element-binding protein correlates with the anti-inflammatory activity of complement protein C1q in human monocytes. J Biol Chem, 282, 7360–7367

[163] Delgado, M,, Munoz-Elias, E.J., Kan, Y., Gozes, I., Fridkin, M., Brenneman, D.E., Gomariz, R.P., Ganea, D. (1998) Vasoactive intestinal peptide and pituitary adenylate cyclase-activating polypeptide inhibit tumor necrosis factor alpha transcriptional activation by regulating nuclear factor-kB and cAMP response element-binding protein/c-Jun. J Biol Chem, 273, 31427–31436

[164] Li S, Ni Z, Cong B, Gao W, Xu S, Wang C, Yao Y, Ma C, Ling Y. (2007) CCK-8 inhibits LPS-induced IL-1beta production in pulmonary interstitial macrophages by modulating PKA, p38, and NF-kappaB pathway. Shock, 27, 678–686.

[165] Sousa LP, Carmo AF, Rezende BM, Lopes F, Silva DM, Alessandri AL, Bonjardim CA, Rossi AG, Teixeira MM, Pinho V. (2009) Cyclic AMP enhances resolution of allergic pleurisy by promoting inflammatory cell apoptosis via inhibition of PI3 K/Akt and NF-kappaB. Biochem Pharmacol, 78, 396–405.

[166] Koga K, Takaesu G, Yoshida R, Nakaya M, Kobayashi T, Kinjyo I, Yoshimura A. (2009) Cyclic adenosine monophosphate suppresses the transcription of proinflammatory cytokines via the phosphorylated c-Fos protein. Immunity, 30, 372–383.

[167] Davies, S.P., Reddy, H., Caivano, M., and Cohen, P. (2000) Specificity and mechanism of action of some commonly used protein kinase inhibitors. Biochem J, 35, 95–105.

[168] Hsiung, S.C., Tin, A., Tamir, H., Franke, T.F., and Liu, K.P. (2008) Inhibition of 5-HT1A receptor-dependent cell survival by cAMP/protein kinase A: role of protein phosphatase 2A and Bax. J Neurosci Res 86, 2326–2338.

[169] Delgado, M., and Ganea, D. (2003) Vasoactive intestinal peptide inhibits IL-8 production in human monocytes by downregulating nuclear factor kappaB-dependent transcriptional activity. Biochem Biophys Res Commun 302(2):275–283

[170] Kirisako, T., Kamei, K., Murata, S., Kato, M., Fukumoto, H., Kanie, M., Sano, S., Tokunaga, F., Tanaka, K., and Iwai, K. (2006) A ubiquitin ligase complex assembles linear polyubiquitin chains. EMBO J., 25, 4877-87.

[171] Chen, Z.J., Parent, L., and Maniatis, T. (1996) Site-Specific Phosphorylation of IkBa by a Novel Ubiquitination-Dependent Protein Kinase Activity, Cell, 84, 853-862.

[172] Gerlach, B., Cordier, S.M., Schmukle, A.C., Emmerich, C.H., Rieser, E., Haas, T.L., Webb, A.I., Rickard, J.A., Anderton, H., Wong, W.W., Nachbur, U., Gangoda, L., Warnken, U., Purcell, A.W., Silke, J., and Walczak, H. (2011) Linear ubiquitination prevents inflammation and regulates immune signalling. Nature, 471, 591-6.

[173] Hochstrasser, M. (2006) Lingering mysteries of ubiquitin-chain assembly. Cell. 124, 27-34.

[175] Chen, Z.J., and Sun, L.J. (2009) Nonproteolytic functions of ubiquitin in cell signaling. Mol Cell. 33, 275-86.

[176] Niu,J., Shi, Y., Iwai, K., and Wua, Z.H. (2011) LUBAC regulates NF-κB activation upon genotoxic stress by promoting linear ubiquitination of NEMO. EMBO J. 30, 3741–3753.

[177] Skaug, B., Jiang, X., and Chen, Z.J. (2009) The role of ubiquitin in NF-kappaB regulatory pathways. Annu Rev Biochem.,78, 769-96.

[178] Tokunaga, F., Sakata, S., Saeki, Y., Satomi, Y., Kirisako, T., Kamei, K., Nakagawa, T., Kato, M., Murata, S., Yamaoka, S., Yamamoto, M., Akira, S., Takao, T., Tanaka, K., and Iwai, K. (2009) Involvement of linear polyubiquitylation of NEMO in NF-kappaB activation. Nat Cell Biol., 11,123-32.

[179] Regnier, C. H., Song, H. Y., Gao, X., Goeddel, D. V., Cao, Z., and Rothe, M. (1997) Identification and Characterization of an IkB Kinase. Cell, 90, 373-383.

[180] Verma, I.M., and Stevenson, J. (1997) IkB kinase:Beginning, not theend, PNAS, 94, 11758-11760.

[181] Mercurio, F., Zhu, H., Murray, B., Shevchenko, A., Bennett, B. L., Li, J.W., Young, D. B., Barbosa, M., and Mann, M. (1997) IKK-1 and IKK-2:Cytokine - Activated IkB Kinases Essential for NF-kB Activation. Science, 278, 860-866.

[182] Rothwarf, D. M., zandi, E., Natoli, G., and Karin, M. (1998) IKK-g is an essential regulatory subunit of the IkB kinase complex. Nature, 395, 297-300.